Coupled cycling of metals with nitrogen and carbon in marine sediments

by

Jennifer S. Karolewski

B.S., California Institute of Technology (2015)

Submitted to the Department of Earth, Atmospheric, and Planetary Sciences in partial fulfillment of the requirements for the degree of

Doctor of Philosophy

at the
MASSACHUSETTS INSTITUTE OF TECHNOLOGY
and
WOODS HOLE OCEANOGRAPHIC INSTITUTION

May 2024

Signature of Author

Jennifer S. Karolewski
Joint Program in Oceanography/Applied Ocean Science and Engineering
Massachusetts Institute of Technology
and Woods Hole Oceanographic Institution
May 3rd, 2024

Certified by

Dr. Scott D. Wankel
Thesis Supervisor
Woods Hole Oceanographic Institution

Accepted by

Dr. Ed Boyle
Chair, Joint Committee for Chemical Oceanography
Massachusetts Institute of Technology

Abstract

Coupled cycling of metals with nitrogen and carbon in marine sediments

by

Jennifer S. Karolewski

Submitted to the MIT-WHOI Joint Program in Oceanography and Applied Ocean Science and Engineering on May 3rd 2024, in Partial Fulfilment of the Requirements for the Degree of Doctor of Philosophy

Cross element processes are complex and often understudied components within biogeochemical cycles. In this thesis, I use stable isotopes of carbon, nitrogen, and oxygen as the primary tools to interrogates these complex reactions. First, I report abiotic oxidation of nitrite to nitrate by manganese(III)-pyrophosphate. This reaction can occur even in the absence of oxygen, unlike biological nitrite oxidation. Reaction rates were measured at a range of environmentally relevant pH values (5-8) with the reaction proceeding more quickly at lower pH. Reaction order was second order with respect to manganese(III) and first order with respect to nitrous acid. No reversibility of reaction was observed upon addition of isotopically distinct nitrate. An inverse kinetic isotope effect of +19.9 ± 0.7‰ was calculated, which was comparable in magnitude and direction to that of biological nitrite oxidation. In natural waters, such as estuaries, this reaction could potentially play an important role in the nitrogen cycle. Next, I report an abiotic reaction between hydroxylamine and manganese(III)-pyrophosphate which forms nitrous oxide, nitrite, and likely dinitrogen gas. In artificial seawater (pH = 8), this reaction proceeds rapidly, with the ratio of products highly dependent on the reactant ratio. Nitrous oxide site preference (SP) of +35.5 ± 0.6‰ was observed, consistent with the isotopic signatures of several marine nitrifying organisms. This suggests that "leakage" of intermediate hydroxylamine from nitrifier cells could potentially react with manganese(III) in a mixed biotic-abiotic process without previously being noticed. Finally, I performed experiments using carbon-13 labelling to measure rates of anaerobic oxidation of methane (AOM) in cold seep sediments collected at Cascadia Margin. Four forms of oxidized manganese and four forms of oxidized iron were added to treatments in order to evaluate how these altered rates of AOM. In contrast to previous work, addition of metals did not overall increase rates of AOM above those of an unamended control and some treatments in fact reduced it. However, energy yields from microbes using metal as an electron acceptor are higher per mole of methane reduced than that of using sulfate so even with these lower rates, energy yields would have exceeded those of controls. Additionally, doubling times for the archaea performing AOM are long enough that the microbial community may not have been able to adapt on the timescale of the experiment. Overall, the results of this thesis illuminate the need for further study of abiotic and coupled cycling reactions when considering biogeochemical cycles.

Thesis Supervisor: Dr. Scott D. Wankel
Title: Associate Scientist, Woods Hole Oceanographic Institution

Acknowledgements

This thesis would not have been possible without contributions from countless individuals, some of whom I'm sure I have forgotten to mention here but have nonetheless provided essential aid.

Susan Kauzlarich provided a wide-eyed 15-year-old the opportunity to begin doing chemistry in her lab at UC Davis. I'm not sure why she trusted me to handle molten tin, oxygen-acetylene torches, and arc-welding but her faith allowed me to discover my love of wet chemistry.

Paul Asimow, George Rossman, and Jeff Mendez were my guiding lights while slogging through the intense workload at Caltech. Thank you for nudging me into geochemistry where I actually get to see the sun!

Rachel Stanley invited me to work in her lab in the summer of 2014, thus starting my journey into oceanography. Evan Howard provided invaluable mentorship that summer and beyond (only sometimes in the form of adorable bunny pictures).

My adviser Scott has provided so much encouragement and enthusiasm over this (long, long) journey. My committee Colleen, Jeff, and Kristin have improved this thesis immeasurably through their considerable expertise. I'm grateful for Ann acting as an amazing thesis chair and NSF 1826940 and WHOI OVF for funding.

The Hankel/Wansel crew over the years including Carly, Kevin, Net, Sam, Danny, Luke, Brooke, Noah, Jarek, Zoe, Emily, Julia, Gabi, Kalina, Vero, Lina, Hayley, Chad, Erica, Luciana, Eric, JenN, and Kate are some of the most inspiring people I've ever had the privilege of working with. Shout out to the best dogs Molly, Mola, and Moxie for providing office snuggles.

My cohort of Jellyfish were the best classmates I could have dreamed of. Thanks for many years of friendship, laughter, and support. Maybe our first summer in OP really was the best summer of our lives? Sometimes I wish we all still lived in those little bungalows instead of being spread all around the world.

I've been lucky to go to sea seven (!) times since starting my PhD and have been fortunate to spend that time with brilliant scientists who have become lifelong friends.

Karen Casciotti and her lab have provided me with my dream job. Thank you, Nicole, Colette, Andrew, Noah, Hanif, Meléa, Luke, Jackie, and Hannah, for welcoming me to Stanford.

To my parents for encouraging my curiosity from the beginning and supporting my educational goals even when you didn't understand what the heck I was studying.

I want to thank my amazing team of doctors who took my chronic pain seriously and have kept my disabled body going despite its best efforts to quit on me. Healthcare should not be a privilege, but I have been extremely lucky to have access to world-class care.

My chosen family fills my heart every single day. Hannah, Allison, and Kayla we finally all got (or yeeted) the D! My friends here made the move out to CA so full of joy.

Finally, to my partner Nathan. I love everything about our little life together (even Mapes).

Table of contents

1. Introduction

Biogeochemistry involves the study of biological, geological, chemical, and physical processes and reactions that govern the distribution and cycling of elements in the environment. Among biogeochemists, it is common to discuss cycling in the context of a single element, such as the carbon or nitrogen cycle. Chapters 2 and 3 focus on the nitrogen cycle which I will briefly review here. Nitrogen is an essential element for life and often acts as a limiting nutrient within the ocean (Moore et al. 2013). Human impacts on the nitrogen cycle are substantial; the amount of artificially fixed nitrogen produced for fertilizers and other industrial applications is equivalent or greater than the amount fixed biologically per year (Galloway et al. 2004). Within the marine environment, nitrogen cycling reactions can be divided into those that occur in oxic and anoxic regions of the ocean (Figure 1). In surface waters, dinitrogen gas is fixed into ammonium or organic matter ($N_2 \rightarrow NH_4^+$) primarily by photoautotrophs such as *Trichodesmium* (Tang et al. 2019). Also occurring in oxic regions is nitrification ($NH_4^+ \rightarrow NO_2^- \rightarrow NO_3^-$) which will be discussed further below. In anoxic regions, denitrification ($NO_3^- \rightarrow NO_2^- \rightarrow NO \rightarrow N_2O \rightarrow N_2$) is performed primarily by heterotrophs which use fixed nitrogen as an electron acceptor (Devol 2015). Dissimilatory reduction of nitrate to ammonium (DNRA; $NO_3^- \rightarrow NO_2^- \rightarrow NH_4^+$) is performed by a similar nutritional class of microbes (chemoorganoheterotrophs) but does not result in the loss of fixed nitrogen from the system (Gruber 2008). Finally, anammox ($NH_4^+ + NO_2^- \rightarrow N_2$) is performed by chemoautotrophs as an energy source and also results in the loss of fixed nitrogen (Kuenen 2008). Chapter 4 focuses on a specific portion of the carbon cycle, namely that of methane. Methane is the most abundant organic molecule on Earth and acts as a supply of energy to both humans and microbes (Whiticar 2020). Additionally, methane is a potent greenhouse gas that is the second most impactful to the climate after CO_2 (Whiticar 2020). Methane is biologically produced in aquatic systems through methanogenesis which primarily occurs through the hydrogenotrophic pathway (from hydrogen and carbon dioxide) or the acetoclastic pathway (from breaking down acetate) (Whiticar 2020). Once formed methane can then be consumed through aerobic methanotrophy or anaerobic oxidation of methane (AOM) which will be discussed further below (Guerrero-Cruz et al. 2021). Aerobic methanotrophy is performed by bacteria which use methane as their sole source of carbon and energy and tend to accumulate the surface of sediments (Fenibo et al. 2023)

While it may be easier to limit biogeochemical studies to primarily one element, nature does not restrict itself in the same way and thus this approach omits important cross-element reactions. Coupled cycling can take many forms in the environment. Microbes can use redox-active species in order to gain energy (dissimilatory) and/or acquire biomass (assimilatory) (Kappler et al. 2021). Dissimilatory pathways can also be divided in anaerobic respiration, wherein oxidized forms of nitrogen, metals, sulfur, etc. are used as electron acceptors to break down organic matter, and chemolithotrophy, wherein inorganic redox reactions are used to directly harvest energy (Burgin et al. 2011). Chapter 4 of this thesis focuses on one such biological coupled cycling process: anaerobic oxidation of methane (AOM) which transforms methane (CH_4) to carbon dioxide (CO_2). This reaction serves as a pathway for microbes to acquire energy and also as a source of carbon. Generally, this process is thought to be most commonly tied to sulfate reduction (sulfate-AOM) performed by consortia of anaerobic methanotrophic archaea (ANME) and sulfate-reducing bacteria (SRB); though, oxidized metals such as iron (Fe(III)) and manganese (Mn(IV)) have also been linked to AOM (metal-AOM) (Beal et al. 2009; Boetius et al. 2000; Nauhaus et al. 2002; Sivan et al. 2011). In Chapter 4, I discuss a study of AOM in marine sediments, wherein the potential for oxidized forms of iron and manganese to oxidize methane to carbon dioxide is explored.

Abiotic reactions can also play an important role in coupled cycling. It has been demonstrated that many of the reactions in the conventional biotic view of the nitrogen cycling can also be performed abiotically, often by redox active metals such as iron and manganese (Figure 2, Doane 2017; Zhu-Barker et al. 2015). For instance, "chemodenitrification" has linked the iron and nitrogen cycles (Buchwald et al. 2016; Grabb et al. 2017; Jones et al. 2015). The most important nitrogen cycle reaction in this thesis is the process of nitrification. Nitrification is generally written as NH_3 (ammonia) → NO_2^- (nitrite) → NO_3^- (nitrate) and can thus be divided into the steps of ammonia oxidation and nitrite oxidation (Ward 2008). Conventional views of nitrification suggest that these steps are performed in sequence to gain energy by obligately aerobic microbes, including ammonia-oxidizing archaea (AOA), ammonia-oxidizing bacteria (AOB), nitrite-oxidizing bacteria (NOB), and more recently discovered comammox bacteria which are capable of oxidizing both ammonia and nitrite (Könneke et al. 2005; Kowalchuk and Stephen 2001; Van Kessel et al. 2015; Watson et al. 1981). In Chapters 2 and 3, I make a detailed examination of abiotic nitrification

reactions between nitrogen and manganese species (Figure 3). In Chapter 2, I explore an alternative mechanism for nitrite oxidation which is both abiotic and agnostic to the presence of oxygen. Nitrification is also known to produce nitrous oxide (N_2O) as a side product through a process that is still not well understood but may involve the reactive intermediate hydroxylamine (NH_2OH). In Chapter 3, I investigate a second potential abiotic reaction mechanism that can transform NH_2OH to N_2O under environmental conditions. Coupled cycling may also play an important role in mixed abiotic-biotic reactions; for instance, leakage of a reactive intermediate such as hydroxylamine from an ammonia-oxidizing bacterial or archaeal cell may promote reaction with dissolved metals ions present outside the cell (Kits et al. 2019; Kozlowski et al. 2016; Liu et al. 2017; Soler-Jofra et al. 2021). In Chapter 3, I discuss one of these potential reactions: the abiotic reaction of manganese with biologically produced hydroxylamine.

When attempting to study these complex, multi-element processes, stable isotopes can provide a crucial tool. Within both carbon and nitrogen cycling, natural abundance stable isotopes have been used to help disentangle co-occurring processes (Casciotti 2016; Wagner and Herrle 2014). Additions of enriched isotope tracers have also been utilized to measure rates of reaction. In this thesis I use stable isotopes of nitrogen (^{15}N, ^{14}N), oxygen (^{18}O, ^{16}O), and carbon (^{13}C, ^{12}C) to track reaction pathways, measure reaction rates, and calculate isotope effects. The goal of this thesis is to use stable isotopes as a tool to probe coupled cycling reactions between the trace metals iron and manganese and the nutrients carbon and nitrogen. This thesis consists of three data chapters. Chapters 2 and 3 focus on abiotic interactions between manganese (III) and nitrogen species nitrite and hydroxylamine, respectively. I establish that these reactions can occur under environmentally relevant conditions and that their isotopic signatures are similar or even identical to those of the corresponding biological reaction. I also use stable isotopes in these chapters to measure rates of reaction and evaluate potential back-reactions or further reaction of products, to better understand reaction mechanisms. Chapter 4 is a study of anaerobic oxidation of methane (AOM) in the presence of manganese, iron, and sulfur. Using ^{13}C labeled methane as a tracer, I establish that the addition of oxidized metals to cold-seep sediments does not universally increase rates of AOM and may actually be inhibitory under some conditions. Finally, I conclude with Chapter 5, wherein I summarize the relevance and major findings of this thesis as well as briefly discuss future directions for study for each chapter.

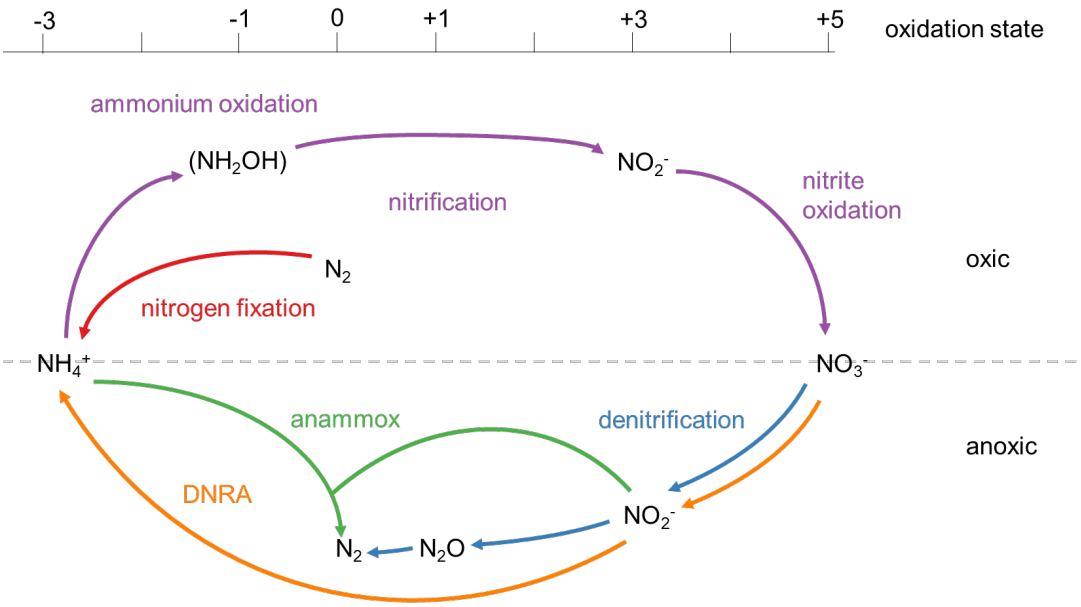

Figure 1: Major microbially driven processes and chemical species in the marine nitrogen cycle plotted against oxidation state of N. Processes above the dashed line occur in oxic environments and processes below occur in anoxic environments. DNRA = Dissimilatory Nitrate Reduction to Ammonium

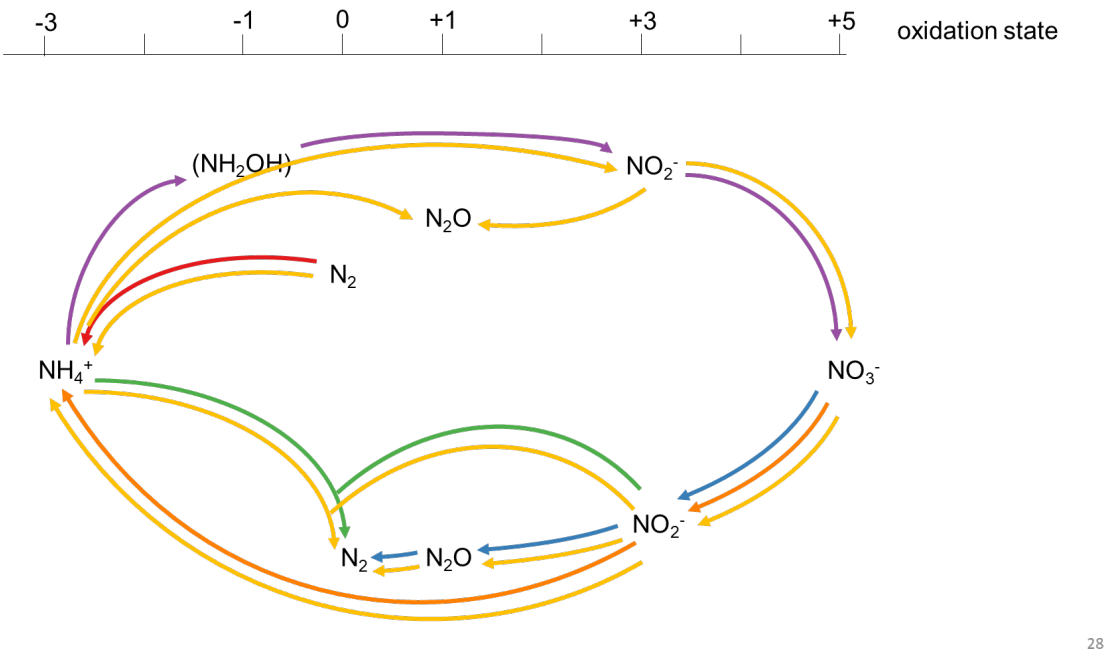

Figure 2: Major microbially driven processes and chemical species in the marine nitrogen cycle plotted against oxidation state of N (red, orange, green, blue, and purple arrows) alongside a selection of abiotic process (yellow arrows). Adapted from Doane 2017.

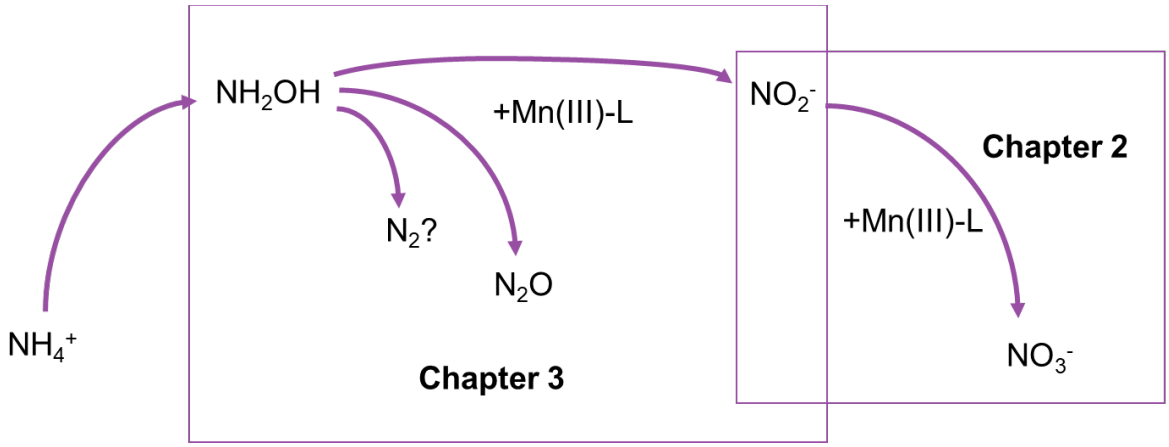

Figure 3: Conceptual diagram showing the abiotic reactions discussed in chapters 2 and 3.

References

Beal, E. J., House, C. H., & Orphan, V. J. (2009). Manganese- and iron-dependent marine methane oxidation. *Science*, *325*(5937), 184–187.

Boetius, A., Ravenschlag, K., Schubert, C. J., Rickert, D., Widdel, F., Gleseke, A., Amann, R., Jørgensen, B. B., Witte, U., & Pfannkuche, O. (2000). A marine microbial consortium apparently mediating anaerobic oxidation of methane. *Nature*, *407*(6804), 623–626.

Buchwald, C., Grabb, K., Hansel, C. M., & Wankel, S. D. (2016). Constraining the role of iron in environmental nitrogen transformations: Dual stable isotope systematics of abiotic NO2− reduction by Fe(II) and its production of N2O. *Geochimica et Cosmochimica Acta*, *186*, 1–12.

Canfield, D. E., Glazer, A. N., & Falkowski, P. G. (2010). The evolution and future of earth's nitrogen cycle. *Science*, *330*(6001), 192–196.

Casciotti, K. L. (2016). Nitrogen and Oxygen Isotopic Studies of the Marine Nitrogen Cycle. *Annual Review of Marine Science*, *8*, 379–407.

Devol, A. H. (2015). Denitrification, anammox, and N2 production in marine sediments., *7*(Volume 7, 2015), 403–423

Doane, T. A. (2017). The Abiotic Nitrogen Cycle. ACS Earth and Space Chemistry, 1(7), 411–421.

Fenibo, E. O., Selvarajan, R., Wang, H., Wang, Y., & Abia, A. L. K. (2023). Untapped talents: insight into the ecological significance of methanotrophs and its prospects. *Science of The Total Environment*, *903*, 166145.

Galloway, J. N., Dentener, F. J., Capone, D. G., Boyer, E. W., Howarth, R. W., Seitzinger, S. P., Asner, G. P., Cleveland, C. C., Green, P. A., Holland, E. A., Karl, D. M., Michaels, A. F., Porter, J. H., Townsend, A. R., & Vörösmarty, C. J. (2004). Nitrogen cycles: Past, present, and future. *Biogeochemistry*, *70*(2), 153–226.

Godfrey, L. v., & Glass, J. B. (2011). The Geochemical Record of the Ancient Nitrogen Cycle, Nitrogen Isotopes, and Metal Cofactors. *Methods in Enzymology*, *486*(C), 483–506.

Grabb, K. C., Buchwald, C., Hansel, C. M., & Wankel, S. D. (2017). A dual nitrite isotopic investigation of chemodenitrification by mineral-associated Fe(II) and its production of nitrous oxide. *Geochimica et Cosmochimica Acta*, *196*, 388–402.

Gruber, N. (2008). The Marine Nitrogen Cycle: Overview and Challenges. *Nitrogen in the Marine Environment*, 1–50.

Guerrero-Cruz, S., Vaksmaa, A., Horn, M. A., Niemann, H., Pijuan, M., & Ho, A. (2021). Methanotrophs: Discoveries, Environmental Relevance, and a Perspective on Current and Future Applications. *Frontiers in Microbiology*, *12*, 678057.

Hansel, C. M. (2017). Manganese in Marine Microbiology. *Advances in Microbial Physiology*, *70*, 37–83.

Jones, L. C., Peters, B., Lezama Pacheco, J. S., Casciotti, K. L., & Fendorf, S. (2015). Stable isotopes and iron oxide mineral products as markers of chemodenitrification. *Environmental Science and Technology*, *49*(6), 3444–3452.

Kappler, A., Bryce, C., Mansor, M., Lueder, U., Byrne, J. M., & Swanner, E. D. (2021). An evolving view on biogeochemical cycling of iron. *Nature Reviews Microbiology 2021 19:6*, *19*(6), 360–374.

Kits, K. D., Jung, M. Y., Vierheilig, J., Pjevac, P., Sedlacek, C. J., Liu, S., Herbold, C., Stein, L. Y., Richter, A., Wissel, H., Brüggemann, N., Wagner, M., & Daims, H. (2019). Low

yield and abiotic origin of N2O formed by the complete nitrifier Nitrospira inopinata. *Nature Communications 2019 10:1*, *10*(1), 1–12.

Könneke, M., Bernhard, A. E., de La Torre, J. R., Walker, C. B., Waterbury, J. B., & Stahl, D. A. (2005). Isolation of an autotrophic ammonia-oxidizing marine archaeon. *Nature 2005 437:7058*, *437*(7058), 543–546.

Kowalchuk, G. A., & Stephen, J. R. (2001). Ammonia-oxidizing bacteria: A model for molecular microbial ecology. *Annual Review of Microbiology*, *55*(Volume 55, 2001), 485–529.

Kozlowski, J. A., Stieglmeier, M., Schleper, C., Klotz, M. G., & Stein, L. Y. (2016). Pathways and key intermediates required for obligate aerobic ammonia-dependent chemolithotrophy in bacteria and Thaumarchaeota. *The ISME Journal 2016 10:8*, *10*(8), 1836–1845.

Kuenen, J. G. (2008). Anammox bacteria: from discovery to application. *Nature Reviews Microbiology 2008 6:4*, *6*(4), 320–326.

Liu, S., Han, P., Hink, L., Prosser, J. I., Wagner, M., & Brüggemann, N. (2017). Abiotic Conversion of Extracellular NH2OH Contributes to N2O Emission during Ammonia Oxidation. *Environmental Science and Technology*, *51*(22), 13122–13132.

Moore, C. M., Mills, M. M., Arrigo, K. R., Berman-Frank, I., Bopp, L., Boyd, P. W., Galbraith, E. D., Geider, R. J., Guieu, C., Jaccard, S. L., Jickells, T. D., la Roche, J., Lenton, T. M., Mahowald, N. M., Marañón, E., Marinov, I., Moore, J. K., Nakatsuka, T., Oschlies, A., … Ulloa, O. (2013). Processes and patterns of oceanic nutrient limitation. *Nature Geoscience 2013 6:9*, *6*(9), 701–710.

Nauhaus, K., Boetius, A., Krüger, M., & Widdel, F. (2002). In vitro demonstration of anaerobic oxidation of methane coupled to sulphate reduction in sediment from a marine gas hydrate area. *Environmental Microbiology*, *4*(5), 296–305.

Sivan, O., Adler, M., Pearson, A., Gelman, F., Bar-Or, I., John, S. G., & Eckert, W. (2011). Geochemical evidence for iron-mediated anaerobic oxidation of methane. *Limnology and Oceanography*, *56*(4), 1536–1544.

Soler-Jofra, A., Pérez, J., & van Loosdrecht, M. C. M. (2021). Hydroxylamine and the nitrogen cycle: A review. *Water Research*, *190*, 116723.

Stüeken, E. E., Kipp, M. A., Koehler, M. C., & Buick, R. (2016). The evolution of Earth's biogeochemical nitrogen cycle. *Earth-Science Reviews*, *160*, 220–239.

Tagliabue, A., Bowie, A. R., Boyd, P. W., Buck, K. N., Johnson, K. S., & Saito, M. A. (2017). The integral role of iron in ocean biogeochemistry. *Nature*, *543*(7643), 51–59.

Tang, W., Wang, S., Fonseca-Batista, D., Dehairs, F., Gifford, S., Gonzalez, A. G., Gallinari, M., Planquette, H., Sarthou, G., & Cassar, N. (2019). Revisiting the distribution of oceanic N2 fixation and estimating diazotrophic contribution to marine production. *Nature Communications 2019 10:1*, *10*(1), 1–10.

van Kessel, M. A. H. J., Speth, D. R., Albertsen, M., Nielsen, P. H., Op Den Camp, H. J. M., Kartal, B., Jetten, M. S. M., & Lücker, S. (2015). Complete nitrification by a single microorganism. *Nature 2015 528:7583*, *528*(7583), 555–559.

Wagner, T., & Herrle, J. O. (2014). C-Isotopes. *Encyclopedia of Marine Geosciences*, 1–8.

Wang, X., Xie, G. J., Tian, N., Dang, C. C., Cai, C., Ding, J., Liu, B. F., Xing, D. F., Ren, N. Q., & Wang, Q. (2022). Anaerobic microbial manganese oxidation and reduction: A critical review. *Science of The Total Environment*, *822*, 153513.

Ward, B. B. (2008). Nitrification in Marine Systems. *Nitrogen in the Marine Environment*, 199–261.

Watson, S. W., Valois, F. W., & Waterbury, J. B. (1981). The Family Nitrobacteraceae. *The Prokaryotes*, 1005–1022.

Whiticar, M. J. (2020). The Biogeochemical Methane Cycle. *Hydrocarbons, Oils and Lipids: Diversity, Origin, Chemistry and Fate*, 1–78.

Zhu-Barker, X., Cavazos, A. R., Ostrom, N. E., Horwath, W. R., & Glass, J. B. (2015). The importance of abiotic reactions for nitrous oxide production. *Biogeochemistry 2015 126:3*, *126*(3), 251–267.

2. An isotopic study of abiotic nitrite oxidation by ligand-bound manganese (III)

This chapter was originally published as: Karolewski, J. S., Sutherland, K. M., Hansel, C. M., & Wankel, S. D. (2021). An isotopic study of abiotic nitrite oxidation by ligand-bound manganese (III). *Geochimica et Cosmochimica Acta*, *293*, 365–378.

Abstract

Redox transformations of nitrogen (N) play a critical role in determining its speciation and biological availability, thus defining the magnitude and extent of productivity in many ecosystems. A range of important nitrogen transformations often co-occur in regions hosting redox-active elements, including sulfur, iron and manganese (Mn), especially along sharp redox gradients within aquatic sediments. This proximity produces conditions under which multi-element interactions and coupled cycling are thermodynamically favored. While previous work has reported anoxic nitrification linked to the presence of manganese (Mn) oxides in sediments, a clear connection between the cycling of Mn and N has remained elusive. Soluble Mn(III), which is stabilized via ligand-complexation, has recently been shown to represent the dominant dissolved Mn species in many environments. Here, we examined the reactivity of ligand-stabilized Mn(III) with nitrite, using natural abundance stable nitrogen and oxygen isotopes to explore reaction dynamics under a range of conditions. Oxidation of nitrite to nitrate by Mn(III)-pyrophosphate proceeded abiotically under both oxygen replete and nitrogen-purged conditions. Kinetics and isotope systematics of this reaction were measured over a range of pH (5 to 8), with reaction rates decreasing with increasing pH. Under all treatments, an inverse kinetic isotope effect of -19.9 ± 0.7‰ was observed for N, remarkably similar with previously documented fractionation by nitrite-oxidizing organisms. Experiments using ^{18}O-labeled water confirmed that the source of the additional oxygen atom was from water. These findings suggest that nitrite oxidation in environments hosting abundant ligand-bound Mn(III), including porewaters, estuaries and coastal waters, may be facilitated in part by abiotic reactions with Mn, even under functionally anoxic conditions.

2.1 Introduction

As a primary nutrient for sustaining life, the processes governing the transformations of nitrogen (N) have long been a topic of interest. The N cycle is also intricately linked with the cycling of other important elements in aquatic environments, including carbon, oxygen, phosphorous, sulfur, iron, and manganese (Mn) (Gruber and Galloway, 2008; Burgin et al., 2011; Melton et al., 2014). While the cycling of nitrogen has traditionally been attributed to microbially-mediated transformations, recent studies have highlighted abiotic processes as likely important and understudied aspects of nitrogen cycling under some conditions (Zhu-Barker et al., 2015; Heil et al., 2016; Doane, 2017; Cavazos et al., 2018; Stanton et al., 2018).

Redox interactions between Mn and N in sediments have been the focus of previous studies, however, their importance in global cycling is still poorly understood (Zhu-Barker et al., 2015; Doane, 2017). For example, Luther et al. (1997) showed in laboratory and field studies that reactions between ammonia (NH_3) and Mn(III,IV) (oxy)(hydr)oxides (hereinafter Mn oxides) in sediments could act to "short circuit" the nitrogen cycle by providing a direct pathway to the formation of dinitrogen gas ($2NH_3 + 3MnO_2 + 6H^+ \rightarrow 3Mn^{2+} + N_2 + 6H_2O$). Subsequent work also found indirect evidence for anoxic nitrification coupled to reduction of Mn oxides to Mn(II) (Hulth et al., 1999; Anschutz et al., 2000). In contrast, however, targeted studies using incubations amended with $^{15}NH_4^+$ failed to find conclusive evidence that reactions between ammonia and manganese were occurring in a Mn oxide rich continental basin sediment (Thamdrup and Dalsgaard, 2000). More recent field studies have suggested that the specific geochemical conditions, including the concentration and age of the Mn oxides, are key factors controlling the efficacy of Mn oxide catalyzed anaerobic nitrification (Bartlett et al., 2007; Bartlett et al., 2008), or that reactions may only occur in presence of colloidal Mn oxides or more reactive Mn(III) species (Luther and Popp, 2002; Lin and Taillefert, 2014).

While many biogeochemical models of Mn in sediments include only soluble Mn(II) and solid Mn(III,IV) oxides, soluble Mn(III) can be stabilized via complexation by ligands and has been recently shown to represent the dominant dissolved Mn species in many environments (Madison et al., 2013; Oldham et al., 2015). With a reduction potential close to that of molecular oxygen (Luther et al., 1997; Luther III, 2010), Mn(III)-ligand (Mn(III)-L) complexes have the capacity to

be potent and important environmental oxidants. For instance, Mn(III)-L complexes can directly oxidize carbon, ferrous iron, and sulfide (Kostka et al., 1995). Ultimately, the extent to which Mn(III)-L complexes interact with other redox-active elements and molecules will depend on the specific ligand and subsequent strength of Mn(III) complexation. While the composition of Mn(III) ligands in natural systems is presently unknown, a diversity of ligand compositions and complex strengths has been predicted, ranging from weaker ligands such as pyrophosphate to complex humics with strong ligand moieties (Yakushev et al., 2009; Oldham et al., 2015; Oldham et al., 2017a).

The role of Mn(III) in Mn-N redox interactions is a potentially important component in the biogeochemical cycles of both elements that has not been fully addressed by previous studies (Luther et al., 1997; Luther et al., 2018). One major challenge to studying coupled cycling reactions is determining the importance of a single process from a range of potential biotic and abiotic reactions occurring in the environment. Stable isotope studies of nitrogen and oxygen have proven to be powerful tools in decoupling complex processes in the nitrogen cycle across a range of environments and contexts (Kendall et al., 2007; Casciotti, 2016). The abundance ratio of the two stable isotopes of N (^{14}N and ^{15}N) as well as O (^{16}O and ^{18}O) can vary as the result of isotope fractionation during processes including enzymatic or chemical reactions. As specific reactions may yield unique isotopic fractionation patterns, measurements of isotope ratios can be used to disentangle complex processes in the environment (Granger and Wankel, 2016). Hence, a focus of this study is to characterize the isotopic fractionation of specific reactions in order to identify abiotic, anoxic nitrite oxidation by ligand-stabilized Mn(III). Here we hypothesize that Mn(III) is a viable and environmentally relevant oxidant of nitrite (NO_2^-) in aquatic systems. We present a series of experiments describing one such potentially important reaction between Mn(III) and NO_2^- and provide the first examination of the stable N and O isotope dynamics captured by the reaction.

2.2 Methods

2.2.1 Experimental Overview

Aspects of the reaction between Mn(III) and NO_2^- were targeted through a variety of experimental approaches. Specifically, experiments were conducted to evaluate 1) the influence of reactant concentrations and pH on the reaction kinetic expression, 2) the kinetic nitrogen isotope effect of

NO_2^- oxidation by measurement of reactant and product isotopic compositions over reaction progress, 3) the influence of dissolved O_2 on reaction rates by varying solution and headspace composition, 4) the possible role of chemically catalyzed equilibrium (or back-reaction) between NO_2^- and reaction products (by use of NO_3^- with an elevated $\delta^{15}N$), and 5) the source of O atoms in reaction product NO_3^- (by use of ^{18}O-labeled water).

2.2.2 Preparation of solutions

Manganese(III)-pyrophosphate (Mn(III)-PP) solutions were prepared as previously described (Madison et al., 2011). A 5 mM solution of sodium pyrophosphate was prepared in de-oxygenated milliQ water and the pH adjusted to 7.0 using 6M hydrochloric acid (HCl). Manganese(III)-acetate salt (0.91 mM) was added to form a clear pink Mn(III)-PP solution (approximately 1 mM) which was subsequently filtered (0.45 μm) to remove any incidental particulate Mn oxides formed via disproportionation. The pH of Mn(III)-PP was adjusted by addition of 6M HCl before filter sterilization (0.2 μm). Additional solutions of Mn(III)-PP were prepared in ^{18}O-labeled water. Solid Mn oxides in the form of buserite were prepared as described previously (Mandernack et al., 1995). Sodium nitrite and sodium nitrate solutions (10 mM) were prepared in milliQ water and sterilized by autoclaving. Solutions of ^{18}O-labeled nitrite were prepared by equilibrating solutions of autoclaved nitrite in ^{18}O-labeled water in a 50°C oven for 7 days (Buchwald and Casciotti, 2013). All experiments were initiated in 160 mL serum bottles by the addition of 1 mL of 10 mM nitrite to 100 mL of ~1 mM Mn(III)-PP in excess pyrophosphate, giving a starting nitrite concentration of ~100 μM. Subsamples were collected over time by removing 3 mL of solution with a sterile syringe and replacing the headspace with air or N_2 gas depending on the experimental treatment. The presence of Mn(III)-PP complex was found to interfere with nitrite and nitrate concentration measurements and was thus removed prior to analysis by precipitation of all Mn as Mn oxides by the addition of 10 μL of 6M NaOH, followed by filtration of Mn precipitate (0.2 μm) and neutralization by addition of HCl.

2.2.3 Chemical speciation

Concentrations of nitrate plus nitrite were measured using chemiluminescent NO_x detection (Teledyne, T200) after reduction in hot acidic vanadyl sulfate solution (Braman and Hendrix, 1989). Nitrite concentrations were monitored using Griess reagent (Pai et al., 1990), and nitrate

concentration estimated by difference. Samples were diluted 10-fold with milliQ water to a final volume of 3 mL, treated with 60 µL sulfanilamide (SAN) and 60 µL *N*-(1-Naphthyl)ethylenediamine (NED) and measured for absorbance at 543 nm. Mn(III) concentrations were measured using the leucoberbelin blue method referenced to a standard curve of potassium permanganate and adjusted to account for the oxidation state offset (Krumbein and Altman, 1973; Jones et al., 2019).

2.2.4 Isotopic measurements

Isotopic ratios ($^{15}N/^{14}N$, $^{18}O/^{16}O$) are reported using standard delta notation where $\delta^{15}N = [(^{15}R_{sample}/^{15}R_{N2\text{-}ATM})\text{-}1)*1000]$ and $^{15}R = {}^{15}N/^{14}N$ and where $\delta^{18}O = [(^{18}R_{sample}/^{18}R_{VSMOW})\text{-}1)*1000]$ and $^{18}R = {}^{18}O/^{16}O$. Isotopic composition of nitrite was measured after conversion of 20-30 nmol to nitrous oxide (N_2O) using the azide method (McIlvin and Altabet, 2005) in 20 mL crimp-sealed headspace vials. Nitrate N and O isotopes were measured using the denitrifier method (Sigman et al., 2001; Casciotti et al., 2002) to convert samples to nitrous oxide after removal of nitrite by sulfamic acid addition (Granger and Sigman, 2009). The resulting N_2O was then purified and trapped on a modified TraceGas (IsoPrime, Inc.) purge and trap system coupled with a Gilson autosampler before isotopic analysis on an isotope ratio mass spectrometer (IRMS) (IsoPrime 100, Elementar Inc.). Isotope reference materials for nitrate (USGS 32, USGS 34, USGS 35) or nitrite (WILIS 10, WILIS 11 and WILIS 20) were run before and after samples at 3 different sizes to normalize reported isotope values and correct for variations in sample size and any instrument drift. Values of USGS 32, USGS 34, and USGS 35 are +180, -1.8, and +2.7‰ for $\delta^{15}N$ and +25.4, -27.8, and +56.8‰ for $\delta^{18}O$, respectively (Brand et al., 2009). Inter-laboratory comparisons set the values of WILIS 10, WILIS 11, and WILIS 20 at -1.7, +57.1, and -7.8‰ for $\delta^{15}N$ and +13.2, +8.6 and +47.6‰ for $\delta^{18}O$ (Wankel et al., 2017). Typical reproducibility is ±0.2‰ for both $\delta^{15}N$ and $\delta^{18}O$ using the azide method and ±0.2‰ for $\delta^{15}N$ and ±0.5‰ for $\delta^{18}O$ using the denitrifier method. Here we adopt the isotope notation convention wherein reactions resulting in products with a preference for lighter isotopes are indicated by a ‘normal’ isotope effect with a positive sign; thus, a negative sign indicates an inverse isotope effect.

2.3 Results

2.3.1 Concentrations of nitrite and nitrate

Nitrite (100 μM) was reacted with Mn(III)-PP (~1 mM) under a headspace of air over a period of 11 days at three pH treatments (pH = 5.0, 5.7, 6.5) with four replicates. Over the course of the experiment, nitrite concentrations were monitored and found to decrease to undetectable levels (<1 μM) by the end of the experiment, with higher pH treatments reacting more slowly (Figure 1a). At the conclusion of the experiment, concentrations of nitrate produced were 1:1 with nitrite consumed (not shown). Parallel controls without pyrophosphate or Mn(III)-PP showed no loss of nitrite during the experiment.

2.3.2 Isotopic fractionation

Nitrite $\delta^{15}N$ values universally decreased from their starting value (-2.3‰) during the course of the reaction in relation with the proportion of nitrite consumed. Oxygen isotope ratios showed no statistical difference between starting and ending values. Calculation of the N isotope effect of nitrite oxidation by Mn(III)-PP ($^{15}\varepsilon_{NO2ox,MnIII}$) assuming closed-system Rayleigh dynamics (Mariotti et al., 1981) yielded $^{15}\varepsilon_{NO2ox,MnIII}$ values of -19.1 ± 0.5‰ for pH = 5.0 (r^2 = 0.997) and $^{15}\varepsilon_{NO2ox,MnIII}$ = -18.2 ± 0.4‰ for pH = 5.7 (r^2 = 0.997) in initial experiments. Nitrogen isotope effects were also calculated during a subset of reaction kinetics experiments described below and ranged from -19.2 ± 0.4‰ to -20.6 ± 0.2‰ (Figure 1b; Table 1).

2.3.3 Reaction kinetics

Two experiments were conducted in order to determine the reaction kinetics and order with respect to Mn(III)-PP and nitrite. The isolation method was used, in which initial concentration of one reagent was varied while other variables were held constant. Solutions of varying Mn(III)-PP concentration were prepared by v/v dilution of an approximately 1 mM solution with 5 mM pyrophosphate. All experiments were run with air as the headspace at pH = 5.0 (Table 1).

To determine the role of pH in the kinetics of reaction, incubations were conducted at pH = 5.0, 5.7, and 6.5. Solution pH was buffered by excess pyrophosphate with pH stability confirmed by measurement at the conclusion of the experiment. Solid oxides were added to minimize influence of Mn(III)-PP loss during the reaction (additional Mn(III)-PP complex will form in the presence

of excess Mn oxides and pyrophosphate ligand). An additional control with Mn oxides and no pyrophosphate ligand displayed no reactivity with nitrite.

Using the balanced reaction (Eq. 1), a general rate law (Eq. 2) was written to derive the rate of reaction. Concentrations in Eq. 2 represent the total concentration of each reactant. For simplicity of notation, $[NO_2^-]$ also includes any nitrous acid (HNO_2) present. $NO_2^- + 2Mn(III)\text{-}PP + H_2O \rightarrow NO_3^- + 2Mn^{2+} + 2PP + 2H^+$ [1]

$$\frac{d[NO_3^-]}{dt} = k[Mn(III)PP]^a[NO_2^-]^b[H^+]^c \quad [2]$$

$$rate = \frac{d[NO_3^-]}{dt} = -2\frac{d[Mn(III)PP]}{dt} = -\frac{d[NO_2^-]}{dt} \quad [3]$$

where *a*, *b, c* represent the order of the reaction with respect to Mn(III)-PP, NO_2^-, and H^+, respectively, and *k* is the rate constant. When [Mn(III)-PP] is varied while pH and $[NO_2^-]$ held constant equation 2 simplifies to:

$$rate = k_{obs,1}[Mn(III)PP]^a \quad [4]$$

where

$$k_{obs,1} = k[NO_2^-]^b[H^+]^c \quad [5]$$

Using the instantaneous rate method equation 4 can be rewritten as:

$$\log(rate_{ins}) = \log(k_{obs,1}) + a \log([Mn(III)PP_{in}]) \quad [6]$$

where $rate_{ins}$ is the instantaneous rate and $[Mn(III)PP_{in}]$ is the initial concentration of Mn(III)-PP. Thus, the slope (a) of $\log([Mn(III)PP_{in}]$ vs. $\log(rate_{ins})$ indicated a 2nd order reaction with respect to Mn(III)-PP (a = 1.95±0.1; Figure 2a).

Similarly, when $[NO_2^-]$ is varied and [Mn(III)-PP] is held constant equation 2 can be written as:

$$rate = k_{obs,2}[NO_2^-]^b \quad [7]$$

with

$$k_{obs,2} = k[Mn(III)PP]^a[H^+]^c \quad [8]$$

As above this can be expressed as:

$$\log(rate_{int}) = \log(k_{obs,2}) + b \log([NO_2^-]_{in}) \quad [9]$$

The slope (b) of $\log([NO_2^-]_{in})$ vs. $\log(rate_{int})$ gave a value of 1.03±0.04, indicating the reaction is 1st order with respect to NO_2^- (Figure 2b).

To determine the role of pH, reactions were conducted in the presence of excess Mn oxides and pyrophosphate, to minimize any changes in the concentration of Mn(III)-PP. Thus assuming constant [Mn(III)-PP], kinetics appeared pseudo-first order with respect to nitrite and rate constants were calculated from the slope of time vs. ln ($[NO_2^-]$) (Figure 2c). As above the rate expression was simplified:

$$rate = k_{obs,3}[H^+]^c \quad [10]$$

with

$$k_{obs,3} = k[Mn(III)PP]^a[NO_2^-]^b \quad [11]$$

Using the pseudo-first order rate constants derived as described above:

$$\log(rate) = \log(k_{obs,3}) + c \log([H^+]) \quad [12]$$

Equation 12 was solved for the slope c, indicating the reaction is 1st order with respect to concentration of protons (Figure 2d; c = 0.96±0.01). The overall rate expression is thus:

$$\frac{d[NO_3^-]}{dt} = k[Mn(III)PP]^2[NO_2^-][H^+] \quad [13]$$

This rate expression can also be simplified as:

$$\frac{d[NO_3^-]}{dt} = k[Mn(III)PP]^2[HNO_2]K_a \quad [14]$$

Where K_a represents the acid dissociation constant of nitrous acid. Thus we conclude the reactant is HNO_2, rather than NO_2^-.

2.3.4 Reaction rates

Based on observed changes in concentrations over time for experiments at pH = 5.0, 5.7, and 6.5 (starting NO_2^- = 100 µM and Mn(III)-PP = 1000 µM, four replicates), nitrite reduction rates of 518 ± 16.8, 108 ± 4.8, and 21.6 ± 2.4 µM d^{-1} were calculated, respectively (Table 2). Additional incubation experiments were performed with the same starting concentrations at pH 7 and 8 using isotopically labeled $^{15}NO_2^-$ to determine the reaction rates at pH values relevant to the marine system (Ward, 2011; Beman et al., 2013). Unlabeled nitrite (9 mM), ^{15}N-nitrite (1 mM), and unlabeled nitrate (4 mM) were pre-mixed and aliquotted into bottles as described above and then sampled over 3 months to track accumulation of ^{15}N in the NO_3^- pool over time. Under these reaction conditions rates of nitrite oxidation by Mn(III)-PP at pH 7 and 8 were 5.8 ± 1.3 and 3.9 ± 0.6 µM d^{-1}, respectively (Table 2).

2.3.5 Effect of dissolved oxygen

To determine the potential role of oxygen in the oxidation of nitrite to nitrate by Mn(III)-PP, two parallel incubations were conducted either with a headspace of laboratory air or after vigorously purging with N_2 gas for 15 minutes to substantially reduce the amount of dissolved oxygen. Experiments were run at pH 5 and sampled over 4 days. No significant difference in reaction rates was found between the oxic and N_2-sparged treatments (Table 1, Figure 3). Similarly, the observed N isotope fractionation was unaltered by oxygen level ($p = 0.28$).

2.3.6 Potential reversibility of reaction

To test the possibility of reaction reversibility, experiments were run with the addition of nitrate having an elevated $\delta^{15}N$ value (USGS 32, $\delta^{15}N = +180$). Two treatments contained an additional 10 μM (10% of nitrite added) and 100 μM (100% of nitrite added) nitrate at the beginning of each experiment at two pH values (pH = 5.0, 5.5). Sub-samples were collected over a period of 8 days. Again, no observed change in $^{15}\varepsilon_{NO2ox,MnIII}$ was noted among treatments receiving high $\delta^{15}N\text{-}NO_3^-$ in comparison to previous experiments receiving no NO_3^- amendment (Table 1).

2.3.7 Source of additional oxygen atom

In order to determine the source of the additional oxygen atom in nitrate, an experiment using ^{18}O-labeled water was performed. Two ^{18}O-labeled water samples having $\delta^{18}O$ values of approximately +18‰ and +40‰ were prepared by dilution from a stock solution (~+5000‰), with an unlabeled water sample with $\delta^{18}O \sim -5‰$ used as a third condition. As nitrite oxygen isotopes equilibrate with water quickly at the pH conditions of our experiments (Casciotti et al., 2007), ^{18}O-labeled nitrite stock solutions were also prepared as described above in an aliquot of each labeled water sample. As the result of equilibrium isotope fractionation between NO_2^- and H_2O, fully equilibrated nitrite has a $\delta^{18}O$ value ~14‰ higher than its surrounding water (Casciotti et al., 2007; Buchwald and Casciotti, 2013). Average starting values of $\delta^{18}O\text{-}NO_2^-$ were +11, +32, and +54‰ after equilibration with ^{18}O-labeled water.

Five treatments ($\delta^{18}O_{water} = -5‰$, +18‰, +40‰ oxic, $\delta^{18}O = -5‰$ N_2-sparged, oxic no Mn control) were run at three pH conditions (pH = 5.0, 5.7, 6.5) and subsampled over 17 days. Samples of nitrite and nitrate were analyzed for $\delta^{18}O$. No differences in rates or $\delta^{18}O$ values were found

between $\delta^{18}O\text{-}NO_3^-$ produced under oxic or N_2-sparged conditions ($p = 0.59$). The slope of $\delta^{18}O\text{-}H_2O$ vs. $\delta^{18}O\text{-}NO_3^-$ was very close to 1 under all three pH conditions, indicating water was the source of the third O-atom in nitrate (Figure 4; Table 3). Examination of the y-intercept of these data also allows calculation of the kinetic isotope effect associated with incorporation of the O atom from water ($^{18}\varepsilon_{k,H2O}$), which was determined to be +20.3 ± 1.5‰.

2.4 Discussion

Environmental transformations of nitrogen play a fundamental role in determining its fate as a nutrient and contaminant across ecosystems. While the framework for these processes is complex, it is widely understood that microbially driven reactions comprise the large majority of these transformations. Nevertheless, there also exists an array of abiotic transformations that may contribute to the complex framework of environmental nitrogen transformations under some conditions (Luther 2010; Zhu-Barker et al., 2015; Heil et al., 2016; Doane, 2017; Luther et al. 2018). Among these are redox reactions involving commonly abundant transition metals, especially Mn and Fe (Heil et al., 2015; Zhu-Barker et al., 2015; Buchwald et al., 2016; Doane, 2017; Grabb et al., 2017; Cavazos et al., 2018; Stanton et al., 2018). Here we demonstrate that ligand bound Mn(III) can serve as an important oxidant of nitrite, producing nitrate under environmentally relevant conditions and independent of molecular oxygen concentrations. We further present our stable isotopic interrogation of this process, shedding light on source O atoms and associated kinetic isotope effects, and discuss its possible relevance in environmental N cycling.

2.4.1 Mn(III) is an effective oxidant of NO_2^- - with possible environmental relevance

Foremost, our results demonstrate that ligand bound Mn(III) is an effective oxidant of nitrite under the conditions evaluated including circumneutral pH and modestly elevated concentrations. While Mn is present in the environment in three oxidation states (II, III, and IV), most studies exploring the oxidative potential of oxidized Mn on the N cycle have only examined the reactivity of Mn oxide minerals, thus overlooking the possible influence of dissolved, oxidized Mn (Bartlett, 1981; Stone and Morgan, 1984; Nelson et al., 2002). Additionally, Mn oxide minerals may vary widely in structure, oxidation state and reactivity (Post, 1999). To the best of our knowledge, the potential relevance of Mn to nitrite oxidation has only been examined in two previous studies, both

involving solid-phase Mn oxides (Bartlett, 1981; Luther and Popp, 2002). Bartlett (1981) first observed abiotic oxidation of nitrite to nitrate in sterilized soils upon addition of Mn oxides, while Luther and Popp (Luther and Popp, 2002) more formally evaluated the kinetics of nitrite oxidation by colloidal Mn oxides. In contrast to these solid Mn oxide phases, ligand bound Mn(III) forms have recently been shown to comprise the majority of dissolved Mn across a range of aquatic systems (Kostka et al., 1995; Madison et al., 2011; Oldham et al., 2015; Oldham et al., 2017a). These Mn(III)-L complexes have been shown to easily pass through conventional filtration (0.2-0.45 μm) (Wilczak et al., 1993; Kostka et al., 1995; Luther and Popp, 2002) and ultrafiltration (0.02 μm) (Oldham et al., 2017a; Oldham et al., 2017b), suggesting that previous studies assuming that all dissolved Mn was present as Mn(II) may have overlooked an important and reactive fraction of soluble Mn. Indeed our experimental results demonstrate that Mn(III)-L complexes are viable oxidants of nitrite under conditions of environmental relevance.

2.4.2 Reaction rate

Over the range of conditions we evaluated, observed rates of Mn(III)-L induced nitrite oxidation ranged from 3.9 μM d^{-1} up to 518.4 μM d^{-1} over pH values from 8.0 to 5.0, respectively (Table 2). While direct comparison with other studies of nitrite oxidation by bacterial cultures or in aqueous environments is not straightforward, to a first order, our observed rates are similar to those reported in a wide variety of studies. For example, recently reported rates of aerobic nitrite oxidation by axenic cultures of nitrite-oxidizing *Nitrobacter* and *Nitrospira* bacteria yielded half saturation constants (Km) of 49 to 544 μM and 9 to 27 μM, and V_{max} values of 64 to 164 and 18 to 48 μmol mg $protein^{-1}$ hr^{-1}, respectively (Nowka et al., 2015). Under our experimental conditions (all other factors being equal), a nitrite-oxidizer cell density corresponding to hypothetical protein concentration of 100 μg/L, would yield initial nitrite oxidation rates of 17 to 500 μM d^{-1} – similar in magnitude to the initial Mn(III)-L induced rates we observed at pH 5.0 and 5.7 of 518 μM d^{-1} and 108 μM d^{-1}, respectively.

Rates of nitrite oxidation in aqueous environments, of course, are much lower than those observed in bacterial cultures or lab experiments and are therefore commonly measured by addition of $^{15}NO_2^-$ and measured accumulation of $^{15}NO_3^-$ with time (Ward, 2011). In particular, much effort has focused on characterization of nitrite oxidation rates in oxygen deficient hotspots of nitrogen

transformation in the global ocean – yielding values ranging from 0 to ~600 nM d^{-1} (Ward et al., 1989; Lupschultz et al., 1990; Beman et al., 2013; Peng et al., 2015; Bristow et al., 2016; Sun et al., 2017). Other studied environments include coastal environments, open ocean, estuaries, and coral reefs, also typically exhibit rates ranging from ~0 up to several hundred nM d^{-1} (Dore and Karl, 1996; Bianchi et al., 1997; Heiss and Fulweiler, 2016). While microbial nitrite oxidation is generally considered to be an aerobic process, under oxygen-restricted conditions, the anaerobic oxidation of ammonium (anammox) is also known to oxidize NO_2^- to NO_3^- at stoichiometry of ~0.19 moles of NO_3^- produced per mole of NH_4^+ oxidized (Jetten et al., 1999; Strous et al., 2006; Kartal et al., 2011). Extrapolating from measured anammox rates in oceanic oxygen deficient zones (ODZs) and groundwaters suggests that environmental anammox based nitrite oxidation rates may range from <1 nM d^{-1} up to 70 nM d^{-1} (Kuypers et al., 2003; Dalsgaard et al., 2005; Lam et al., 2007; Moore et al., 2011).

Turning to the only previously reported rates of Mn induced nitrite oxidation, Luther and Popp (2002) reported a rate constant (k) of 493 M^{-1} min^{-1} at pH = 5.00 for reaction of NO_2^- with "polymeric" (colloidal) Mn oxides. Thus, relative to rates we observe in our experiment, at [MnO_2] = 1 mM and [NO_2^-] = 100 μM, the predicted rate of NO_3^- formation would be several orders of magnitude greater than rates we observed. Nevertheless, Mn oxides, including colloids, will be considerably lower than 1 mM in most environments, and could be less reactive due to surface adsorbates and/or co-precipitates. Further, Mn(III)-L and Mn oxides are oftentimes decoupled spatially. For instance, along redoxclines in stratified systems, Mn(III)-L span a wide redox gradient, while Mn oxides have a distinct peak in their distribution along the gradient (Trouwborst et al., 2006; Yakushev et al., 2007; Yakushev et al., 2009; Dijkstra et al., 2018). In any regards, predicted rates of nitrite oxidation by Mn(III)-L are similar in magnitude to biological rates described above. For example, under conditions that might typify porewaters close to an estuarine sediment-water interface (pH 6.5, [NO_2^-] = 10 μM, [Mn(III)-PP] = 80 μM) an estimate of 14 nM d^{-1} would be feasible (Madison et al., 2013). This result suggests that abiotic nitrite oxidation by Mn(III)-L complexes may be competitive with corresponding microbial processes, particularly at pH < 7 (Table 4). When taken together with the previously demonstrated potential for Mn oxides to also oxidize nitrite, Mn may therefore represent an important and currently underappreciated oxidant of nitrite within some ecosystems.

2.4.3 Stable isotope dynamics

Nitrite does not readily accumulate in most aquatic environments, with concentrations rarely reported above more than a few μM. Nevertheless, as with other reactive intermediates, its low concentrations reflect its high reactivity and fluxes involving nitrite can be high. As a consequence of these low ambient levels, nitrite has only recently been interrogated by stable isotope analyses. As both a reductive and oxidative intermediate of several transformation processes, the nitrogen and oxygen isotope dynamics of nitrite are often complex and reflect multiple processes (Casciotti et al., 2011; Buchwald and Casciotti, 2013; Casciotti, 2016; Buchwald et al., 2018). Thus, there still remains much to be learned from gaining an improved understanding of the systematics that govern its natural isotopic composition across environments in particular those with strong redox variations.

Our experiments yielded a number of insights that shed light on the nature of the reaction examined. First, abiotic nitrite oxidation by Mn(III)-PP yielded an average inverse nitrogen isotope effect ($^{15}\varepsilon_{NO2ox,MnIII}$) of -19.9 ± 0.7‰ across all experiments. No significant differences in this N isotope effect were observed between experiments, indicating that both pH ($p = 0.59$) and O_2 ($p = 0.28$) did not influence N isotopic fractionation. While inverse isotope effects are not commonly observed, it is notable that biological nitrite oxidation has also been shown to exhibit this same dynamic. In a study of *Nitrococcus mobilis*, Casciotti (2009) first demonstrated this isotope behavior, suggesting that the lower zero point energy for the transition state of the ^{14}N isotopologue over the ^{15}N isotopologue for the N-O bond forming reaction favored the net transition of ^{15}N into the product pool – thereby yielding a unique ^{15}N depletion of the reactant nitrite pool over the course of the reaction. A similar dynamic has been demonstrated with anaerobic NO_2^- oxidation by anammox bacteria (Brunner et al., 2013; Kobayashi et al., 2019). This inverse isotope effect has since been invoked to explain large differences in $\delta^{15}N$ of NO_2^- and NO_3^- in oxygen deficient zones of the oceans (up to ~40‰) (Casciotti and McIlvin, 2007; Gaye et al., 2013; Bourbonnais et al., 2015; Peters et al., 2018), and in ocean sediment porewaters reported as high as 54‰ (Buchwald et al., 2018). Thus, the nitrogen isotope signature imparted by abiotic Mn-catalyzed oxidation of NO_2^- to NO_3^- appears similar in direction and magnitude to biological nitrite oxidation. Our study falls within the range of reported biological isotope effects for nitrite

oxidation (-12.8‰ to -45.3‰) (Casciotti, 2009; Kobayashi et al., 2019) with differences in magnitude likely resulting from differences in bond strengths in transition states.

Second, our results also indicate no significant variation in the observed values of $^{15}\varepsilon_{NO2ox,MnIII}$, despite substantial differences in reaction rates among experimental conditions. Additionally, our evaluation of whether the unique inverse isotope effect might be explained by chemically catalyzed isotopic equilibrium between NO_2^- and NO_3^- confirmed that no backwards isotopic transfer occurred during the reaction. Had any sort of nitrogen isotope equilibrium occurred during the reaction, in-growth of ^{15}N from labeled NO_3^- (added prior to experimental initiation) back into the reactant nitrite pool would have impacted the observed kinetic isotope effect. As such, our results suggest that the reaction proceeds in a single, irreversible step.

Third, no changes in reaction rate ($p = 0.74$) or $^{15}\varepsilon_{NO2ox,MnIII}$ ($p = 0.28$) were observed whether the reaction occurred under oxygen-saturated or oxygen-depleted (N_2-sparged) conditions, illustrating that the oxidation of nitrite to nitrate by Mn(III)-pyrophosphate is effectively agnostic to oxygen and occurs under hypoxic conditions. A similar observation was also previously reported during soil incubations of soils and synthetic Mn oxides, in which no differences in reaction extent or stoichiometry were observed between vessels open to air and those purged with N_2 or CO_2 (Bartlett, 1981).

The $\delta^{18}O$ of the product nitrate derives from both reactant nitrite and the addition of a third O atom. Our experiments conducted in ^{18}O-labeled water reveal the origin of this O atom – clearly deriving from water. By pre-equilibrating reactant NO_2^- with waters having different $\delta^{18}O$ compositions, we observed a near 1:1 relationship between the experimental waters and the newly added oxygen (Figure 4). Luther and Popp (2002) postulated that this additional O atom might derive from Mn oxide, due to balancing of loss of two protons in the reaction. Although the formation of Mn oxide particles was not observed in our study, transient formation of Mn oxides via Mn(III) disproportionation is possible. However, if Mn-bound oxygen (or even O_2) had been the source of the third oxygen atom, then the regression of $\delta^{18}O_{H2O}$ vs. $\delta^{18}O_{NO3}$ (Figure 4) would yield a slope of ~0.66, as the contribution of the third additional O atom would have the same $\delta^{18}O$ value in all treatments (while the other two atoms from NO_2^- were in equilibrium with water). In all cases, the

near 1:1 slope unequivocally reflects incorporation of O atoms from water during formation of nitrate.

In contrast to the behavior of N isotopes in this system, nitrite O isotopes quickly equilibrate with the ambient water oxygen isotopes at the pH of our experiments (Casciotti et al., 2007; Buchwald and Casciotti, 2013). Resulting from this rapid oxygen isotope equilibration of NO_2^- with ambient H_2O at our experimental pH conditions, no differences between starting and ending $\delta^{18}O$ of NO_2^- were observed. This complete oxygen isotope equilibration between nitrite and water allows us to determine the isotope effect associated with the incorporation of hydration shell water-oxygen into nitrate. Following derivations by Buchwald and Casciotti (2010), we calculate an overall kinetic isotope effect for incorporation of O from water $^{18}\varepsilon_{k,H2O}$ = +20.3±1.5‰. As with the inverse N isotope effect, the isotope effect associated with incorporation of an O atom from water during Mn(III)-induced nitrite oxidation to nitrate is also analogous to the comparable isotope effect observed in nitrite oxidizing bacteria of +12.8 to +18.2‰ (Buchwald and Casciotti, 2010; Hollocher, 1984). Thus, abiotic NO_2^- oxidation by Mn(III) could conceivably operate in parallel to biological nitrite oxidation with no impact on the expected isotope dynamics of reactant NO_2^- or product NO_3^-.

2.4.4 Coupling of Mn and N cycling in the environment

Despite the favorable thermodynamic conditions for reactions coupling Mn and N transformations, and the commonly overlapping zonation of Mn and N species in redox transition regimes, direct evidence for the occurrence of these reactions in the environment remains limited. Coupled redox reactions between N and Mn species have been proposed by a number of previous studies using a range of approaches (Luther et al., 1997; Hulth et al., 1999; Anschutz et al., 2000; Thamdrup and Dalsgaard, 2000; Luther and Popp, 2002; Mortimer et al., 2004; Lin and Taillefert, 2014; Aigle et al., 2017). Notably, Luther and colleagues (Luther et al., 1997; Luther 2010; Luther et al., 2018) highlighted the thermodynamic favorability of reactions between Mn and N over a range of environmentally relevant conditions. Indeed, these thermodynamically favorable reactions have justified the search for microbial mediation of coupled Mn/N reactions. Studies of soils, freshwater lakes, marine sediments and even wastewater treatment operations have variably reported either the presence or absence of evidence for redox interactions of Mn and N (Dhakar and Burdige,

1996; Luther et al., 1997; Hulth et al., 1999; Anschutz et al., 2000; Thamdrup and Dalsgaard, 2000; Mortimer et al., 2002; Bartlett et al., 2007; Taillefert, 2014; Fernandes et al., 2015; Heil et al., 2015; Lin and Swathi et al., 2017). Nevertheless, while the apparent energetic yields of many Mn/N redox couples would appear to easily support microbial metabolisms, little evidence exists implicating any direct involvement in support of metabolic energy conservation.

Our data provide some intriguing insight into possible environmental links, specifically that soluble Mn(III)-ligands may readily oxidize NO_2^- to NO_3^- – an abiotic analog of the second step in bacterial nitrification – without the notable requirement of molecular oxygen. Indeed, several studies have concluded that so-called 'anoxic nitrification' may be important in marine and estuarine sediments (Luther et al., 1997; Hulth et al., 1999; Anschutz et al., 2000; Mortimer et al., 2002; Mortimer et al., 2004; Bartlett et al., 2008), with at least one study providing evidence for Mn-linked abiotic nitrification in soils (Bartlett, 1981). If important, anoxic nitrification could provide an important link and N loss term without a requirement of molecular oxygen. Most N loss (as N_2) in soils and aquatic sediments is attributed to denitrification or anaerobic ammonium oxidation (anammox), both proceeding under low O_2 conditions and requiring oxidized forms of N as electron acceptors (e.g., NO_3^- or NO_2^-). In general, production and delivery of these electron acceptors is linked to the activity of aerobic nitrifying organisms. Hence, a process by which N is oxidized in the absence of molecular oxygen could represent an important shunt in the N cycle.

A number of previous studies have highlighted the apparent occurrence of oxidative nitrogen cycling under anoxic conditions – with associated implications for involvement of Mn (Luther et al., 1997; Lin and Taillefert, 2014). For example, several studies examining highly resolved porewater profiles noted accumulation of NO_3^- at depths below what would be expected from diffusion alone, speculating that Mn oxides must play a role as environmental oxidant of reduced N in the absence of dissolved oxygen (Anschutz et al., 2000; Mortimer et al., 2004; Hulth et al., 2005; Bartlett et al., 2008). Other studies have used experimental amendments in sediment incubations of marine sediments – specifically, looking for responses of systemic nitrogen cycling to increased availability of Mn oxides – mostly focused on reactivity of solid phase Mn (III/IV) oxides (Bartlett et al., 2007; Lin and Taillefert, 2014). Accumulation of NO_3^- and/or NO_2^- has been reported from anoxic lab incubations of Mn-rich surface sediments and sediments amended with

various Mn oxides (Hulth et al., 1999; Bartlett et al., 2007). While it was suggested that differences in Mn mineral structure (e.g., phase, defects, composition, see Luther et al., 2018) could underlie variability among different environmental systems in results, it is unclear whether products of Mn reduction, which could include Mn(III)-ligand bound forms, may have played a role in the observed dynamics.

Interestingly, evidence for the oxidative 'recycling' of NO_2^- back to NO_3^- in low oxygen systems has been mounting, in both marine and terrestrial systems (Casciotti, 2016; Granger and Wankel, 2016). In low oxygen marine systems, including oxygen deficient zones (ODZs) and porewaters, nitrate N and O isotope data have consistently required substantial re-oxidative fluxes of NO_2^- to NO_3^-, albeit under low O_2 conditions (Sigman et al., 2005; Casciotti and McIlvin, 2007; Gaye et al., 2013; Buchwald et al., 2018). The mechanism of this apparently large back-flux has remained enigmatic. Intriguingly, ^{15}N-label rate measurements of nitrite oxidation in these systems have also indicated nitrite oxidation under very low O_2 (Füssel et al., 2012; Beman et al., 2013; Sun et al., 2017; Babbin et al., in press), although some preservation approaches may induce potential artifacts (Ostrom et al., 2016). In parallel to these observational studies, multi-process multi-isotope modeling studies have also consistently concluded that substantial conversion of NO_2^- to NO_3^- under anoxic conditions is needed to explain dynamics observed in redox transition zones of ODZs, marine porewaters and groundwater (Casciotti, 2016; Granger and Wankel, 2016; Buchwald et al., 2018;). While our data cannot directly implicate the occurrence of abiotic N transformations in the environment, it is intriguing to consider the possible role of Mn(III)-L in driving some of this purported NO_2^- oxidation under low oxygen conditions. In freshwater systems, where pH is often <7 and levels of dissolved metals are elevated, a possible role for Mn-based NO_2^- oxidation seems particularly feasible. In the absence of O_2, this mechanism provides an abiotic avenue for active NO_2^- reoxidation – promoting coupled biotic/abiotic cycling between NO_3^- and NO_2^- as suggested by modeling studies (Granger and Wankel, 2016). Reports of anoxic nitrification in soils and sediments may also reflect such a unique biotic/abiotic coupling. In comparison, marine redox transition zones exhibit higher pH and lower levels of dissolved metals (Landing and Bruland, 1987; Lewis and Landing, 1991; Lewis and Luther, 2000; Nameroff et al., 2002; Moffett et al., 2007; Kondo and Moffett, 2015). Under these conditions, oxidation of NO_2^- by Mn(III)-L is likely to be much slower. Speciation of Mn (including Mn(III)) in oxygen deficient

zones (ODZs) has not been widely examined, with only a few studies examining coincident N cycling features. Notably, Mn(III) was implicated as a controlling factor in fluxes of phosphorus within the redoxcline of the Black Sea through formation of Mn(III)-pyrophosphate complexes with proposed concentrations of ca. 50 nM within the suboxic zone (Dijkstra et al., 2018). Additionally Trouwborst et al. (2006) reported Mn(III)-L concentrations in the Black Sea up to 5 μM. Interestingly, reported maxima in dissolved Mn in the Arabian Sea ODZ were always highly correlated with secondary nitrite maxima (Lewis and Luther, 2000) – a zone coinciding with active NO_2^- turnover in the absence of oxygen (Füssel et al., 2012; Beman et al., 2013; Sun et al., 2017). Future examination of such interactions seems duly warranted.

2.5 Summary

We demonstrate that a Mn(III)-L complex can facilitate abiotic NO_2^- oxidation under a wide range of environment conditions relevant to freshwater, marine, and sedimentary environments. We characterized the kinetics and N- and O- stable isotope systematics of Mn(III)-PP reaction with nitrite. The overall reaction is second order with respect to Mn(III)-PP, and first order with respect to both nitrite and H^+. An inverse nitrogen isotope effect of -19.9 ± 0.7‰ was observed between the product nitrate and the reactant nitrite. While inverse isotope effects such as the one we measured here are not common in kinetically-controlled reactions, it is similar in direction and magnitude to its biological analog in nitrification. The overall similarity in reaction rates and stable isotope effects of nitrite oxidation by Mn(III)-L complexes and by biologically-mediated nitrification demands further consideration of the relative importance of abiotic processes involving Mn(III)-L complexes in local nitrogen cycling.

Intriguingly, Mn(III)-PP oxidation of NO_2^- is insensitive to oxygen concentration, raising the possibility of an abiotic analog to nitrification under oxygen-poor conditions. Although Mn has long been implicated as an important player in suboxic and anoxic redox transformations, the consideration of Mn(III)-L complexes offers an additional avenue of inquiry that provides a greater mechanistic understanding for N-redox cycling in functionally anoxic environments and environments in which redox gradients facilitate interactions between Mn- and N- species of intermediate valence. Although Mn(III)-L complexes are widespread in natural waters, there is very little known about the diversity of Mn-binding ligands, including their composition, origin,

and binding strength. These are all critical factors in ultimately determining the environmental conditions under which Mn(III)-L complexes facilitate N redox reactions. In any case, interactions between Mn(III)-L complexes and nitrite are a potentially critical missing link in understanding local nitrogen budgets, the ultimate fate of these two important electron acceptors, and the energetic limits of life in the absence of oxygen.

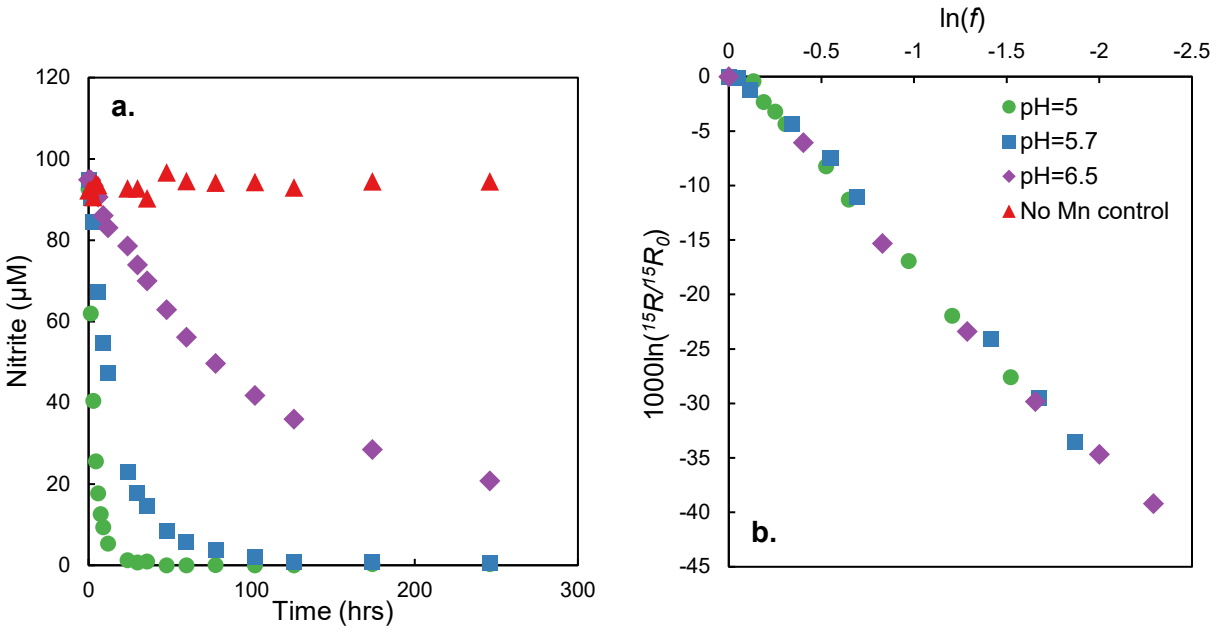

Figure 1. Nitrite concentration (a.) and closed-system Rayleigh distillation of δ^{15}N-NO_2^- (b.) over the course of a timeseries experiment. Data points represent the average of four replicates with standard deviations smaller than the points. Higher pH treatments reacted more slowly and no measureable change in nitrite was observed in a no Mn addition control. Slope of ln([NO_2^-]) vs. ln(^{15}R) was used to calculate $^{15}\varepsilon_{NXR,MnIII,}$ but are plotted here as ln(f) vs. 1000ln($^{15}R/^{15}R_0$).

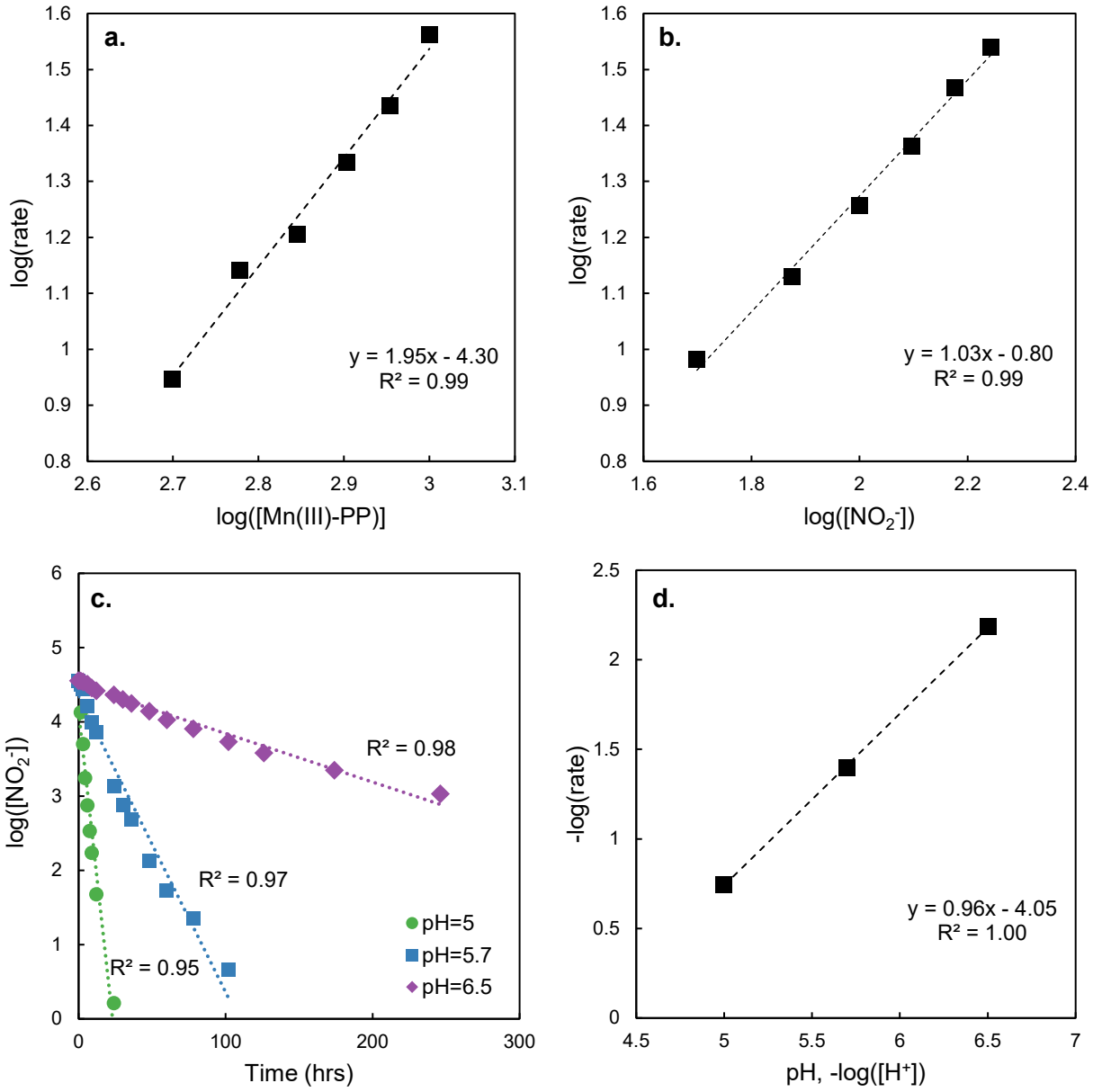

Figure 2. Log(rate) vs. log([Mn(III)-PP] (a.), log([NO_2^-]) (b.), and –log([H^+]) (d.). Slope of linear regression represents the order of reaction with respect to that reactant, thus the reaction is second order in Mn(III)-PP and first order in NO_2^- and H^+.

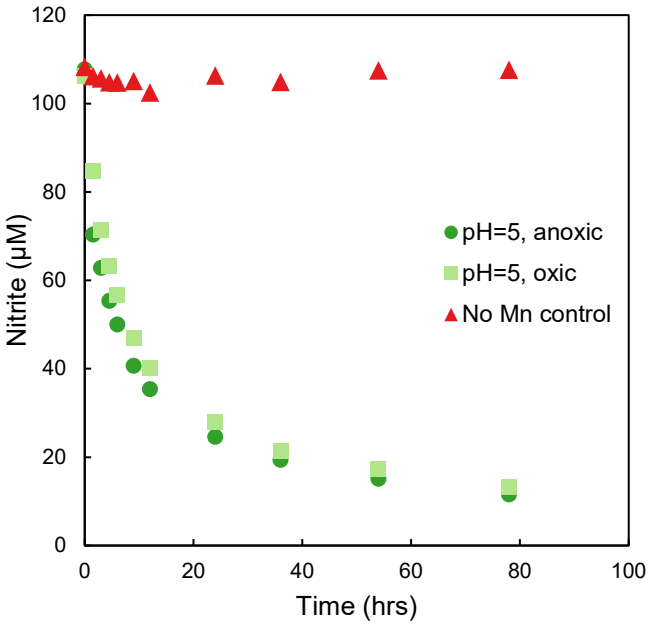

Figure 3. Time course of nitrite concentration at pH=5. No significant difference in rate was observed between air and N_2-purged headspace treatments. A control treatment with no Mn addition showed no significant decrease in nitrite.

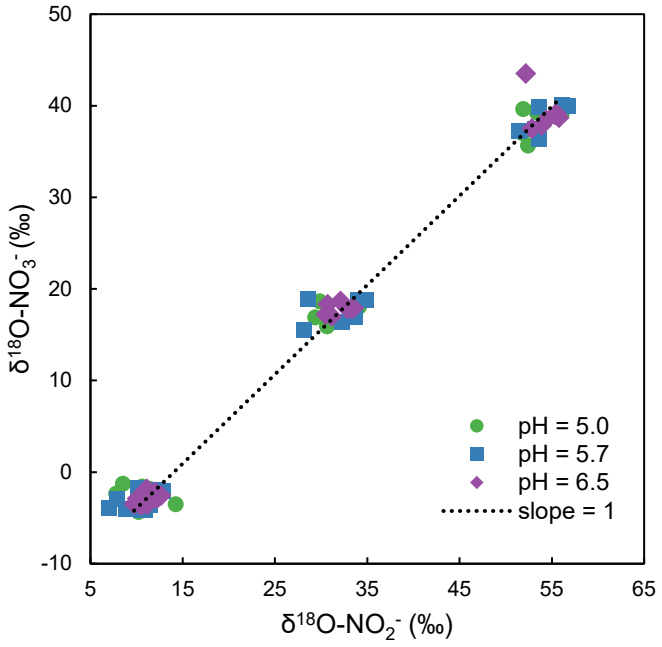

Figure 4. $\delta^{18}O\text{-}NO_3^-$ produced from NO_2^- equilibrated with different ^{18}O-labeled H_2O samples. Slopes of best-fit lines were indistinguishable from a 1:1 line for all three pH treatments. Intercepts of the linear regressions were used to calculate $^{18}\varepsilon_{k,H2O}$, as shown in Table 3.

Table 1: Summary of isotope effects for nitrite oxidation by Mn(III)-PP ($^{15}\varepsilon_{NXR,MnIII}$).

pH	Mn(III)-PP (μM)	NO_2^- (μM)	Headspace	$^{15}NO_3^-$ (μM)	$^{15}\varepsilon_{NXR,\ Mn(III)}$ (‰)		
5.0	1000	100	Air	–	−19.1	±	0.5
5.7	1000	100	Air	–	−18.2	±	0.4
5.0	1000	100	Air	–	−20.3	±	0.3
5.0	900	100	Air	–	−20.2	±	0.3
5.0	800	100	Air	–	−19.9	±	0.3
5.0	700	100	Air	–	−20.1	±	0.4
5.0	600	100	Air	–	−20.1	±	0.4
5.0	500	100	Air	–	−19.6	±	0.5
5.0	1000	50	Air	–	−19.8	±	0.3
5.0	1000	75	Air	–	−20.6	±	0.2
5.0	1000	100	Air	–	−19.6	±	0.5
5.0	1000	125	Air	–	−19.9	±	0.2
5.0	1000	150	Air	–	−20.2	±	0.2
5.0	1000	175	Air	–	−19.9	±	0.2
5.0	1000	100	N_2-purged	–	−19.8	±	0.3
5.0	1000	100	Air	–	−20.1	±	0.1
5.0	1000	100	Air	10	−19.6	±	0.6
5.0	1000	100	Air	100	−19.4	±	0.3
5.7	1000	100	Air	10	−19.2	±	0.4
5.7	1000	100	Air	100	−20.5	±	0.2

Table 2: Rates of nitrite oxidation and rate constants, pH = 5.0–8.0.

	Nitrite oxidation rate			Rate constant (k_{pH})		
pH	μM d^{-1}			$\mu M^{-2}\ hr^{-1}$		
5.0	518.4	±	16.8	2.16E−07	±	7.00E−09
5.7	108	±	4.8	4.50E−08	±	2.00E−09
6.5	21.6	±	2.4	9.00E−09	±	1.00E−09
7.0	5.8	±	1.3	2.40E−11	±	5.38E−10
8.0	3.9	±	0.6	1.62E−11	±	2.33E−10

Table 3: Results from ^{18}O-labeled water experiments.

pH	$\delta^{18}O$-H_2O (‰)	Headspace	Slope $\delta^{18}O$ (NO_2^- vs NO_3^-)	Intercept $^{18}\varepsilon_{k,H2O}$ (‰)
5.0	−5	Air	0.95 ± 0.03 ($r^2 = 0.988$)	+20.5 ± 0.8
5.0	18	Air		
5.0	40	Air		
5.0	−5	N_2-purged		
5.7	−5	Air	0.94 ± 0.02 ($r^2 = 0.991$)	+20.2 ± 0.8
5.7	18	Air		
5.7	40	Air		
5.7	−5	N_2-purged		
6.5	−5	Air	0.97 ± 0.03 ($r^2 = 0.992$)	+22.5 ± 0.4
6.5	18	Air		
6.5	40	Air		
6.5	−5	N_2-purged		

Table 4: Theoretical rates of nitrite oxidation under environmentally relevant conditions.

pH	[Mn(III)PP] μM	$[NO_2^-]$ μM	Oxidation Rate nM d^{-1}
6.0	10	10	0.6
6.0	50	10	14.2
6.0	100	10	56.9
6.5	10	10	0.2
6.5	50	10	5.4
6.5	100	10	21.6
7.0	10	10	5.8E−04
7.0	50	10	1.4E−02
7.0	100	10	5.8E−02

References

Aigle, A., Bonin, P., Iobbi-Nivol, C., Mejean, V. and Michotey, V. (2017) Physiological and transcriptional approaches reveal connection between nitrogen and manganese cycles in Shewanella algae C6G3. Scientific Reports 7, 44725.

Anschutz, P., Sundby, B., Lefrancois, L., Luther, G.W., III and Mucci, A. (2000) Interactions between metal oxides and species of nitrogen and iodine in bioturbated marine sediments. Geochimica et Cosmochimica Acta 64, 2751-2763.

Babbin, A.R., Buchwald, C., Morel, F.M.M., Wankel, S.D. and Ward, B.B. (2020) Nitrite oxidation exceeds reduction and fixed nitrogen loss in anoxic Pacific waters. Marine Chemistry 224.

Bartlett, R., Mortimer, R.J. and Morris, K.M. (2007) The biogeochemistry of a manganese-rich Scottish sea loch: Implications for the study of anoxic nitrification. Continental Shelf Research 27, 1501-1509.

Bartlett, R., Mortimer, R.J.G. and Morris, K. (2008) Anoxic nitrification: Evidence from Humber Estuary sediments (UK). Chemical Geology 250, 29-39.

Bartlett, R.J. (1981) Nonmicrobial nitrite-to-nitrate transformation in soils. Soil Science Society of America Journal 45, 1054-1058.

Beman, J.M., Shih, J.L. and Popp, B.N. (2013) Nitrite oxidation in the upper water column and oxygen minimum zone of the eastern tropical North Pacific Ocean. The ISME Journal 7, 2192-2205.

Bianchi, M., Feliatra, F., Treguer, P., Vincendeau, M.-A. and Morvan, J. (1997) Nitrification rates, ammonium and nitrate distribution in upper layer of the water column and in sediments of the Inidian sector of the Southern Ocean. Deep Sea Research Part II 44, 1017-1032.

Bourbonnais, A., Altabet, M.A., Charoenpong, C., Larkum, J., Hu, H., Bange, H.W. and Stramma, L. (2015) N-loss isotope effects in the Peru oxygen minimum zone studied using a mesoscale eddy as a natural tracer experiment. Global Biogeochemical Cycles 29, 793-811.

Braman, R.S. and Hendrix, S.A. (1989) Nanogram nitrite and nitrate determination in environmental and biological materials by vanadium (III) reduction with chemiluminescence detection. Analytical Chemistry 61, 2715-2718.

Brand, W.A., Coplen, T.B., Aerts-Bijma, A.T., Böhlke, J.K., Gehre, M., Geilmann, H., Gröning, M., Jansen, H.G., Meijer, H.A.J., Mroczkowski, S.J., Qi, H., Soergel, K., Stuart-Williams, H., Weise, S.M. and Werner, R.A. (2009) Comprehensive inter-laboratory calibration of reference materials for $\delta^{18}O$ versus VSMOW using various on-line high-temperature conversion techniques. Rapid Communications in Mass Spectrometry 23, 999-1019.

Bristow, L.A., Dalsgaard, T., Tiano, L., Mills, D.B., Baertagnolli, A.D., Wright, J.J., Hallam, S.J., Ulloa, O., Canfield, D.E., Revsbech, N.P. and Thamdrup, B. (2016) Ammonium and nitrite oxidation at nanomolar oxygen concentrations in oxygen minimum zone waters. Proceedings of the National Academy of Sciences 113, 10601-10606.

Brunner, B., Contreras, S., Lehmann, M.F., Matantseva, O., Rollog, M., Kalvelage, T., Klock, G., Lavik, G., Jetten, M.S.M., Kartal, B. and Kuypers, M.M. (2013) Nitrogen isotope effects induced by anammox bacteria. Proceedings of the National Academy of Sciences 110, 18994-18999.

Buchwald, C. and Casciotti, K.L. (2010) Oxygen isotopic fractionation and exchange during bacterial nitrite oxidation. Limnology and Oceanography 55, 1064-1074.

Buchwald, C. and Casciotti, K.L. (2013) Isotopic ratios of nitrite as tracers of the sources and age of oceanic nitrite. Nature Geoscience 6, 309-313.

Buchwald, C., Grabb, K.C., Hansel, C.M. and Wankel, S.D. (2016) Constraining the role of iron in environmental nitrogen transformations: Dual stable isotope systematics of abiotic NO_2^- reduction by Fe(II) and its production of N_2O. Geochimica et Cosmochimica Acta 186, 1-12.
Buchwald, C., Homola, K., Spivack, A.J., Estes, E.R., Murray, R.W. and Wankel, S.D. (2018) Isotopic constraints on nitrogen transformation rates in the deep sedimentary marine biosphere. Global Biogeochemical Cycles 32, 1688-1702.
Burgin, A.J., Yang, W.H., Hamilton, S.K. and Silver, W.L. (2011) Beyond carbon and nitrogen: how the microbial energy economy couples elemental cycles in diverse ecosystems. Frontiers in Ecology and Environment 9, 44-52.
Casciotti, K.L. (2009) Inverse kinetic isotope fractionation during bacterial nitrite oxidation. Geochimica et Cosmochimica Acta 73, 2061-2076.
Casciotti, K.L. (2016) Nitrogen and Oxygen Isotopic Studies of the Marine Nitrogen Cycle. Annual Review of Marine Science 8, 379-407.
Casciotti, K.L., Böhlke, J.K., McIlvin, M., Mroczkowski, S. and Hannon, J. (2007) Oxygen isotopes in nitrite: Analysis, calibration and equilibration. Analytical Chemistry 79, 2427-2436.
Casciotti, K.L., Buchwald, C., Santoro, A.E. and Frame, C. (2011) Assessment of Nitrogen and Oxygen Isotopic Fractionation During Nitrification and Its Expression in the Marine Environment, Methods in Enzymology. Elsevier.
Casciotti, K.L. and McIlvin, M.R. (2007) Isotopic analyses of nitrate and nitrite from reference mixtures and application to Eastern Tropical North Pacific waters. Marine Chemistry 107, 184-201.
Casciotti, K.L., Sigman, D.M., Galanter-Hastings, M., Böhlke, J.K. and Hilkert, A. (2002) Measurement of the oxygen isotopic composition of nitrate in seawater and freshwater using the denitrifier method. Analytical Chemistry 74, 4905-4912.
Cavazos, A.R., Taillefert, M., Tang, Y. and Glass, J.B. (2018) Kinetics of nitrous oxide production from hydroxylamine oxidation by birnessite. Marine Chemistry 202, 49-57.
Dalsgaard, T., Thamdrup, B. and Canfield, D.E. (2005) Anaerobic ammonium oxidation (anammox) in the marine environment. Research in Microbiology 156, 457-464.
Dhakar, S.P. and Burdige, D.J. (1996) A coupled, non-linear, steady-state model for early diagenesis processes in pelagic sediments. American Journal of Science 296, 296-330.
Dijkstra, N., Krall, P., Seguret, M., Flores, M., Gonzalez, S., Rijkenberg, M. and Slomp, C.P. (2018) Phosphorus dynamics in and below the redoxcline in the Black Sea and implications for phosphorus burial. Geochimica et Cosmochimica Acta 222, 685-703.
Doane, T.A. (2017) The Abiotic Nitrogen Cycle. Earth and Space Chemistry 1, 411-421.
Dore, J.E. and Karl, D.M. (1996) Nitrification in the euphotic zone as a source of nitrite, nitrate, and nitrous oxide at Station ALOHA. Limnology and Oceanography 41, 1619-1628.
Fernandes, S.O., Javanaud, C., Aigle, A., Michotey, V.D., Guasco, S., Deborde, J., Deflandre, B., Anschutz, P. and Bonin, P. (2015) Anaerobic nitrification-denitrification mediated by Mn-oxides in meso-tidal sediments: Implications for N_2 and N_2O production. Journal of Marine Systems 144, 1-8.
Füssel, J., Lam, P., Lavik, G., Jensen, M.M., Holtappels, M., Günter, M. and Kuypers, M.M. (2012) Nitrite oxidation in the Namibiam oxygen minimum zone. The ISME Journal 6, 1200-1209.

Gaye, B., Nagel, B., Dähnke, K., Rixen, T. and Emeis, K.-C. (2013) Evidence of parallel denitrification and nitrite oxidation in the ODZs of the Arabian Sea from paired stable isotopes of nitrate and nitrite. Global Biogeochemical Cycles 27, 1059-1071.

Grabb, K.C., Buchwald, C., Hansel, C.M. and Wankel, S.D. (2017) A dual isotopic investigation of chemodenitrification by mineral-associated Fe(II) and its production of nitrous oxide. Geochimica et Cosmochimica Acta 196, 388-402.

Granger, J. and Sigman, D.M. (2009) Removal of nitrite with sulfamic acid for nitrate N and O isotope analysis with the denitrifier method. Rapid Communications in Mass Spectrometry 23, 3753-3762.

Granger, J. and Wankel, S.D. (2016) Isotopic overprinting of nitrification on denitrification as a ubiquitous and unifying feature of environmental nitrogen cycling. Proceedings of the National Academy of Sciences of the United States of America 113, E6391-E6400.

Gruber, N. and Galloway, J.N. (2008) An Earth-system perspective of the global nitrogen cycle. Nature 451, 293-296.

Heil, J., Liu, S., Verecken, H. and Brüggeman, N. (2015) Abiotic nitrous oxide production from hydroxylamine in soils and their dependence on soil properties. Siol Biology and Biochemistry 84, 107-115.

Heil, J., Verecken, H. and Brüggeman, N. (2016) A review of chemical reactions of nitrification intermediates and their role in nitrogen cycling and nitrogen trace gas formation in soil. European Journal of Soil Science 67, 23-39.

Heiss, E.M. and Fulweiler, R.W. (2016) Coastal water column ammonium and nitrite oxidation are decoupled in summer. Estuarine, Coastal and Shelf Science 178, 110-119.

Hollocher, T.C. (1984) Source of the Oxygen Atoms of Nitrate in the Oxidation of Nitrite by *Nitrobacter agilis* and Evidence against a P-O-N Anhydride Mechanism in Oxidative Phosphorylation. Archives of Biochemistry and Biophysics 233, 721-727.

Hulth, S., Aller, R.C., Canfield, D.E., Dalsgaard, T., Engström, P., Gilbert, F., Sundbäck, K. and Thamdrup, B. (2005) Nitrogen removal in marine environments: Recent findings and future research challenges. Marine Chemistry 94, 125-145.

Hulth, S., Aller, R.C. and Gilbert, F. (1999) Coupled anoxic nitrification/manganese reduction in marine sediments. Geochimica et Cosmochimica Acta 63, 49-66.

Jetten, M.S., Strous, M., van de Pas-Schoonen, K.T., Schalk, J., van Dongen, U.G., van de Graaf, A.A., Logemann, S., Muyzer, G., van Loosdrecht, M.C. and Kuenen, J.G. (1999) The anaerobic oxidation of ammonium. FEMS Microbiology Reviews 22, 421-437.

Jones, M.R., Luther, G.W., Mucci, A. and Tebo, B.M. (2019) Concentrations of reactive Mn(III)-L and MnO2 in estuarine and marine waters determined using spectrophotometry and the leuco base, leucoberbelin blue. Talanta 200, 91-99.

Kartal, B., Maalcke, W.J., de Almeida, N.M., Cirpus, I., Gloerich, J., Geerts, W., op den Camp, H.J., Harhangi, H.R., Janssen-Megens, E.M., Francoijs, K.-J., Stunnenberg, H.G., Keltjens, J.T., Jetten, M.S. and Strous, M. (2011) Molecular mechanims of anaerobic ammonium oxidation. Nature 479, 127-130.

Kendall, C., Elliott, E.M. and Wankel, S.D. (2007) Tracing anthropogenic inputs of nitrogen to ecosystems, in: Michener, R.H., Lajtha, K. (Eds.), Stable isotopes in ecology and environmental science, 2nd ed. Blackwell Publishing, p. 592.

Kobayashi, K., Makabe, A., Yano, M., Oshiki, M., Kindaichi, T., Casciotti, K.L. and Okabe, S. (2019) Dual nitrogen and oxygen isotope fractionation during anaerobic ammonium oxidation by anammox bacteria The ISME Journal.

Kondo, Y. and Moffett, J.W. (2015) Iron redox cycling and subsurface offshore transport in the eastern tropical South Pacific oxygen minimum zone. Marine Chemistry 168, 95-103.
Kostka, J.E., Luther, G.W., III and Nealson, K.H. (1995) Chemical and biological reduction of Mn(III)-pyrophosphate complexes: Potential importance of dissolved Mn(III) as an environmental oxidant. Geochimica et Cosmochimica Acta 59, 885-894.
Krumbein, W.E. and Altman, H.J. (1973) A new method for detection and enumeration of manganese-oxidizing and -reducing microorganisms. Helgol. Wiss. Meeresunters 25, 347-356.
Kuypers, M.M.M., Sliekers, A.O., Lavik, G., Schmid, M., Jorgensen, B.B., Kuenen, J.G., Damste, J.S.S., Strous, M. and Jetten, M.S.M. (2003) Anaerobic ammonium oxidation by anammox bacteria in the Black Sea. Nature 422, 608-610.
Lam, P., Jensen, M.M., Lavik, G., McGinnis, D.F., Muller, B., Schubert, C.J., Amann, R., Thamdrup, B. and Kuypers, M.M.M. (2007) Linking crenarchaeal and bacterial nitrification to anammox in the Black Sea. Proceedings of the National Academy of Sciences of the United States of America 104, 7104-7109.
Landing, W.M. and Bruland, K.W. (1987) The contrasting biogeochemistry of iron and manganese in the Pacific Ocean. Geochimica et Cosmochimica Acta 51, 29-43.
Lewis, B.L. and Landing, W.M. (1991) The biogeochemistry of manganese and iron in the Black Sea. Deep Sea Research Part A - Oceanographic Research Papers 38, S773-S803.
Lewis, B.L. and Luther, G.W., III (2000) Processes controlling the distribution and cycling of manganese in the oxygen minimum zone of the Arabian Sea. Deep Sea Research Part II 47, 1541-1561.
Lin, H. and Taillefert, M. (2014) Key geochemical factors regulating Mn(IV)-catalyzed anaerobic nitrification in coastal sediments. Geochimica et Cosmochimica Acta 133, 17-33.
Lupschultz, F., Wofsy, S.C., Ward, B.B., Codispoti, L.A., Friedrich, G. and Elkins, J. (1990) Bacterial transformations of inorganic nitrogen in the oxygen-deficient waters of the Eastern Tropical South Pacific Ocean. Deep-Sea Research 37, 1513-1541.
Luther, G.W., III and Popp, J.I. (2002) Kinetics of the abiotic reduction of polymeric manganese dioxide by nitrite: An anaerobic nitrification reaction. Aquatic Geochemistry 8, 15-36.
Luther, G.W., III, Sundby, B., Lewis, B.L., Brendel, P.J. and Silverberg, N. (1997) Interactions of manganese with the nitrogen cycle: Alternative pathways to dinitrogen. Geochimica et Cosmochimica Acta 61, 4043-4052.
Luther III, G.W. (2010) The role of one- and two-electron transfer reactions in forming thermodynamically unstable intermediates as barriers in multi-electron redox reactions. Aquat. Geochem. 16, 395-420.
Luther, G.W., Thibault de Chanvalon, A., Oldham, V.E., Estes, E.R., Tebo, B.M. and Madison, A.S. (2018) Reduction of Manganese Oxides: Thermodynamic, Kinetic and Mechanistic Considerations for One- Versus Two-Electron Transfer Steps. Aquat. Geochem. 24, 257-277.
Madison, A.S., Tebo, B.M. and Luther III, G.W. (2011) Simultaneous determination of soluble manganse(III), manganese(II) and total manganese in natural (pore)waters. Talanta 84, 374-381.
Madison, A.S., Tebo, B.M., Mucci, A., Sundby, B. and Luther, G.W., III (2013) Abundant porewater Mn(III) is a major component of the sedimentary redox system. Science 341, 875-878.

Mandernack, K.W., Fogel, M., L, Tebo, B.M. and Usui, A. (1995) Oxygen isotope analyses of chemically and microbially produced manganese oxides and manganates. Geochimica et Cosmochimica Acta 59, 4409-4425.
Mariotti, A., Germon, J.C., Hubert, P., Kaiser, P., Letolle, R., Tardieux, A. and Tardieux, P. (1981) Experimental determination of nitrogen kinetic isotope fractionation: some principles; illustration for the denitrification and nitrification processes. Plant Soil 62, 413-430.
McIlvin, M. and Altabet, M.A. (2005) Chemical conversion of nitrate and nitrite to nitrous oxide for nitrogen and oxygen isotopic analysis in freshwater and seawater. Analytical Chemistry 77, 5589-5595.
Melton, E.D., Swanner, E.D., Behrens, S., Schmidt, C. and Kappler, A. (2014) The interplay of microbially mediate and abiotic reactions in the biogeochemical Fe cycle. Nature Reviews in Microbiology 12, 797-808.
Moffett, J.W., Goepfert, T.J. and Naqvi, S.W.A. (2007) Reduced iron associated with secondary nitrite maxima in the Arabian Sea. Deep Sea Research Part II 54, 1341-1349.
Moore, T.A., Xing, Y., Lazenby, B., Lynch, M.D., Schiff, S.L., Robertson, W.D., Timlin, R., Lanza, S., Ryan, M.C., Aravena, R., Fortin, D., Clark, I.D. and Neufeld, J.D. (2011) Prevalence of anaerobic ammonium-oxidizing bacteria in contaminated groundwater. Environmental Science & Technology 45, 7217-7225.
Mortimer, R.J., Harris, S.J., Krom, M.D., Freitag, T.E., Prosser, J.I., Barnes, J., Anschutz, P., Hayes, P.J. and Davies, I.M. (2004) Anoxic nitrification in marine sediments. Marine Ecology Progress Series 276, 37-51.
Mortimer, R.J., Krom, M.D., Harris, S.J., Hayes, P.J., Davies, I.M., Davison, W. and Zhang, H. (2002) Evidence for suboxic nitrification in recent marine sediments. Marine Ecology Progress Series 236, 31-35.
Nameroff, T., Balistrieri, L. and Murray, J.W. (2002) Suboxic trace metal geochemistry in the Eastern Tropical North Pacific. Geochimica et Cosmochimica Acta 66, 1139-1158.
Nelson, Y.M., Lion, L.W., Shuler, M.L. and Ghiorse, W.C. (2002) Effect of oxide formation mechanisms on lead adsorption by biogenic manganese (hydr)oxides, iron (hydr)oxides and their mixtures. Environmental Science & Technology 36, 421-425.
Nowka, B., Diams, H. and Spieck, E. (2015) Comparison of oxidation kinetics of nitrite-oxidizing bacteria: Nitrite availability as a key factor in niche differentiation. Applied and Environmental Microbiology 81, 745-753.
Oldham, V.E., Jones, M.R., Tebo, B.M. and Luther, G.W., III (2017a) Oxidative and reductive processes contributing to manganese cycling at oxic-anoxic interfaces. Marine Chemistry 195, 122-128.
Oldham, V.E., Miller, M.T., Jensen, L.T. and Luther, G.W., III (2017b) Revisiting Mn and Fe removal in humic rich estuaries. Geochimica et Cosmochimica Acta 209, 267-283.
Oldham, V.E., Owings, S.M., Johnes, M.R., Tebo, B.M. and Luther, G.W., III (2015) Evidence for the presence of strong Mn(III)-binding ligands in the water column of Chesapeake Bay. Marine Chemistry 171, 58-66.
Ostrom, N.E., Gandhi, H., Trubl, G. and Murray, A.E. (2016) Chemodenitrification in the cryoecosystem of Lake Vida, Victoria Valley, Antarctica. Geobiology 14, 575-587
Pai, S.-C., Yang, C.-C. and Riley, J.P. (1990) Formation kinetics of the pink azo dye in the determination of nitrite in natural waters. Analytica Chimica Acta 232, 345-349.

Peng, Z., Fuchsman, C.A., Jayakumar, A., Oleynik, S., Martens-Habbena, W., Devol, A.H. and Ward, B.B. (2015) Ammonia and nitrite oxidation in the Eastern Tropical North Pacific. Global Biogeochemical Cycles 29, 2034-2049.

Peters, B., Horak, R., Devol, A.H., Fuchsman, C.A., Forbes, M., Mordy, C.W. and Casciotti, K.L. (2018) Estimating fixen nitrogen loss and associated isotope effects using concentration and isotope measurements of NO_3^-, NO_2^-, and N_2 from the Eastern Tropical South Pacific oxygen deficient zone. Deep-Sea Research Part II 156, 121-136.

Post, J. (1999) Manganese oxide minerals: Crystal structures and economic and environmental significance. Proc Natl Acad Sci U S A 96, 3447-3454.

Sigman, D.M., Casciotti, K.L., Andreani, M., Barford, C., Galanter, M. and Böhlke, J.K. (2001) A Bacterial Method for the Nitrogen Isotopic Analysis of Nitrate in Seawater and Freshwater. Analytical Chemistry 73, 4145-4153.

Sigman, D.M., Granger, J., DiFiore, P.J., Lehmann, M.F., Ho, R., Cane, G. and van Geen, A. (2005) Coupled nitrogen and oxygen isotope measurements of nitrate along the eastern North Pacific margin. Global Biogeochemical Cycles 19, GB4022.

Stanton, C.L., Reinhard, C.T., Kasting, J.F., Ostrom, N.E., Haslun, J.A., Lyons, T.W. and Glass, J.B. (2018) Nitrous oxide from chemodenitrification: A possible missing link in the Proterozoic greenhouse and the evolution of the aerobic respiration. Geobiology, 1-13.

Stone, A.T. and Morgan, J.J. (1984) Reduction and dissolution of manganese(III) and manganese(IV) oxides by organics. 2. Survey of the reactivity of organics. Environmental Science & Technology 18, 617-624.

Strous, M., Pelletier, E., Mangenot, S., Rattei, T., Lehner, A., Taylor, M.W., Horn, M., Diams, H., Bartol-Mavel, D., Winkcer, P., Barbe, V., Fonknechten, N., Vallenet, D., Segurens, B., Schenowitz-Truong, C., Medigue, C., Collingro, A., Snel, B., Dutilh, B.E., op den Camp, H.J., van der Drift, C., Cirpus, I., van de Pas-Schoonen, K., Harhangi, H.R., van Niftrik, L.A., Schmid, M., Keltjens, J., van de Vossenberg, J., Kartal, B., Meier, H., Frishman, D., Huynen, M.A., Mewes, H.-W., Weissenbach, J., Jetten, M.S., Wagner, M. and Le Paslier, D. (2006) Deciphering the evolution and metabolism of an anammox bacterium from a community genome. Nature 440, 790-794.

Sun, X., Ji, Q., Jayakumar, A. and Ward, B.B. (2017) Dependence of nitrite oxidation on nitrite and oxygen in low-oxygen seawater. Geophysical Research Letters 44, 7883-7891.

Swathi, D., Sabumon, P. and Maliyekkal, S. (2017) Microbial mediated anoxic nitrification-denitrification in the presence of nanoscale oxides of manganese. International Biodeterioration and Biodegradation 119, 499-510.

Thamdrup, B. and Dalsgaard, T. (2000) The fate of ammonium in anoxic manganese oxide-rich marine sediment. Geochimca et Cosmochimica Acta 64, 4157-4164.

Trouwborst, R.E., Clement, B.G., Tebo, B.M., Glazer, B.T. and Luther, G.W. (2006) Soluble Mn(III) in suboxic zones. Science 313, 1955-1957.

Wankel, S.D., Ziebis, W., Buchwald, C., Charoenpong, C., de Beer, D., Dentinger, J., Xu, Z. and Zengler, K. (2017) Evidence for non-traditional N_2O formation pathways in nitrogen-impacted coastal ecosystems: fungal and chemodentrification. Nature Communications 8, 15595.

Ward, B.B. (2011) Measurement and distribution of nitrification rates in the oceans. Methods in Enzymology 486, 307-323.

Ward, B.B., Kilpatrick, K.A., Renger, E.H. and Eppley, R.W. (1989) Biological nitrogen cycling in the nitracline. Limnology and Oceanography 34, 493-513.

Wilczak, A., Aieta, E., Knocke, W. and Hubel, R. (1993) Manganese control during ozonation of water containing organic compounds. Journal of the American Water Works Association 85, 10.

Yakushev, E., Pakhomova, S., Sorensen, K. and Skei, J. (2009) Importance of the different manganese species in the formation of water column redox zones: observations and modeling. Marine Chemistry 117, 59-70.

Yakushev, E., Pollehne, F., Jost, F., Kuznetsov, I., Schneider, B. and Umlauf, L. (2007) Analysis of the water column oxic/anoxic interface in the Black and Baltic seas with a numerical model. Marine Chemistry 107, 388-410.

Zhu-Barker, X., Cavazos, A.R., Ostrom, N.E., Horwath, W.R. and Glass, J.B. (2015) The importance of abiotic reactions for nitrous oxide production. Biogeochemistry 126, 251-267.

3. Abiotic production of nitrous oxide from hydroxylamine and ligand-bound manganese(III)

Abstract

Nitrous oxide (N_2O) is a potent greenhouse gas whose main source in the ocean has historically been attributed to biological reactions. Here, we report the abiotic reaction of a biologically derived nitrogen cycle intermediate hydroxylamine (NH_2OH) with manganese(III)-pyrophosphate (Mn(III)-PP) which rapidly produces N_2O under environmental conditions. The concentration of N_2O formed following the addition of hydroxylamine (10 μM) to solutions of [Mn(III)-PP] = 5 - 80 μM was quantified. At lower concentrations of Mn(III)-PP, a small amount of nitrite (NO_2^-) was formed in addition to N_2O. Approximately 30-60% of the product remained uncharacterized but is posited to be N_2. The formation of N_2O was found not to be a result from back reaction of product NO_2^- with reactant NH_2OH; in other words, it was not due to the combination of two different nitrogen species or "hybrid" formation. During all experiments, the N_2O site preference (SP) of +35.5 ± 0.6‰ was consistent, and identical to those of N_2O produced by marine nitrifying microorganisms. As NH_2OH is known to leak from nitrifying cells, this suggests that abiotic oxidation of hydroxylamine may be occurring unnoticed in the environment or could be a source of N_2O emissions previously attributed solely to biological nitrification reactions.

3.1 Introduction

Nitrous oxide (N_2O) is a greenhouse gas with 300 times the warming potential of CO_2 over its 100-year lifetime in the atmosphere (Myhre et al. 2014; Prather et al. 2012). Additionally, N_2O is implicated in the destruction of stratospheric ozone and has been predicted to be the dominant ozone-depleting substance of the 21st century (Ravishankara et al. 2009). Nitrous oxide concentrations in the atmosphere have been increasing since the industrial revolution and this increase has begun to accelerate (Park et al. 2012; Thompson et al. 2019). The majority of N_2O flux to the atmosphere originates from terrestrial sources with an estimated ~20% coming from the ocean (Ji et al. 2018).

Traditionally N_2O production in the environment has been attributed to biological processes such as nitrification and denitrification (Freing et al. 2012). In contrast to denitrification, in which N_2O

is an obligate intermediate, nitrification ($NH_3 \rightarrow NO_2^- \rightarrow NO_3^-$) produces N_2O as a by-product through multiple poorly understood pathways (Soler-Jofra et al. 2021). Generally, the first step of nitrification is performed by either ammonia-oxidizing archaea (AOA) or ammonia-oxidizing bacteria (AOB), while only nitrite-oxidizing bacteria (NOB) have been found to complete the second step of nitrification (Ward 2008). Microbes capable of performing complete nitrification (comammox) have also been found in the environment (Daims et al. 2015; van Kessel et al. 2015). While there remain open questions as to the exact process by which N_2O is produced during nitrification, hydroxylamine (NH_2OH) has been found to be a biologically produced intermediate of AOA, AOB, and comammox bacteria (Lee 1952, Liu et al. 2017a, Vajrala et al. 2013) and may be a substrate used to enzymatically produce N_2O in AOB (Caranto et al. 2016).

In recent years, increasing evidence has emerged implicating abiotic processes in N_2O production (Doane 2017; Zhu-Barker et al. 2015). Manganese (Mn) in the form of Mn(III,IV) (oxy)(hydr)oxides (hereinafter Mn oxides) has also been linked to production of N_2O both in laboratory experiments (Toyoda et al. 2005; Cavazos et al. 2018) and in soils (Bremner et al. 1980; Duan et al. 2020; Heil et al. 2015a; Liu et al. 2017b; Liu et al. 2019; Rue et al. 2018). While many of these studies assume Mn is in the form of either soluble Mn(II) or solid Mn oxides, in recent years soluble Mn(III) has been shown to be stabilized by ligands and may in fact represent the dominant Mn species in some environments (Madison et al. 2013; Oldham et al. 2015). Manganese (III) ligand complexes (Mn(III)-L) have been previously shown to oxidize iron (II) and sulfide (Kostka et al. 1995) as well as nitrite (Karolewski et al. 2021). Due to the recent appreciation of their abundance in the environment, however, their reactivity remains widely understudied. In this study, we use manganese(III)-pyrophosphate (Mn(III)-PP) as a model Mn(III) compound due to its stability under a wide variety environmental conditions and similar binding affinity when compared to Mn(III) ligands found in natural waters (Qian et al. 2019).

The potential for mixed biotic/abiotic reactions to produce N_2O has also received increased attention. Of particular note are reports that N_2O production from nitrification in culture studies may in fact be an abiotic reaction between biological intermediates such as NH_2OH and oxidized metals present in media (Kits et al. 2019; Kozlowski et al. 2016; Liu et al. 2017a). In light of the complex mix of linked processes known to produce N_2O in the environment, isotopes of nitrogen

(^{14}N, ^{15}N) and oxygen (^{16}O, ^{18}O) have been successfully utilized to help disentangle different processes as both biotic and abiotic reactions can impart distinct isotopic signatures (Baggs 2008; Casciotti 2016; Ostrom and Ostrom 2017; Yu et al. 2008). Stable isotope labeling studies have also revealed a "hybrid" mechanism for N_2O formation by AOA, wherein one N is derived from NO_2^- and the other from NH_3 (in the form of the intermediate NH_2OH) (Kozlowski et al. 2016; Steiglmeier et al. 2014; Trimmer et al. 2016). Due to the asymmetry of the nitrous oxide molecule (N-N-O), an additional parameter known as site preference (SP) can be calculated using the intramolecular distribution of ^{15}N (Yoshida and Toyoda 2000). Site preference of N_2O is a particularly powerful tool for tracing potential pathways as it is thought to be independent of substrate composition and reaction progress (Toyoda et al. 2002).

In this thesis chapter we report production of N_2O from an abiotic reaction between hydroxylamine and Mn(III)-PP. Additionally, we characterize the ratio of multiple products produced at a range of different concentrations of Mn(III)-PP and explore N_2O site preference values in the context of other abiotic reactions and culture experiments involving AOA, AOB, and comammox bacteria. Finally, we examine the potential for further reaction of the nitrogen species produced.

3.2 Methods

3.2.1 Reagent preparation

Manganese(III)-pyrophosphate (Mn(III)-PP) was prepared following Madison et al. (2011). Sodium pyrophosphate (5 mM) was dissolved in nitrogen-purged milliQ water and the pH adjusted to 8.0 using 6M hydrochloric acid. Manganese(III)-acetate (final concentration 1 mM) was then added, forming a clear pink solution of Mn(III)-PP (~1 mM). After allowing the solution to rest overnight, it was subsequently 0.2 μm filtered to remove any particulate Mn. Fresh solutions of Mn(III)-PP were prepared monthly. Due to its instability in solution, hydroxylamine solutions were prepared fresh daily from hydroxylamine hydrochloride salt in DI water. Calcium and magnesium-free artificial seawater (ASW) was prepared according to Lyman and Fleming (1940).

3.2.2 Isotopic analyses

Nitrous oxide was purified using a custom purge-and-trap system coupled with a PAL autosampler (McIlvin and Casciotti 2010, Weigand et al. 2016). Gas was then analyzed using an isotope ratio

mass spectrometer (IRMS) (Delta V Plus, Thermo Scientific). A suite of N_2O gases of known isotopic values were run as standards, including B6, 94321, and S2 (Mohn et al. 2014). Isotope data were corrected using the pyisotopomer software package to calculate size corrections, scrambling coefficients, and isotopomer abundances (Kelly et al. 2023). Concentrations were calculated by comparing the areas of sample N_2O peaks to areas produced by running standards of known concentration. Isotopic ratios of nitrogen ($^{15}R = {}^{15}N/{}^{14}N$) and oxygen ($^{18}R = {}^{18}O/{}^{16}O$) are reported using the standard delta notation where $\delta^{15}N = [(^{15}R_{sample}/\ ^{15}R_{N2\text{-}ATM}) - 1) * 1000]$ and $\delta^{18}O = [(^{18}Rsample/^{18}R_{VSMOW}) - 1) * 1000]$, quantified by measurement of masses 44, 45 and 46. Site preference was calculated by taking the difference in $\delta^{15}N$ between the outer ($\delta^{15}N\text{-}N_2O^{\alpha}$) and inner ($\delta^{15}N\text{-}N_2O^{\beta}$) position nitrogen atoms of N_2O, quantified by simultaneous measurement of the abundance of mass 31 and 30 in the NO fragment. Reproducibility was generally ±0.1‰, ±0.2‰, and ±0.7‰ for $\delta^{15}N\text{-}N_2O$, $\delta^{18}O\text{-}N_2O$, and SP, respectively.

Nitrite (NO_2^-) analyses were performed by conversion to N_2O using the azide method (McIlvin and Altabet 2005). Briefly, a 50/50 mixture of sodium azide (2 M) and acetic acid (1.7 M) was prepared and purged with N_2 gas. 0.1 mL was added to each vial and allowed to react for 30 minutes before neutralizing with sodium hydroxide (0.1 mL, 6 M). To correct for internal drift and sample size, RSIL-N23, N7373 and N10219 were run as standards on the IRMS alongside samples (Casciotti et al. 2007). Concentration and isotopic analyses of hydroxylamine were completed by conversion to N_2O using a modified version of the method outlined in Liu et al. 2014. Sulfamic acid (0.5 mL, 5% w/v in water) was added to each bottle to remove any nitrite present, which is known to cause interference. Immediately after, iron(III) chloride (1 mL, 25 mM) was added to convert all hydroxylamine present to N_2O. The resulting gas was then analyzed on the IRMS as described above. Standards were prepared from solutions of hydroxylamine added to 5 mL of ASW. The denitrifier method was used to determine concentration and isotopic composition of nitrate (Sigman et al. 2001). USGS32, USGS34, and USGS35 (Böhlke et al., 2003) were used as nitrate standards. Approximate precision of nitrite and nitrate measurements was ±0.1‰, ±0.2‰, ±0.2‰, and ±0.3‰ for $\delta^{15}N\text{-}NO_2^-$, $\delta^{18}O\text{-}NO_2^-$, $\delta^{15}N\text{-}NO_3^-$, and $\delta^{18}O\text{-}NO_3^-$, respectively.

3.2.3 Gibbs free energy calculations

Gibbs free energy calculations were carried out for potential products N_2, N_2O, NO, NO_2^-, and NO_3^- using ΔG_f^0 values from the literature or derived from equilibrium dissociation constants (Luther et al. 2015; Stumm and Morgan 1996; Zhu-Barker et al. 2015). For each reaction ΔG_{exp} was calculated using experimental concentrations of reagents ([Mn(III)-PP] = 2.5 μM, $[Mn^{2+}]$ = 2.5 μM, [PP] = 2.5 μM, $[NH_2OH]$ = 5 μM, $[N_2O]$ = 2.5 μM, [NO] = 5 μM, $[NO_2^-]$ = 5 μM, $[NO_3^-]$ = 5 μM, pH = 8, 1 atm N_2, T = 25°C). A range of environmental conditions were also used to generate ΔG_{min} and ΔG_{max} values ([Mn(III)-PP] = 30 - 70 nM, $[Mn^{2+}]$ = 30 – 70 nM, [PP] = 100 – 900 μM, $[NH_2OH]$ = 5 – 20 nM, $[N_2O]$ = 10 – 200 nM, [NO] = 50 – 250 pM, $[NO_2^-]$ = 0.1 – 10 μM, $[NO_3^-]$ = 1 – 50 μM, pH = 5 – 8, 1 atm N_2, T = 10 – 30°C) (Oldham et al. 2017b; Schweiger et al. 2007; Sundareshwar et al. 2001; Tian et al. 2020).

3.2.4 Experimental set-up

Quadruplicate vials of ASW (5 mL in 20 mL Restek crimp-sealed headspace vials with butyl stoppers) were prepared with varying amounts of Mn(III)-PP (5 to 80 μM) and then vigorously purged with N_2 gas for 15 minutes to remove any N_2O. Hydroxylamine (50 μL, 1 mM; final concentration 10 μM) was added to each vial and then allowed to react for 24 hours. As controls, additional vials were prepared containing no NH_2OH or no Mn(III)-PP. All vials were then analyzed on the IRMS for N_2O. Half of the vials were subsequently treated with azide to convert any product NO_2^- to N_2O and the remaining half with sulfamic acid and $FeCl_3$ to convert any remaining NH_2OH to N_2O. Both sets of headspace vials were then run a second time on the IRMS. Finally, the samples measured for NH_2OH were returned to neutral pH and injected directly into denitrifier vials to convert any product NO_3^- present to N_2O and analyzed on the IRMS. Due to the rapid nature of the reaction (hours), it was assumed that no significant biological activity occurred during experiments. Statistical differences were evaluated using paired t-tests.

3.3 Results

3.3.1 Concentrations of nitrogen species

Nitrous oxide concentrations were 1.2 ± 0.1 μM at Mn(III)-PP = 5 μM and increased rapidly before reaching a maximum of 3.4 ± 0.3 μM at Mn(III)-PP = 30 μM (Figure 4). At higher values of Mn(III)-PP, N_2O concentrations decreased towards a value of 1.9 ± 0.2 μM at the highest addition

of Mn(III)-PP (80 μM) . Between 5 and 20 μM Mn(III)-PP, NO_2^- concentrations were 1 ± 0.1 μM, but then decreased to zero at 40 μM Mn(III)-PP and were similarly undetectable at higher values of Mn(III)-PP (Figure 5). Concentrations of the remaining hydroxylamine were 2.2 ± 0.4 μM at Mn(III)-PP = 5 μM and decreased rapidly to near zero by Mn(III)-PP = 15 μM (Figure 6). Controls with no added Mn(III)-PP had 5.6 ± 0.9 μM of NH_2OH remaining, 0.23 ± 0.5 μM N_2O, and 1.0 ± 0.01 μM NO_2^-. Controls with no added NH_2OH had no detectable N_2O or NH_2OH and NO_2^- concentrations that were comparable to that of reagent blanks (<0.1 μM). Due to trace amounts of NO_3^- contamination in the ASW matrix, NO_3^- concentration measurements had a large blank (~2 μM). No samples or controls had concentrations detectable above the blank. Between 28 and 60% of N added remained unaccounted for (Figure 3).

3.3.2 Isotopes of nitrogen species

Isotopes of N_2O, NO_2^-, NH_2OH, and NO_3^- were measured by IRMS as described above. As Mn(III)-PP increased from 5 to 80 μM, $\delta^{15}N_{bulk}$-N_2O values decreased from -6.2 ± 0.5‰ to -12.6 ± 0.2‰ and $\delta^{18}O$-N_2O values increased from +36.2 ± 0.3‰ to +44.1 ± 0.2‰ (Figure 4). Site preference values were identical within measurement precision across all Mn(III)-PP treatments with an overall average value of +35.2 ± 0.7‰. $\delta^{15}N$-NO_2^- values were approximately -25 to -26‰ for Mn(III)-PP additions between 0 and 20 μM. For Mn(III)-PP treatments 25 to 40 μM, $\delta^{15}N$-NO_2^- increased before stabilizing at -7 to -8‰ for treatments 40 - 80 μM. $\delta^{18}O$-NO_2^- increased slightly from +20.9 ± 0.4‰ to +23.1 ± 0.2‰ between Mn(III)-PP = 5 to 30 μM before decreasing to +13.9 ± 0.4‰ at Mn(III)-PP = 80 μM (Figure 5). NH_2OH increased in $\delta^{15}N$ from -25 ± 2‰ to -5.7 ± 0.6‰ between 5 and 80 μM of Mn(III)-PP added (Figure 6). Controls with no added Mn(III)-PP had $\delta^{15}N_{bulk}$-N_2O = -8.9 ± 0.6‰, $\delta^{18}O$-N_2O = +35.4 ± 0.8‰, SP = +37.2 ± 0.7‰, $\delta^{15}N$-NO_2^- = -25 ± 3‰, $\delta^{18}O$-NO_2^- = +14 ± 8‰, $\delta^{15}N$-NH_2OH = -15 ± 1‰, and $\delta^{18}O$-NH_2OH = +46 ± 2‰. No significant differences in $\delta^{15}N$-NO_3^- or $\delta^{18}O$-NO_3^- were found compared to the blank in any of the samples or controls.

3.3.3 Potential reaction of nitrite and hydroxylamine

In order to investigate whether further reaction occurred between product nitrite and reactant hydroxylamine, NO_2^- with a distinctly low isotopic signature ($\delta^{15}N$ = -79.6‰, 4 μM) was added at the beginning of an additional 24 hr experiment in addition to NH_2OH (10 μM). Concentrations

and isotopes of nitrogen species were measured as described above. Relative to experiments without added nitrite, no significant differences were detected in either the concentration ($p = 0.21$), $\delta^{15}N_{bulk}$ ($p = 0.39$), or SP ($p = 0.13$) of N_2O produced. Differences in hydroxylamine concentrations also remained unchanged relative to the control ($p = 0.31$).

3.3.4 Timeseries

To assess reaction kinetics, multiple reaction vials were prepared as described above and immediately sampled in sequence using the autosampler of the IRMS to generate a timeseries of N_2O production (Figure 7). The time between samples was 10 minutes. Three concentrations of Mn(III)-PP were used: 10, 30, and 50 µM. In the timeseries where Mn(III)-PP = 10 µM, N_2O concentrations rose rapidly to 1.34 ± 0.06 µM and remained stable after 50 minutes. $\delta^{15}N_{bulk}$-N_2O fell slightly from -2.0‰ to -3.0‰ while $\delta^{18}O$-N_2O was constant at +34.5 ± 0.2‰. The site preference had no significant change through the timeseries and averaged +35.8 ± 0.4‰ across 18 samples. In the Mn(III)-PP = 30 µM treatment, the concentration of N_2O similarly rose rapidly to ~3 µM in the first 70 minutes and then increased slowly to 3.25 ± 0.03 µM by the end of the experiment (9.5 hrs). Similarly, the site preference was constant at +35.3 ± 0.5‰ (n=19). $\delta^{15}N_{bulk}$-N_2O fell from -7.0‰ to -12.1‰ while $\delta^{18}O$-N_2O rose from +36.7‰ to +40.8‰ (Figure 7). When Mn(III)-PP was increased to 50 µM, N_2O concentration remained fairly constant at 1.0 ± 0.2 µM throughout the timeseries with SP = +36.3 ± 0.3‰ (n=8). There was no clear trend in $\delta^{15}N_{bulk}$-N_2O or $\delta^{18}O$-N_2O which were -16 ± 1‰ and +49 ± 2‰ respectively.

3.3.5 Gibbs free energy calculations

Results of Gibbs free energy calculations are listed in Table 1 and ranged from -477 to -832 kJ/mol at experimental conditions and -374 to -802 kJ/mol at environmental conditions. All values were negative, indicating favorable forward reactions.

3.4 Discussion

Our data demonstrate that hydroxylamine (NH_2OH) and Mn(III)-PP react rapidly in artificial seawater to form nitrite (NO_2^-), nitrous oxide (N_2O), and a third product, presumed to be dinitrogen gas (N_2). Nitrous oxide is formed from two hydroxylamine molecules and is not the product of nitrite reacting with hydroxylamine, nor does nitrous oxide continue reacting to dinitrogen. The

proportion of these products varies based on the starting stoichiometry of the two reactants, with the maximum amount of N_2O formed at 3:1 Mn(III)-PP:NH_2OH. This N_2O has an isotopic site preference signature identical to that of N_2O produced by nitrifying organisms including AOA, AOB, and comammox bacteria; therefore leakage of NH_2OH from cells in the environment could theoretically be oxidized by Mn(III)-L compounds producing N_2O through an as yet unnoticed mixed biotic-abiotic process (Kits et al. 2019).

3.4.1 Isotopic signature of N_2O

Stable isotopes of N_2O can be used to provide information about its abiotic and/or biotic sources. Of particular interest to this study is the intramolecular site preference (SP), calculated as the difference in $\delta^{15}N$ between the central N ($\delta^{15}N_\alpha$-N_2O) and the outer N ($\delta^{15}N_\beta$-N_2O) (Yoshida and Toyoda 2000). Site preference is a particularly powerful tool as it is thought to arise independent of the isotopic composition of the substrate and reaction progress, thus providing a consistent "fingerprint" for a given process (Toyoda et al. 2002).

In this study, we measured consistent SP values of +35.5 ± 0.6‰ across all experiments (n = 97), which are similar to values reported for other abiotic reactions of NH_2OH. Toyoda et al. (2005) reported a SP = +29.5 ± 1.1‰ for the reaction of NH_2OH with MnO_2. While the exact reactants are unclear, Wunderlin et al. (2013) measured a SP of +30.3 ± 0.2‰ when combining NH_2OH with tap water. Heil et al. (2014) performed experiments combining NH_2OH with NO_2^-, Fe^{3+}, and Cu^{2+} at a variety of concentrations and pH conditions and found a SP = +33.9‰ to +35.6‰ across all treatments. Studies that document abiotic N_2O production from other N species have noted more variation in SP, such as Buchwald et al. (2016) who measured SP from 0.4‰ to +26.0‰ and Jones et al. (2015) who measured SP from +10‰ to +22‰ in studies of "chemodenitrification" of NO_2^- by soluble Fe^{2+} and Fe^{3+} containing minerals. Grabb et al. (2017) observed a more consistent SP value of +26.5‰ ± 0.8‰ emerging from reaction between NO_2^- and the Fe(II)-Fe(III) oxyhydroxide phase green rust. Generally, the SP values measured in our experiments were consistent with those measured by Heil et al. (2014) and 4 - 5‰ higher than those measured by Toyoda et al. (2005) and Wunderlin et al. (2013).

Interestingly, the SP value reported here is also broadly consistent with several studies of N_2O production from AOA and AOB (Duan et al. 2017). For instance, Sutka et al. (2006) reported SP values between +32.5‰ and +35.6‰ when providing NH_2OH to several strains of AOB. Frame and Casciotti (2010) calculated a SP value of +36.3 ± 2.4‰ for N_2O produced from NH_2OH by AOB *Nitrosomonas marina*. Yamazaki et al. (2014) isolated the hydroxylamine oxidoreductase (HAO) enzyme from two species of AOB and measured SP values of +36.3 ± 2.3‰ during *in vitro* incubations with hydroxylamine. Enrichments of marine AOA produced N_2O with SP values of +30.3 ± 2.4‰ (Santoro et al. 2011). Recently discovered comammox bacterium *Nitrospira inopinata* produced N_2O with SP values of +34.2 ± 1.4‰ through a process the authors hypothesized to be mixed biotic/abiotic (Kits et al. 2019).

Taken together, these similarities in SP are suggestive of a common mechanism of N_2O production. In abiotic reactions this is often presumed to be *cis*-hyponitrous acid (HO-^{14}N=^{15}N-OH) with the kinetic isotope effect leading to preferential breaking of the ^{14}N-O bond and thus enriching the central N ($\delta^{15}N_\alpha$-N_2O) leading to a positive site preference (Heil et al. 2014). In AOB it is hypothesized that the HAO enzyme either acts on a similar symmetric intermediate or that it binds two NH_2OH molecules in sequence, with a kinetic preference for binding ^{14}N-NH_2OH over ^{15}N-NH_2OH leading to cleavage of the ^{14}N-O bond (Duan et al. 2017; Schreiber et al. 2012). Caranto et al. (2016) reported that the cytochrome P460 enzyme from the AOB *Nitrosomonas europaea,* although not well understood, is capable of direct stoichiometric formation of N_2O from NH_2OH under anoxic conditions and posited a similar sequential binding mechanism. We hypothesize that the reaction mechanism for N_2O production from NH_2OH and Mn(III)-PP acts through creation of a symmetric intermediate thus leading to a positive site preference due to kinetic preference for breaking the ^{14}N-O bond. The similarities in SP between this study and several biological studies also suggests that this reaction could be occurring in the environment unnoticed due to the assumption that high SP values are indicative of nitrification, although further study will need to be undertaken to validate this.

3.4.2 N_2O production is not "hybrid"

There are several potential pathways that are capable of transforming hydroxylamine into nitrous oxide: 1. oxidation of NH_2OH by Fe(III), 2. oxidation of NH_2OH by O_2 (autoxidation), 3.

disproportionation of NH_2OH, and 4. reaction of NH_2OH with HNO_2 (Schreiber et al. 2012). Of these, pathways 1 and 2 can be excluded here as there was no Fe(III) present in the matrix and O_2 was removed during the sparging process. Disproportionation of NH_2OH generally proceeds very slowly at pH = 8 and is discussed further in 4.4.3 (Bonner et al. 1978). By contrast, reaction of NH_2OH with HNO_2 is known to proceed rapidly and therefore NO_2^- (in equilibrium with HNO_2) formed during biotic or abiotic oxidative pathways could potentially further react with NH_2OH and contribute to production of "hybrid" N_2O from two different N-bearing precursor molecules (Döring and Gehlen 1961).

Hybrid N_2O production from NO_2^- and NH_2OH has been reported in the literature, often linked to abiotic reactions with trace metals. Terada et al. (2017) performed experiments using an enrichment of AOB and isotopic labeling which showed ~50% of N_2O production was due to abiotic reaction of NO_2^- and NH_2OH (pH = 7.8). However, there was no abiotic production of N_2O when similar experiments were performed in water, indicating the synthetic wastewater matrix (containing trace metals Fe, Mn, Cu, Zn, Ni) catalyzed the reaction. Terada et al. (2017) performed further experiments and concluded that Fe(III) was not involved. Harper et al. (2015), using the same media recipe and pH condition, concluded that Cu(II) catalyzed the formation of N_2O from NO_2^- and NH_2OH. When mimicking reaction conditions found in wastewater treatment plants, Soler-Jofra et al. (2016) found a strong correlation between lower pH and faster rates of abiotic reaction of NO_2^- and NH_2OH which they attributed to increasing proportion of HNO_2. At the pH treatment closest to that of our study (pH = 7.6) they measured a rate of 1.4 µM/hr NH_2OH consumption (0.7 µM/hr N_2O production) upon addition of 3.9 mM NO_2^- to 21.4 µM to NH_2OH. The authors concluded trace metals present in the growth media (Fe, Zn, Co, Mn, Cu, Mo, and Ni) could be responsible for accelerating the rate of reaction (Soler-Jofra et al. 2016). Soler-Jofra et al. (2018) reported comparable levels of N_2O production from AOB *Nitrosomonas europaea* cultures (pH = 7.5) and abiotic controls in which NO_2^- and NH_2OH were added to uninoculated media, concluding that observed N_2O production from their culture experiments was due to abiotic reaction between nitrous acid (HNO_2) and NH_2OH potentially also involving metals (Cu, Fe, Mn, Mo, Zn, Co) from the AOB culture media.

Other studies have concluded that the abiotic reaction between NO_2^- and NH_2OH may represent a more minor source of N_2O compared to biotic N_2O production. Su et al. (2019a) measured the rate of abiotic reaction of NO_2^- and NH_2OH in the presence Fe(II) and Fe(III). Between pH 6 and pH 8, the reaction rate fell from 150 nmol/hr to 18 nmol/hr N_2O production, respectively, again indicating that HNO_2 concentration controls the formation of N_2O. Overall these abiotic reaction rates were 1-5 orders of magnitude lower than those measured overall in the reactor, accounting for 0.025% to 2.6% of total N_2O production.

In order to investigate the potential for further reaction of product NO_2^- with reactant NH_2OH, we performed an experiment in which isotopically distinct NO_2^- ($\delta^{15}N$ = -79.6‰) was added at the beginning of the experiment. If this NO_2^- were involved in reactions with NH_2OH, this low $\delta^{15}N$ signal would appear in the N_2O pool. If the rate of reaction was high enough, the overall concentration of N_2O would also rise above those documented in the parallel experiment without amended NO_2^-. In contrast, we saw no statistically significant difference in either the [N_2O] or $\delta^{15}N_{bulk}$-N_2O and thus no evidence of hybrid N_2O production between NO_2^- and NH_2OH. However, it is possible the rate of reaction was too slow to measure with the low concentrations of NO_2^- and NH_2OH used, and the short timescale of the experiment compared to those previously described. Using the reaction rates calculated by Su et al. 2019b and comparable reaction conditions to my experiments (pH = 8, [NO_2^-] = 1 μM, [NH_2OH] = 10 μM) we calculate a rate of N_2O formation on the order of 10^{-13} M/hr which results in only 0.01 nM over 24 hours. If we assume no significant fractionation occurs, an addition of 0.01 nM of N_2O with $\delta^{15}N \cong$ -40‰ results in changes to the overall $\delta^{15}N_{bulk}$-N_2O of <0.1‰. Therefore, hybrid N_2O formation can be excluded, as it would be so minor as to be insignificant under the reaction conditions studied here.

3.4.3 Towards the closing of nitrogen mass balance

In this study, we simultaneously quantified changes in concentrations of reaction products N_2O, NO_2^-, and NO_3^- together with the evolving reactant pool of NH_2OH remaining. However, there remained 30-60% of N unaccounted for when performing a mass balance of the overall reaction. In this section, we discuss potential other products that could account for this "missing" N.

First, we will consider the possibility of further reaction of products [N_2O] and [NO_2^-]. As described above, further reaction of NO_2^- and NH_2OH to N_2O must be insignificant under the reaction conditions studied. However, other further reactions must also be considered. For instance, NO_2^- has been found to react to NO_3^- in the presence of Mn(III)-PP, although the reaction is relatively slow at pH = 8 (Karolewski et al. 2021). Using the reaction conditions of these experiments (pH = 8, [NO_2^-] = 1 μM, [Mn(III)-PP] = 80 μM) we calculate a rate of NO_3^- formation on the order of 10^{-17} M/hr which results in negligible NO_3^- formation over 24 hours. Even in environments with lower pH this reaction is unlikely to substantially affect [NO_2^-]; for instance, at pH = 5, 4 nM/day could be removed which is <1% of NO_2^- produced. These calculations are also supported by the measurements of [NO_3^-] which were undetectable above the blank. Nitrous oxide could also theoretically react with Mn^{2+} to form N_2 and MnO_2 (ie. $N_2O + Mn^{2+} + H_2O \rightarrow N_2 + MnO_2 + 2H^+$) (Cavazos et al. 2018). Notably, however, if N_2O were being both produced and consumed, each process would impart an isotopic signature onto the overall SP of N_2O. However, the SP of N_2O was identical within precision throughout all experiments and did not vary with [N_2O], [Mn(III)-PP] added, fraction of missing N, or time elapsed during time series experiments. Thus, it is unlikely that there are multiple processes impacting SP of N_2O and further reaction of N_2O can also be ruled out.

In order to assess the thermodynamic viability of various products from the direct redox reaction of Mn(III)-PP and NH_2OH, we calculated the Gibbs free energy of reaction for production of N_2, N_2O, NO, NO_2^-, and NO_3^- at both standard state conditions (ΔG°) and relevant reaction conditions (ΔG). For all reactions, the ΔG° and ΔG were both negative, indicating energetically favorability. As [N_2O], [NO_2^-], and [NO_3^-] were already quantified during the experimental process, only N_2 and NO remain as viable candidates. Nitric oxide (NO) is a highly reactive free radical unlikely to persist in solution with other redox-active species. Thus, it seems most parsimonious that N_2 is the likely identity of the missing N, if the reaction is a simple reduction-oxidation. Interestingly, the number of Mn(III)-PP equivalents needed to produce each product did not seem to predict products observed (Table 1; Figure 3). For instance, the production of NO_2^- requires 4 Mn(III)-PP molecules per NH_2OH while the production of N_2O requires only 2 Mn(III)-PP molecules per NH_2OH. However, at the lower ratios of Mn(III)-PP to NH_2OH, NO_2^- was formed while at higher ratios

N_2O was formed. Thus, we were unable to use the stoichiometry of balanced reactions to predict the identity of the missing N.

Because N_2 gas was used to purge vials during these experiments it was not possible to directly measure any production of N_2. However, within the literature similar reactions have been documented. Dinitrogen gas was predicted as a product (along with N_2O) when hydroxylamine was oxidized by manganese(III)-bis(salicylaldimine) (Salem 1995). Additionally, Mn(II/III) was posited to be the active site of the DnfA enzyme which converts NH_2OH to N_2 in dirammox heterotrophic bacteria (Hou et al. 2022). If N_2 is in fact the only missing N species, 65-100% of NH_2OH added would be transformed into non-fixed nitrogen species, therefore potentially removing NH_2OH from aquatic systems under the tested conditions. If all missing N is produced through disproportionation of NH_2OH this value is still 52 - 87% (see below). Currently, most models of N cycling assume the biological processes denitrification and anammox are the primary loss terms of fixed N although other studies have shown production of N_2 from trace metals (Doane 2017; Luther et al. 1997; Moraghan and Buresh 1977).

Disproportionation reactions could also account for some of the missing N, likely also producing N_2. As previously discussed, disproportionation of NH_2OH generally proceeds slowly at pH = 8. However, it has been shown to be catalyzed by Fe(II) and Fe(III) compounds (Allusetti et al. 2004; Bari et al. 2010). Disproportionation can proceed as $4NH_2OH \rightarrow N_2O + 2NH_3 + 3H_2O$ or $3NH_2OH \rightarrow NH_3 + N_2 + 3H_2O$ (Cisneros et al. 2003). If all N_2O formation at [Mn(III)-PP] = 30 µM was due to this disproportionation reaction, ~6.7 µM NH_3 would be formed in addition to the 3.4 µM N_2O (6.7 µM N). However, only 10 µM of N (as NH_2OH) was added at the beginning of the experiment and therefore cannot account for 6.7 µM NH_3 + 6.7 µM N-N_2O = 13.4 µM. Similar results are found for all but the lowest (5 µM) and the highest (80 µM) treatments which suggests disproportionation producing N_2O could only account for a fraction of the N_2O produced. As the site preference remained consistent across experiments, multiple pathways of N_2O formation are also unlikely and therefore disproportionation producing N_2O is likely insignificant. However, disproportionation producing N_2 could account for some or all of the missing N fraction. In this scenario, one-third of the missing N would be in the form of NH_3 and the remaining two-thirds as

N_2. As previously discussed, neither NH_3 nor N_2 concentrations were measured during these experiments so this possibility cannot be fully ruled out.

When examining the ratios of products in Figure 3, it does appear that there may be a shift in dynamics located at around 30 – 35 μM [Mn(III)-PP] where NO_2^- is no longer formed, N_2O begins to decrease, and the fraction of missing N correspondingly increases. It is possible this shift corresponds to disproportionation giving way to redox reactions with Mn(III)-PP as the ratio of Mn(III)-PP to NH_2OH increases. In this scenario, 2/3 of the missing N would be N_2 at [Mn(III)-PP] < 30 μM and all of the missing N would be N_2 at at [Mn(III)-PP] > 30 μM. However, as discussed above, higher ratios of Mn(III)-PP to NH_2OH did not seem to correlate with the formation of more oxidized products, so it is difficult to determine if this visual trend in product ratio is in fact significant.

3.4.4 Potential environmental relevance

While this study did not directly measure rates in the environment, production of N_2O has been correlated with soil Mn content in several previous studies (Heil et al. 2015b; Xu et a. 2022). Due to the relatively recent discovery of Mn(III)-L, no studies measuring N_2O production from NH_2OH have measured Mn(III) directly, although many methods used to quantify Mn would also include Mn(III)-L. For instance, Bremner et al. (1980) added NH_2OH to a suite of sterilized soils containing oxidized Mn and the majority of N was transformed to N_2O with minor amounts of N_2 production. Other studies similarly found total Mn content in soils was correlated with rapid N_2O production from addition of NH_2OH (Heil et al. 2015a; Liu et al. 2017b; Liu et al. 2019). Site preference values of N_2O produced ranged from +31.4 ± 3.6‰ to +35‰, comparable to the value reported here (+35.5 ± 0.6‰) (Duan et al. 2020; Heil et al. 2015a).

Several studies have also directly studied the impact of solid Mn oxides (MnO_2) on N_2O production. Cavazos et al. (2018) performed laboratory experiments that showed rapid production of N_2O from reaction of the phyllomanganate birnessite and NH_2OH under environmental conditions. Similarly, Rue et al. (2018) reacted NH_2OH with pyrolusite and poorly crystalline MnO_2(s) and found 82-86% transformed to N_2O. Taken together, these studies suggest oxidized mineral forms of Mn also play an important role in transforming NH_2OH to N_2O.

Although NH_2OH has been known to accumulate in cultures of AOB, AOA, and comammox bacteria, NH_2OH rarely accumulates to measurable levels in the environment due to its instability and reactivity (Soler-Jofra et al. 2021). However, concentrations up to ~250 nM have been measured in coastal seawater with high nitrification activity (Zhu-Barker et al. 2015). Additionally, rapid rates of reaction can prevent the buildup of NH_2OH, but do not preclude high rates of consumption. Due to the relatively recent discovery of the abundance of Mn(III)-L compounds in the environment, measurements are somewhat sparse (Madison et al. 2013; Oldham et al. 2015). Jones et al. (2020) reported a peak of up to 0.5 - 1 nM of Mn(III)-L at the base of the euphotic zone in oxygenated waters of the Northwest Atlantic, coincident with the peak in nitrification rates often observed at this depth (Ward 2008). Oldham et al. (2017a) found a similar peak at the base of the euphotic zone of 0.2 - 0.4 μM Mn(III)-L in both fully oxygenated waters and above anoxic sediments in profiles from St. Lawrence Estuary. Within sediment porewaters, up to 80 μM Mn(III)-L was reported by Madison et al. (2013) with maxima close to the oxic-suboxic interface where nitrification in sediments is similarly high (Ward 2008). While we are not aware of any studies simultaneously measuring NH_2OH and Mn(III)-L concentrations in the environment, these papers suggest several locations where NH_2OH formation and "leakage" by nitrifiers could overlap with regions high in Mn(III)-L. Comparing measurements from two similar estuarine sites with seasonal anoxia, NH_2OH was measured as 5 - 20 nM and Mn(III)-L was 30 - 70 nM (Oldham et al. 2017b; Schweiger et al. 2007). The ratios of Mn(III)-L:NH_2OH would be between 1.5 to 14 which are of similar stoichiometric ratios as those used in this study (0.5 to 8). However, both studies note high degrees of temporal variability on the scale of hours to days as is to be expected from highly reactive species. Despite this variability, ΔG values calculated at environmental concentrations consistently remained negative, indicating theoretical thermodynamic favorability (Table 1).

The ratio of products observed was highly dependent on the starting stoichiometry, with a peak in N_2O production at [Mn(III)-L] = 30 μM or a ratio of 3:1 Mn(III)-PP:NH_2OH. At lower ratios of Mn(III)-PP, the products have a greater fraction of NO_2^- and missing N (presumed to be primarily N_2). At higher ratios, the fraction of N_2O decreases while the presumed N_2 rises. Thus, in environments higher in Mn(III)-L compounds with fewer nitrifiers releasing NH_2OH, such as in nearly anoxic porewaters, it is more likely that all N undergoing this reaction will be lost as non-

fixed N in the form of N_2O and N_2. At ratios between 1.5 and 6 Mn(III)-PP:NH_2OH, half or more of the N added will be converted to N_2O. In locations such as open ocean oxygen deficient zones (ODZs), with high NH_2OH and generally lower trace metal contents, relatively more NO_2^- could be formed and continue in the nitrification pathway or subsequently be denitrified. If NH_3 is also being formed through a disproportionation pathway, it could also be "recycled" back into nitrification. Further study will be necessary to determine if this reaction is occurring in the environment and to if so, to what degree.

3.5 Conclusion

Here, we have shown that Mn(III)-PP can abiotically oxidize NH_2OH primarily to N_2O, with NO_2^- as a secondary product when the ratio of Mn(III)-PP to NH_2OH was less than 4 to 1. Dinitrogen gas and potentially ammonia were presumed to be the remaining percentage of the products, although neither was measured directly. The isotope dynamics of ^{15}N and ^{18}O were characterized for both the known products and the reactant. Isotopically distinct NO_2^- was used to demonstrate that the formation pathway of N_2O was not a hybrid process between NO_2^- and NH_2OH. The site preference of N_2O formed was highly consistent at +35.5 ± 0.6‰ regardless of reactant ratio or reaction progress, indicating N_2O was likely formed through a symmetric intermediate and through only one production pathway with no further consumption occurring. This SP value is also very close to those reported in multiple studies of AOA, AOB, and comammox bacteria. Although this reaction has yet to be documented in the environment, the similarity in SP values suggests that previous measurements of environmental N_2O could have included abiotic oxidation of NH_2OH by Mn(III)-L while attributing its signature to solely biological nitrification processes. This study supports the hypothesis that abiotic and mixed biotic/abiotic processes potentially could contribute significantly to N_2O emissions and suggests that Mn(III)-L compounds could play an important role in greenhouse gas emissions.

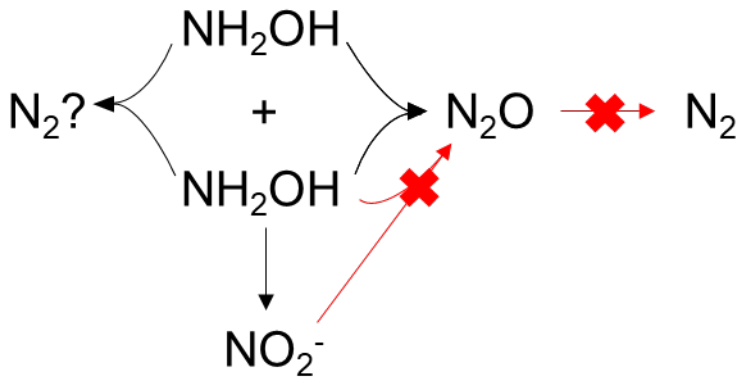

Figure 1: Conceptual diagram illustrating the major reactions occurring in this chapter. Hydroxylamine reacts with Mn(III) pyrophosphate to form nitrous oxide, nitrite, and potentially dinitrogen gas. Two potential reactions were also ruled out during this study, namely "hybrid" formation of nitrous oxide from nitrite and hydroxylamine and reduction of nitrous oxide to dinitrogen by Mn^{2+}.

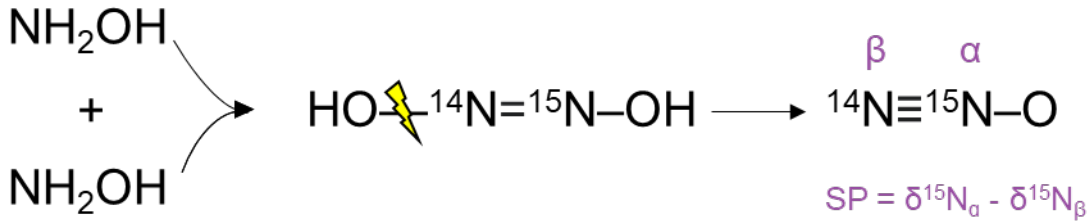

Figure 2: Reaction between two hydroxylamine atoms forms a symmetric intermediate *cis*-hyponitrous acid. Preferential breaking of the ^{14}N-O bond and enriches the central N ($\delta^{15}N_{\alpha}$) compared to the outer N ($\delta^{15}N_{\beta}$) leading to a positive site preference.

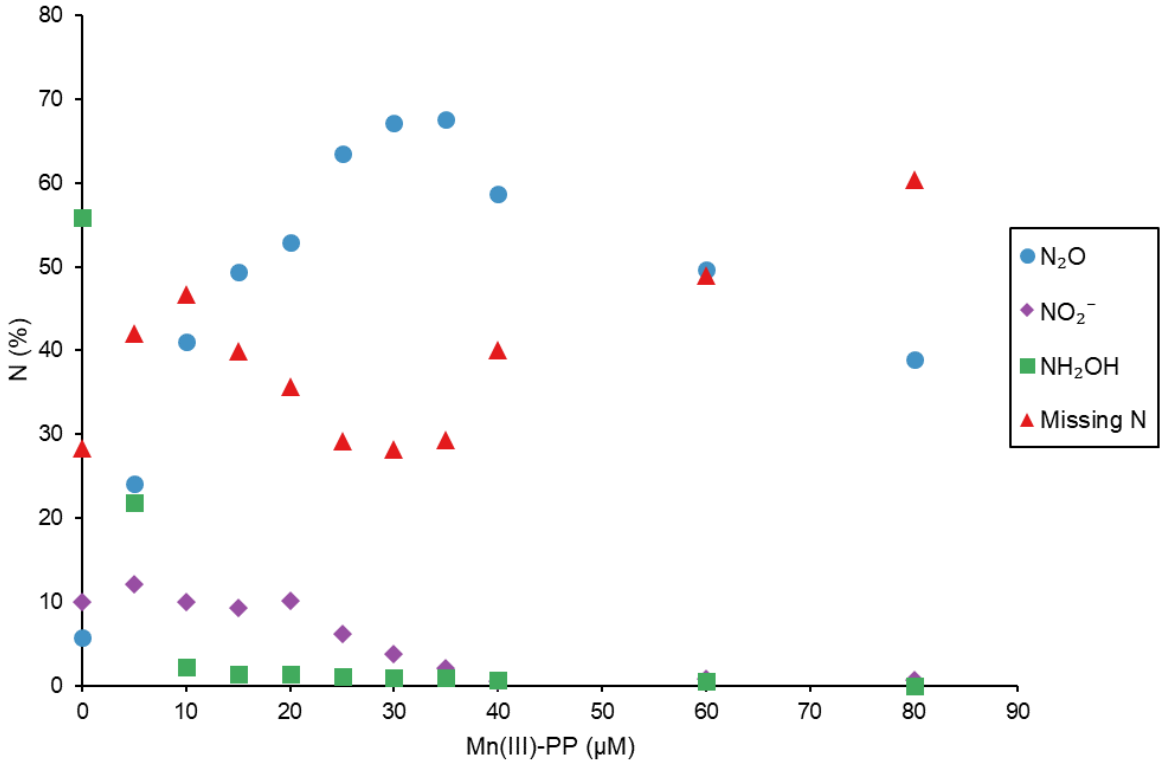

Figure 3: Remaining NH_2OH and produced NO_2^-, N_2O, and missing product (presumed to be N_2) after 24 hrs. of reaction vs. starting Mn(III)-PP (μM). Values are reported in % of N added.

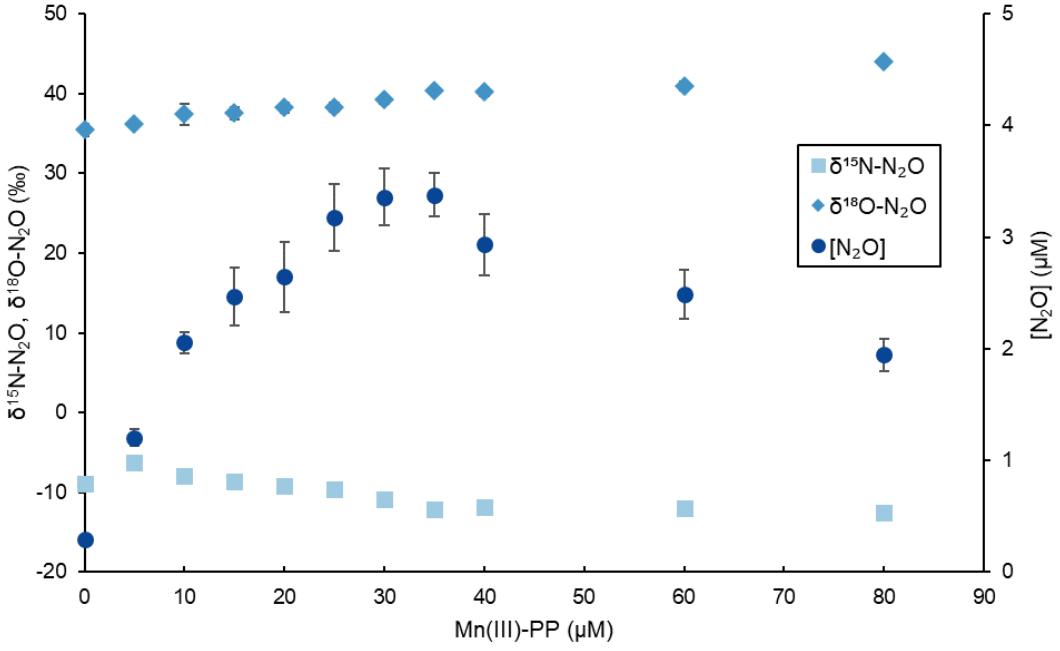

Figure 4: N_2O produced (μM), $\delta^{15}N$-N_2O, and $\delta^{18}N$-N_2O after 24 hrs. of reaction vs. starting Mn(III)-PP (μM). Starting NH_2OH was 10 μM and had an initial $\delta^{15}N$ of -4‰. Error bars represent the standard deviation of measurements (n = 4).

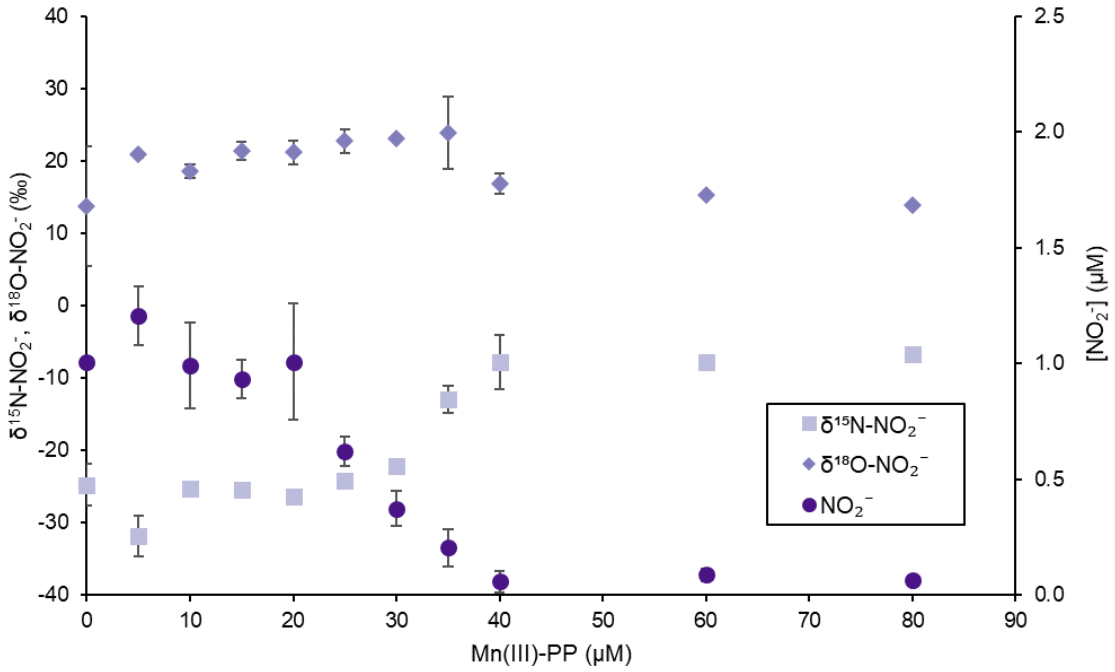

Figure 5: NO_2^- produced (μM), $\delta^{15}N\text{-}NO_2^-$, and $\delta^{18}O\text{-}NO_2^-$ after 24 hrs. of reaction vs. starting Mn(III)-PP (μM). Starting NH_2OH was 10 μM and had an initial $\delta^{15}N$ of -4‰. Error bars represent the standard deviation of measurements (n = 2).

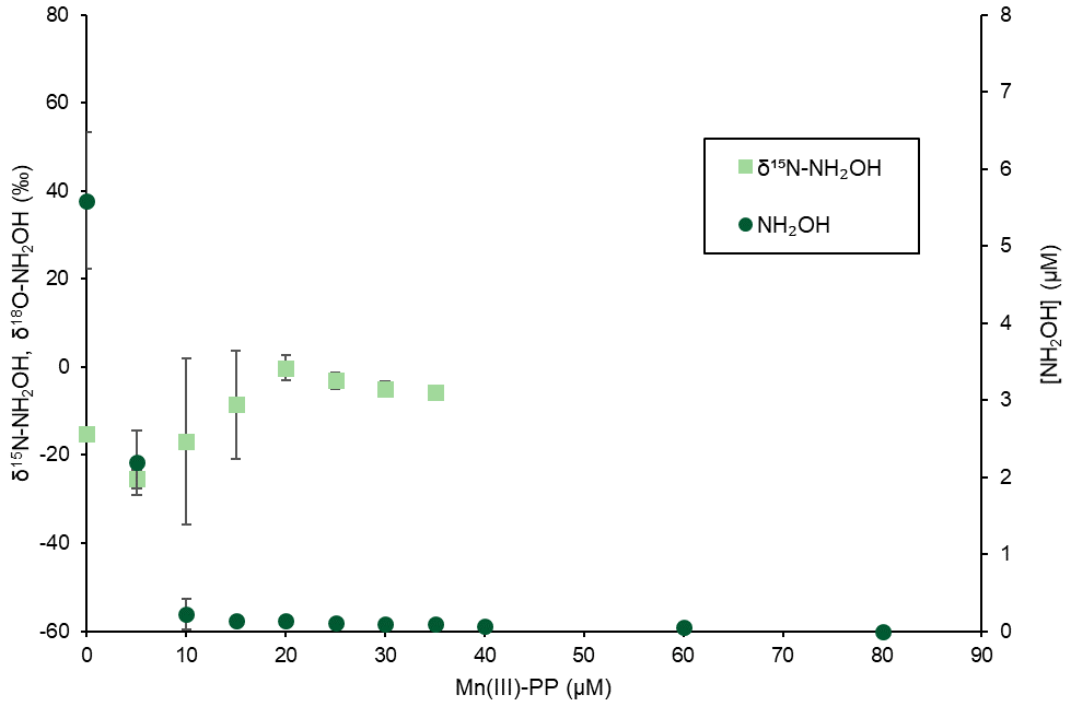

Figure 6: NH_2OH remaining (μM) and $\delta^{15}N\text{-}NH_2OH$ after 24 hrs. of reaction vs. starting Mn(III)-PP (μM). Starting NH_2OH was 10 μM and had an initial $\delta^{15}N$ of -4‰. Error bars represent the standard deviation of measurements (n = 2).

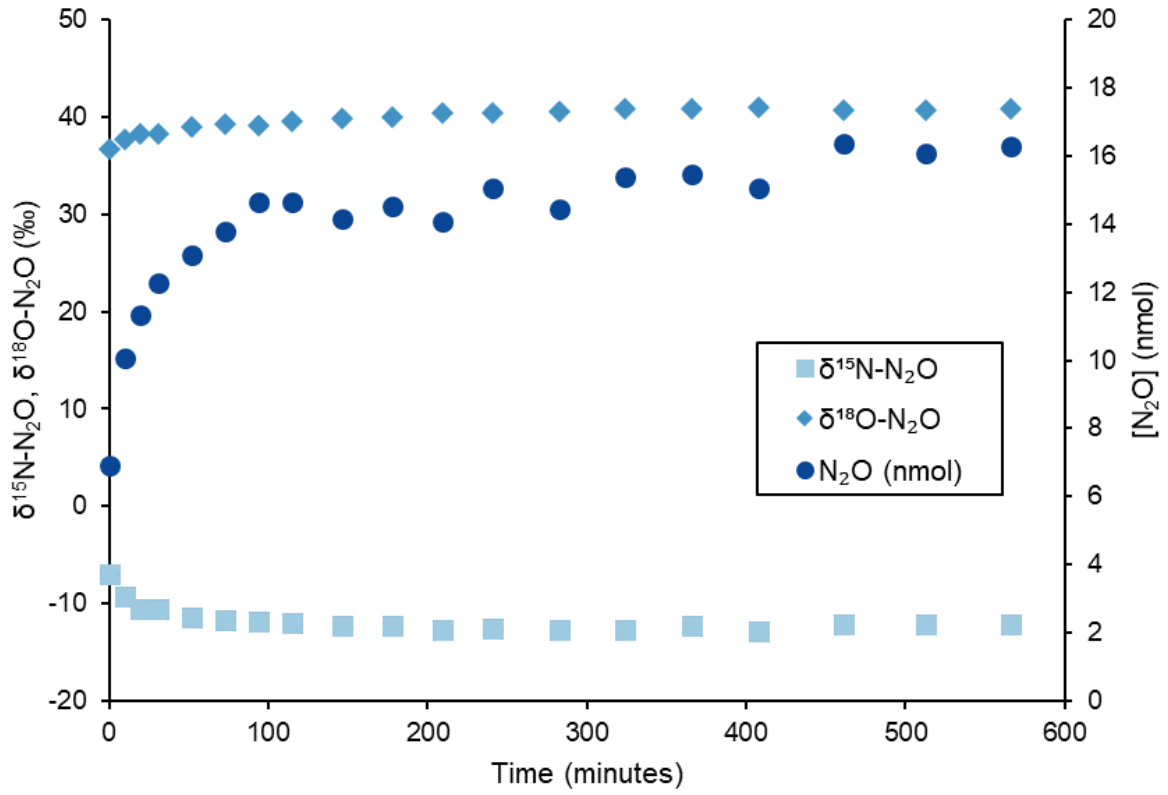

Figure 7: N_2O (nmol), $\delta^{15}N$-N_2O, and $\delta^{18}O$-N_2O vs. time in minutes for [Mn(III)-PP] = 30 µM. Starting NH_2OH was 10 µM and had an initial $\delta^{15}N$ of -4‰.

Balanced reaction	ΔG_{exp}	ΔG_{min}	ΔG_{max}
$2Mn(III)\text{-}PP + 2NH_2OH \rightarrow 2Mn^{2+} + N_2 + 2H^+ + 2H_2O + 2PP$	-764	-728	-666
$4Mn(III)\text{-}PP + 2NH_2OH \rightarrow 4Mn^{2+} + N_2O + 4H^+ + H_2O + 4PP$	-832	-802	-671
$3Mn(III)\text{-}PP + NH_2OH \rightarrow 3Mn^{2+} + NO + 3H^+ + 3PP$	-477	-472	-374
$4Mn(III)\text{-}PP + NH_2OH + H_2O \rightarrow 4Mn^{2+} + NO_2^- + 5H^+ + 4PP$	-600	-563	-431
$6Mn(III)\text{-}PP + NH_2OH + 2H_2O \rightarrow 6Mn^{2+} + NO_3^- + 7H^+ + 6PP$	-820	-787	-575

Table 1: Gibbs free energy calculations for reaction conditions from this study (ΔG_{exp}) and for a variety of environmental conditions (ΔG_{min} and ΔG_{max}). Experimental reaction conditions were [Mn(III)-PP] = 2.5 µM, $[Mn^{2+}]$ = 2.5 µM, [PP] = 2.5 µM, $[NH_2OH]$ = 5 µM, $[N_2O]$ = 2.5 µM, [NO] = 5 µM, $[NO_2^-]$ = 5 µM, $[NO_3^-]$ = 5 µM, pH = 8, 1 atm N_2, T = 25°C and the range of environmental reaction conditions were [Mn(III)-PP] = 30 - 70 nM, $[Mn^{2+}]$ = 30 – 70 nM, [PP] = 100 – 900 µM, $[NH_2OH]$ = 5 – 20 nM, $[N_2O]$ = 10 – 200 nM, [NO] = 50 – 250 pM, $[NO_2^-]$ = 0.1 – 10 µM, $[NO_3^-]$ = 1 – 50 µM, pH = 5 – 8, 1 atm N_2, T = 10 – 30°C All values are negative, indicating favorable reactions.

References

Alluisetti, G. E., Almaraz, A. E., Amorebieta, V. T., Doctorovich, F., & Olabe, J. A. (2004). Metal-catalyzed anaerobic disproportionation of hydroxylamine. Role of diazene and nitroxyl intermediates in the formation of N2, N 2O, NO+, and NH3. *Journal of the American Chemical Society*, *126*(41), 13432–13442.

Anthropogenic and natural radiative forcing. (2013). *Climate Change 2013 the Physical Science Basis: Working Group I Contribution to the Fifth Assessment Report of the Intergovernmental Panel on Climate Change*, *9781107057999*, 659–740.

Baggs, E. M. (2008). A review of stable isotope techniques for N_2O source partitioning in soils: recent progress, remaining challenges and future considerations. *Rapid Communications in Mass Spectrometry*, *22*(11), 1664–1672.

Bari, S. E., Amorebieta, V. T., Gutiérrez, M. M., Olabe, J. A., & Doctorovich, F. (2010). Disproportionation of hydroxylamine by water-soluble iron(III) porphyrinate compounds. *Journal of Inorganic Biochemistry*, *104*(1), 30–36.

Böhlke, J. K., Mroczkowski, S. J., & Coplen, T. B. (2003). Oxygen isotopes in nitrate: new reference materials for 18O:17O:16O measurements and observations on nitrate-water equilibration. *Rapid Communications in Mass Spectrometry*, *17*(16), 1835–1846.

Bonner, F. T., Dzelzkalns, L. S., & Bonucci, J. A. (1978). Properties of Nitroxyl as Intermediate in the Nitric Oxide-Hydroxylamine Reaction and in Trioxodinitrate Decomposition1. *Inorganic Chemistry*, *17*(9), 2487–2494.

Buchwald, C., Grabb, K., Hansel, C. M., & Wankel, S. D. (2016). Constraining the role of iron in environmental nitrogen transformations: Dual stable isotope systematics of abiotic $NO2^-$ reduction by Fe(II) and its production of N_2O. *Geochimica et Cosmochimica Acta*, *186*, 1–12.

Caranto, J. D., Vilbert, A. C., & Lancaster, K. M. (2016a). Nitrosomonas europaea cytochrome P460 is a direct link between nitrification and nitrous oxide emission. *Proceedings of the National Academy of Sciences of the United States of America*, *113*(51), 14704–14709.

Caranto, J. D., Vilbert, A. C., & Lancaster, K. M. (2016b). Nitrosomonas europaea cytochrome P460 is a direct link between nitrification and nitrous oxide emission. *Proceedings of the National Academy of Sciences of the United States of America*, *113*(51), 14704–14709.

Casciotti, K. L. (2016). Nitrogen and Oxygen Isotopic Studies of the Marine Nitrogen Cycle.

Casciotti, K. L., Böhlke, J. K., McIlvin, M. R., Mroczkowski, S. J., & Hannon, J. E. (2007). Oxygen isotopes in nitrite: analysis, calibration, and equilibration. *Analytical Chemistry*, *79*(6),

Cavazos, A. R., Taillefert, M., Tang, Y., & Glass, J. B. (2018). Kinetics of nitrous oxide production from hydroxylamine oxidation by birnessite in seawater. *Marine Chemistry*, *202*, 49–57.

Cisneros, L. O., Wu, X., Rogers, W. J., Mannan, M. S., Park, J., & North, S. W. (2003). Decomposition Products of 50 Mass% Hydroxylamine/Water Under Runaway Reaction Conditions. *Process Safety and Environmental Protection*, *81*(2), 121–124.

Daims, H., Lebedeva, E. v., Pjevac, P., Han, P., Herbold, C., Albertsen, M., Jehmlich, N., Palatinszky, M., Vierheilig, J., Bulaev, A., Kirkegaard, R. H., von Bergen, M., Rattei, T., Bendinger, B., Nielsen, P. H., & Wagner, M. (2015). Complete nitrification by Nitrospira bacteria. *Nature 2015 528:7583*, *528*(7583), 504–509.

Doane, T. A. (2017). The Abiotic Nitrogen Cycle. *ACS Earth and Space Chemistry*, *1*(7), 411–421.

Döring, C., und, H. G.-Z. für anorganische, & 1961, undefined. (1875). Über die Kinetik der Reaktion zwischen Hydroxylamin und salpetriger Säure. *Wiley Online LibraryC Döring, H GehlenZeitschrift Für Anorganische Und Allgemeine Chemie, 1961•Wiley Online Library*, *176*(1–2), 435.

Duan, H., Ye, L., Erler, D., Ni, B. J., & Yuan, Z. (2017). Quantifying nitrous oxide production pathways in wastewater treatment systems using isotope technology - A critical review. *Water Research*, *122*, 96–113.

Duan, P., Shen, H., Jiang, X., Yan, X., & Xiong, Z. (2020). The contributions of hydroxylamine and nitrite to NO and N_2O production in alkaline and acidic vegetable soils. *Journal of Soils and Sediments*, *20*(7), 2903–2911.

Frame, C. H., & Casciotti, K. L. (2010). Biogeochemical controls and isotopic signatures of nitrous oxide production by a marine ammonia-oxidizing bacterium. *Biogeosciences*, *7*(9), 2695–2709.

Freing, A., Wallace, D. W. R., & Bange, H. W. (2012). Global oceanic production of nitrous oxide. *Philosophical Transactions of the Royal Society B: Biological Sciences*, *367*(1593), 1245.

Grabb, K. C., Buchwald, C., Hansel, C. M., & Wankel, S. D. (2017). A dual nitrite isotopic investigation of chemodenitrification by mineral-associated Fe(II) and its production of nitrous oxide. *Geochimica et Cosmochimica Acta*, *196*, 388–402.

Harper, W. F., Takeuchi, Y., Riya, S., Hosomi, M., & Terada, A. (2015). Novel abiotic reactions increase nitrous oxide production during partial nitrification: Modeling and experiments. *Chemical Engineering Journal*, *281*, 1017–1023.

Heil, J., Liu, S., Vereecken, H., & Brüggemann, N. (2015). Abiotic nitrous oxide production from hydroxylamine in soils and their dependence on soil properties. *Soil Biology and Biochemistry*, *84*, 107–115.

Heil, J., Wolf, B., Brüggemann, N., Emmenegger, L., Tuzson, B., Vereecken, H., & Mohn, J. (2014). Site-specific 15N isotopic signatures of abiotically produced N2O. *Geochimica et Cosmochimica Acta*, *139*, 72–82.

Hou, T. T., Miao, L. L., Peng, J. sen, Ma, L., Huang, Q., Liu, Y., Wu, M. R., Ai, G. M., Liu, S. J., & Liu, Z. P. (2022). Dirammox Is Widely Distributed and Dependently Evolved in Alcaligenes and Is Important to Nitrogen Cycle. *Frontiers in Microbiology*, *13*.

Ji, Q., Buitenhuis, E., Suntharalingam, P., Sarmiento, J. L., & Ward, B. B. (2018). Global Nitrous Oxide Production Determined by Oxygen Sensitivity of Nitrification and Denitrification. *Global Biogeochemical Cycles*, *32*(12), 1790–1802.

Jones, L. C., Peters, B., Lezama Pacheco, J. S., Casciotti, K. L., & Fendorf, S. (2015). Stable isotopes and iron oxide mineral products as markers of chemodenitrification. *Environmental Science and Technology*, *49*(6), 3444–3452.

Jones, M. R., Luther, G. W., & Tebo, B. M. (2020). Distribution and concentration of soluble manganese(II), soluble reactive Mn(III)-L, and particulate MnO2 in the Northwest Atlantic Ocean. *Marine Chemistry*, *226*, 103858.

Karolewski, J. S., Sutherland, K. M., Hansel, C. M., & Wankel, S. D. (2021). An isotopic study of abiotic nitrite oxidation by ligand-bound manganese (III). *Geochimica et Cosmochimica Acta*, *293*, 365–378.

Kelly, C. L., Manning, C., Frey, C., Kaiser, J., Gluschankoff, N., & Casciotti, K. L. (2023). Pyisotopomer: A Python package for obtaining intramolecular isotope ratio differences

from mass spectrometric analysis of nitrous oxide isotopocules. *Rapid Communications in Mass Spectrometry*, *37*(11), e9513.

Kits, K. D., Jung, M. Y., Vierheilig, J., Pjevac, P., Sedlacek, C. J., Liu, S., Herbold, C., Stein, L. Y., Richter, A., Wissel, H., Brüggemann, N., Wagner, M., & Daims, H. (2019). Low yield and abiotic origin of N_2O formed by the complete nitrifier Nitrospira inopinata. *Nature Communications 2019 10:1*, *10*(1), 1–12.

Kostka, J. E., Luther, G. W., & Nealson, K. H. (1995). Chemical and biological reduction of Mn (III)-pyrophosphate complexes: Potential importance of dissolved Mn (III) as an environmental oxidant. *Geochimica et Cosmochimica Acta*, *59*(5), 885–894.

Kozlowski, J. A., Stieglmeier, M., Schleper, C., Klotz, M. G., & Stein, L. Y. (2016). Pathways and key intermediates required for obligate aerobic ammonia-dependent chemolithotrophy in bacteria and Thaumarchaeota. *The ISME Journal 2016 10:8*, *10*(8), 1836–1845.

Lees, H., Sherwood, S. L., & Ridley Warren McCulloch, E. S. (1952). Hydroxylamine as an Intermediate in Nitrification. *Nature 1952 169:4291*, *169*(4291), 156–157.

Liu, S., Berns, A. E., Vereecken, H., Wu, D., & Brüggemann, N. (2017). Interactive effects of MnO2, organic matter and pH on abiotic formation of N_2O from hydroxylamine in artificial soil mixtures. *Scientific Reports 2017 7:1*, *7*(1), 1–10.

Liu, S., Han, P., Hink, L., Prosser, J. I., Wagner, M., & Brüggemann, N. (2017). Abiotic Conversion of Extracellular NH_2OH Contributes to N_2O Emission during Ammonia Oxidation. *Environmental Science and Technology*, *51*(22), 13122–13132.

Liu, S., Schloter, M., Hu, R., Vereecken, H., & Brüggemann, N. (2019). Hydroxylamine contributes more to abiotic N_2O production in soils than nitrite. *Frontiers in Environmental Science*, *7*(MAR), 449080.

Liu, S., Vereecken, H., & Brüggemann, N. (2014). A highly sensitive method for the determination of hydroxylamine in soils. *Geoderma*, *232–234*, 117–122.

Luther, G. W., Sundby, B., Lewis, B. L., Brendel, P. J., & Silverberg, N. (1997). Interactions of manganese with the nitrogen cycle: Alternative pathways to dinitrogen. *Geochimica et Cosmochimica Acta*, *61*(19), 4043–4052.

Lyman, J., & Fleming, R. (1940). Composition of sea water. *Journal of Marine Research*, *3*(2). Madison, A. S., Tebo, B. M., & Luther, G. W. (2011). Simultaneous determination of soluble manganese(III), manganese(II) and total manganese in natural (pore)waters. *Talanta*, *84*(2), 374–381.

Madison, A. S., Tebo, B. M., Mucci, A., Sundby, B., & Luther, G. W. (2013). Abundant porewater Mn(III) is a major component of the sedimentary redox system. *Science*, *341*(6148), 875–878.

McIlvin, M. R., & Altabet, M. A. (2005). Chemical conversion of nitrate and nitrite to nitrous oxide for nitrogen and oxygen isotopic analysis in freshwater and seawater. *Analytical Chemistry*, *77*(17), 5589–5595.

McIlvin, M. R., & Casciotti, K. L. (2011). Technical updates to the bacterial method for nitrate isotopic analyses. *Analytical Chemistry*, *83*(5), 1850–1856.

Mohn, J., Wolf, B., Toyoda, S., Lin, C. T., Liang, M. C., Brüggemann, N., Wissel, H., Steiker, A. E., Dyckmans, J., Szwec, L., Ostrom, N. E., Casciotti, K. L., Forbes, M., Giesemann, A., Well, R., Doucett, R. R., Yarnes, C. T., Ridley, A. R., Kaiser, J., & Yoshida, N. (2014). Interlaboratory assessment of nitrous oxide isotopomer analysis by isotope ratio

mass spectrometry and laser spectroscopy: current status and perspectives. *Rapid Communications in Mass Spectrometry : RCM*, *28*(18), 1995–2007.
Moraghan, J. T., & Buresh, R. J. (1977). Chemical Reduction of Nitrite and Nitrous Oxide by Ferrous Iron. *Soil Science Society of America Journal*, *41*(1), 47–50.
Oldham, V. E., Jones, M. R., Tebo, B. M., & Luther, G. W. (2017). Oxidative and reductive processes contributing to manganese cycling at oxic-anoxic interfaces. *Marine Chemistry*, *195*, 122–128.
Oldham, V. E., Mucci, A., Tebo, B. M., & Luther, G. W. (2017). Soluble Mn(III)–L complexes are abundant in oxygenated waters and stabilized by humic ligands. *Geochimica et Cosmochimica Acta*, *199*, 238–246.
Oldham, V. E., Owings, S. M., Jones, M. R., Tebo, B. M., & Luther, G. W. (2015). Evidence for the presence of strong Mn(III)-binding ligands in the water column of the Chesapeake Bay. *Marine Chemistry*, *171*, 58–66.
Ostrom, N. E., & Ostrom, P. H. (2017). Mining the isotopic complexity of nitrous oxide: a review of challenges and opportunities. *Biogeochemistry 2017 132:3*, *132*(3), 359–372.
Park, S., Croteau, P., Boering, K. A., Etheridge, D. M., Ferretti, D., Fraser, P. J., Kim, K. R., Krummel, P. B., Langenfelds, R. L., van Ommen, T. D., Steele, L. P., & Trudinger, C. M. (2012). Trends and seasonal cycles in the isotopic composition of nitrous oxide since 1940. *Nature Geoscience 2012 5:4*, *5*(4), 261–265.
Prather, M. J., Holmes, C. D., & Hsu, J. (2012). Reactive greenhouse gas scenarios: Systematic exploration of uncertainties and the role of atmospheric chemistry. *Geophysical Research Letters*, *39*(9), 9803.
Qian, A., Zhang, W., Shi, C., Pan, C., Giammar, D. E., Yuan, S., Zhang, H., & Wang, Z. (2019). Geochemical Stability of Dissolved Mn(III) in the Presence of Pyrophosphate as a Model Ligand: Complexation and Disproportionation. *Environmental Science and Technology*, *53*(10), 5768–5777.
Ravishankara, A. R., Daniel, J. S., & Portmann, R. W. (2009). Nitrous oxide (N_2O): the dominant ozone-depleting substance emitted in the 21st century. *Science (New York, N.Y.)*, *326*(5949), 123–125.
Rue, K., Rusevova, K., Biles, C. L., & Huling, S. G. (2018). Abiotic hydroxylamine nitrification involving manganese- and iron-bearing minerals. *The Science of the Total Environment*, *644*, 567.
Salem, I. A. (1995). A kinetic study of the homogeneous oxidation of hydroxylamine by manganese(III)-bis(salicylaldimine) complexes. *Transition Metal Chemistry*, *20*(3), 312–315.
Santoro, A. E., Buchwald, C., McIlvin, M. R., & Casciotti, K. L. (2011). Isotopic signature of N2O produced by marine ammonia-oxidizing archaea. *Science*, *333*(6047), 1282–1285.
Schreiber, F., Wunderlin, P., Udert, K. M., & Wells, G. F. (2012). Nitric oxide and nitrous oxide turnover in natural and engineered microbial communities: Biological pathways, chemical reactions, and novel technologies. *Frontiers in Microbiology*, *3*(OCT), 28255.
Schweiger, B., Hansen, H. P., & Bange, H. W. (2007). A time series of hydroxylamine (NH2OH) in the southwestern Baltic Sea. *Geophysical Research Letters*, *34*(24).
Sigman, D. M., Casciotti, K. L., Andreani, M., Barford, C., Galanter, M., & Böhlke, J. K. (2001). A bacterial method for the nitrogen isotopic analysis of nitrate in seawater and freshwater. *Analytical Chemistry*, *73*(17), 4145–4153.

Soler-Jofra, A., Pérez, J., & van Loosdrecht, M. C. M. (2021). Hydroxylamine and the nitrogen cycle: A review. *Water Research*, *190*, 116723.

Soler-Jofra, A., Picioreanu, C., Yu, R., Chandran, K., van Loosdrecht, M. C. M., & Pérez, J. (2018). Importance of hydroxylamine in abiotic N2O production during transient anoxia in planktonic axenic Nitrosomonas cultures. *Chemical Engineering Journal*, *335*, 756–762.

Soler-Jofra, A., Stevens, B., Hoekstra, M., Picioreanu, C., Sorokin, D., van Loosdrecht, M. C. M., & Pérez, J. (2016). Importance of abiotic hydroxylamine conversion on nitrous oxide emissions during nitritation of reject water. *Chemical Engineering Journal*, *287*, 720–726.

Stumm, W., & Morgan, J. J. (1996). *Aquatic chemistry: chemical equilibria and rates in natural waters*. 1022.

Su, Q., Domingo-Félez, C., Jensen, M. M., & Smets, B. F. (2019). Abiotic Nitrous Oxide (N 2 O) Production Is Strongly pH Dependent, but Contributes Little to Overall N 2 O Emissions in Biological Nitrogen Removal Systems. *Environmental Science and Technology*, *53*(7), 3508–3516.

Sundareshwar, P. v., Morris, J. T., Pellechia, P. J., Cohen, H. J., Porter, D. E., & Jones, B. C. (2001). Occurrence and ecological implications of pyrophosphate in estuaries. *Limnology and Oceanography*, *46*(6), 1570–1577.

Sutka, R. L., Ostrom, N. E., Ostrom, P. H., Breznak, J. A., Gandhi, H., Pitt, A. J., & Li, F. (2006). Distinguishing nitrous oxide production from nitrification and denitrification on the basis of isotopomer abundances. *Applied and Environmental Microbiology*, *72*(1), 638–644.

Terada, A., Sugawara, S., Hojo, K., Takeuchi, Y., Riya, S., Harper, W. F., Yamamoto, T., Kuroiwa, M., Isobe, K., Katsuyama, C., Suwa, Y., Koba, K., & Hosomi, M. (2017). Hybrid Nitrous Oxide Production from a Partial Nitrifying Bioreactor: Hydroxylamine Interactions with Nitrite. *Environmental Science and Technology*, *51*(5), 2748–2756.

Tian, Y., Yang, G. P., Liu, C. Y., Li, P. F., Chen, H. T., & Bange, H. W. (2020). Photoproduction of nitric oxide in seawater. *Ocean Science*, *16*(1), 135–148.

Thompson, R. L., Lassaletta, L., Patra, P. K., Wilson, C., Wells, K. C., Gressent, A., Koffi, E. N., Chipperfield, M. P., Winiwarter, W., Davidson, E. A., Tian, H., & Canadell, J. G. (2019). Acceleration of global N_2O emissions seen from two decades of atmospheric inversion. *Nature Climate Change*, *9*(12), 993–998.

Toyoda, S., Mutobe, H., Yamagishi, H., Yoshida, N., & Tanji, Y. (2005). Fractionation of N2O isotopomers during production by denitrifier. *Soil Biology and Biochemistry*, *37*(8), 1535–1545.

Trimmer, M., Chronopoulou, P. M., Maanoja, S. T., Upstill-Goddard, R. C., Kitidis, V., & Purdy, K. J. (2016). Nitrous oxide as a function of oxygen and archaeal gene abundance in the North Pacific. *Nature Communications 2016 7:1*, *7*(1), 1–10.

Vajrala, N., Martens-Habbena, W., Sayavedra-Soto, L. A., Schauer, A., Bottomley, P. J., Stahl, D. A., & Arp, D. J. (2013). Hydroxylamine as an intermediate in ammonia oxidation by globally abundant marine archaea. *Proceedings of the National Academy of Sciences of the United States of America*, *110*(3), 1006–1011.

van Kessel, M. A. H. J., Speth, D. R., Albertsen, M., Nielsen, P. H., Op Den Camp, H. J. M., Kartal, B., Jetten, M. S. M., & Lücker, S. (2015). Complete nitrification by a single microorganism. *Nature 2015 528:7583*, *528*(7583), 555–559.

Ward, B. B. (2008). Nitrification in Marine Systems. *Nitrogen in the Marine Environment*, 199–261.

Weigand, M. A., Foriel, J., Barnett, B., Oleynik, S., & Sigman, D. M. (2016). Updates to instrumentation and protocols for isotopic analysis of nitrate by the denitrifier method. *Rapid Communications in Mass Spectrometry*, *30*(12), 1365–1383.

Wunderlin, P., Lehmann, M. F., Siegrist, H., Tuzson, B., Joss, A., Emmenegger, L., & Mohn, J. (2013). Isotope signatures of N_2O in a mixed microbial population system: Constraints on N2O producing pathways in wastewater treatment. *Environmental Science and Technology*, *47*(3), 1339–1348.

Xu, C., Qi, M., Lin, W., & Li, X. (2022). Nitrous Oxide from Abiotic Processes of Hydroxylamine and Nitrite in Estuarine and Coastal Ecosystems: A Review. *Journal of Marine Science and Engineering 2022, Vol. 10, Page 623*, *10*(5), 623.

Yamazaki, T., Hozuki, T., Arai, K., Toyoda, S., Koba, K., Fujiwara, T., & Yoshida, N. (2014). Isotopomeric characterization of nitrous oxide produced by reaction of enzymes extracted from nitrifying and denitrifying bacteria. *Biogeosciences*, *11*(10), 2679–2689.

Yoshida, N., & Toyoda, S. (2000). Constraining the atmospheric N_2O budget from intramolecular site preference in N_2O isotopomers. *Nature 2000 405:6784*, *405*(6784), 330–334.

Yu, L., Harris, E., Lewicka-Szczebak, D., Barthel, M., Blomberg, M. R. A., Harris, S. J., Johnson, M. S., Lehmann, M. F., Liisberg, J., Müller, C., Ostrom, N. E., Six, J., Toyoda, S., Yoshida, N., & Mohn, J. (2020). What can we learn from N_2O isotope data? – Analytics, processes and modelling. *Rapid Communications in Mass Spectrometry*, *34*(20), e8858.

Zhu-Barker, X., Cavazos, A. R., Ostrom, N. E., Horwath, W. R., & Glass, J. B. (2015). The importance of abiotic reactions for nitrous oxide production. *Biogeochemistry 2015 126:3*, *126*(3), 251–267.

4. Insights into metal-mediated methane oxidation in seep sediments of the Cascadia Margin

Abstract

Anaerobic oxidation of methane (AOM) can be coupled to a variety of electron acceptors including manganese and iron; however, relatively little is understood about how various forms of oxidized metals may impact metal coupled AOM rates. In this chapter, we present a series of cold-seep sediment incubations from Cascadia Margin amended with a diverse range of oxidized manganese and iron species, including different mineral phases and soluble metal-ligand complexes. Rates of AOM were measured by tracking the incorporation of ^{13}C from labeled methane into the DIC pool over the course of 8.5 months. Overall, rates were comparable to previous studies in similar environments, however, no oxidized metal addition consistently elevated rates of AOM. In fact, many metal species treatments lowered rates below that of the unamended control. We discuss possible explanations for this trend including that coupling of AOM to metal results in greater energy yields per mol of methane or that the microbial community was unable to adapt over the course of the experiment. Despite the overall lower rates of AOM, presumed metal-AOM did appear to occur at rates up to 13 μmol CH_4 cm^{-3} yr^{-1} in incubations containing little to no sulfate.

4.1 Introduction

Methane (CH_4) is a potent greenhouse gas with a projected 28-34 larger global warming potential than that of carbon dioxide (CO_2) on a centennial time scale and is estimated to contribute to about 20% of present global warming (Myhre et al. 2014, Etminan et al. 2016). Despite its climatic relevance, estimates of oceanic contributions to the natural atmospheric methane budget remain limited (Weber et al. 2019). In marine environments, methane is primarily produced in anoxic sediments by methanogenesis. Up to 90% of this seafloor methane is then oxidized to CO_2 through microbially mediated anaerobic oxidation of methane (AOM) (Knittel and Boetius 2009). Anaerobic oxidation of methane was initially found to proceed through coupling to sulfate reduction (sulfate-AOM) performed by consortia of anaerobic methanotrophic archaea (ANME) and sulfate-reducing bacteria (SRB) (Boetius et al. 2000; Nauhaus et al. 2002); though more recently, nitrate- and nitrite-dependent AOM have also been documented (Ettwig et al. 2010;

Haroon et al. 2013; Raghoebarsing et al. 2006), reflecting a wider range of possible metabolic couplings.

Metal-dependent AOM (metal-AOM) has also been demonstrated, wherein oxidized iron (Fe) or manganese (Mn), in the form of Fe(III) and Mn(IV), may serve as electron acceptors (Fe-AOM or Mn-AOM, respectively) (Beal et al. 2009; Egger et al. 2015; Riedinger et al. 2014; Rooze et al. 2016; Sivan et al. 2011). Generally, metal-AOM has been less studied compared to sulfate-AOM, so evaluation of its distribution and rates in the environment remains poorly constrained. In the marine environment, it has been primarily studied in sediments rich in methane such as those found near cold seeps (Beal et al. 2009) or in other areas with a high degree of spatial overlap between metals and methane (Egger et al. 2015; Riedinger et al. 2014; Segarra et al. 2013; Wankel et al. 2012). In freshwater environments, most reports of AOM have stemmed from studies of metal-rich lake sediments (Crowe et al. 2011; Mostovaya et al. 2021; Norði et al. 2013; Sivan et al. 2011; Torres et al. 2014).

Several studies have compared rates of AOM when incubations are supplemented with Fe(III) oxides (ferrihydrite) or Mn(III,IV) oxides (birnessite), with no clear trend when comparing relative rates, despite thermodynamic evidence that Mn-AOM may be favored under environmental conditions (Beal et al. 2009; Ettwig et al. 2016; Segarra et al. 2013). However, only a few experiments have compared rates of metal-AOM when incubated with different forms of oxidized iron (Ettwig et al. 2016; Li et al. 2021; Scheller et al. 2016) and, to our knowledge, none has compared different forms of Mn oxides. Thus, our study fills a gap in the literature by not only comparing between Fe-AOM and Mn-AOM rates, but also examining relative differences between different forms of oxidized manganese and iron, including soluble desferrioxamine B (DFOB) complexes. In other reactions that reduce iron and manganese, for instance those catalyzed by dissimilatory metal reducing bacteria (DMRB), the chemical form of the metal has been found to impact the reactivity, with poorly crystalline oxides more quickly reduced than crystalline ones, and soluble, ligand-bound species reacting even faster (Lovley et al. 2004; Nealson and Saffarini 1994; Weber et al. 2006). Additionally, higher surface area and reactive site concentrations have been shown to result in faster reactions rates (Roden and Zachara 1996). With manganese minerals, the degree of hydration has been shown to alter the ability to accept electrons and more hydrous

phases are also prone to interacting with soluble anions (Nealson et al. 2002). Therefore, we predicted that addition of different forms of oxidized metals may impact relative rates of AOM.

Here, we present the results from experiments designed to further examine the potential role of oxidized Fe and Mn in anaerobic methane oxidation rates near seafloor cold seeps, with a focus on comparing different minerals as well as soluble ligand bound forms. In addition to AOM rate measurements, we examine changes in Fe and SO_4^{2-} concentration over time.

4.2 Methods

4.2.1 Study site description

Sediments were collected at Cascadia Margin, a convergent accretionary margin stretching between the northern tip of Vancouver Island and Cape Mendocino, Northern California where the Juan de Fuca plate under-thrusts the North American plate (Figure 1a, Kulm et al. 1986). Due to the presence of abundant methane hydrates and methane gas trapped within organic-rich sediments, this region hosts numerous active bubble flares (Johnson et al. 2015). Over 3,500 bubble streams, clustered at 1,300 sites have been documented using multibeam sonar surveys along the US Cascadia Margin (Merle et al. 2021). During August and September of 2018, areas of interest for sampling were identified using multibeam surveys aboard R/V *Falkor* and then further examined using ROV *SuBastian* (Schmidt Ocean Institute "Hunting Bubbles" Cruise – FK180824).

4.2.2 Experimental setup

Sediment collection

Sediments were collected from the vicinity of active methane seepage located along the Cascadia Margin off the coast of Oregon. Two different areas were included in this study: Hydrate Ridge (44.57° N, 125.15° W) and McArthur Canyon (45.85° N, 124.90° W) (Figure 1b). At each location, two sites were selected, one close to active bubble emission and one approximately 20 m away from any visible activity. Sediments were collected using pushcores inserted into selected areas using ROV *SuBastian*.

Preparation of minerals

The following minerals were synthesized or purchased, in preparation for sediment amendment experiments. Solid manganese treatments included manganite, δ-MnO_2, and birnessite while solid iron treatments included oxide minerals ferrihydrite and goethite, as well as clay mineral nontronite.

Manganite (MnOOH) was synthesized following Larsen et al. (1998). A solution of $MnSO_4$ (0.06 M, 1000 mL) was continuously stirred while hydrogen peroxide (8.82 M, 20.4 mL) was added, followed by addition of ammonium (0.2 M, 300 mL). The mixture was then brought to a boil on a hotplate and allowed to react for 6 hours before decanting excess supernatant. The resulting material was then washed repeatedly with deionized water and stored suspended in clean deionized water.

δ-MnO_2 was prepared as described in Villalobos et al. (2003). Potassium permanganate (0.2 M, 1280 mL) was added to sodium hydroxide (0.5 mM, 1440 mL) while stirring. Manganese chloride (0.3 M, 1280 mL) was then added to the mixture over the course of 30 minutes forming a black precipitate. Supernatant was discarded after allowing the solids to settle over the course of several hours. To remove excess hydroxide and salts, the product was repeatedly centrifuged and washed with deionized water until the overlying solvent pH measured circumneutral.

Birnessite was synthesized following previously outlined methods as follows (Mandernack et. al 1995, Golden et al. 1987). Cold sodium hydroxide (6 M, 125 mL) was added to a stirring solution of manganese chloride (0.5 M, 125 mL) while sparging with oxygen using an air stone. The resulting black solution was transferred to an ice bath and sparged for an additional 4 hours. The product was then washed with deionized water until the overlying water pH was neutral, followed by freeze drying to produce a fine black powder.

Ferrihydrite (2-line) was prepared following Schwertmann and Cornell (2000). Potassium hydroxide (0.4 M, ~330 mL) was added slowly to a flask of $Fe(NO_3)_3 \cdot 9H_2O$ (0.2 M, 500 mL) while stirring until a stable pH of 7.5 was maintained. The product was washed thoroughly with deionized water to remove electrolytes.

Goethite was synthesized according to Schwertmann and Cornell 2000. Potassium hydroxide (5 M, 180 mL) was added to a flask of $Fe(NO_3)_3 \cdot 9H_2O$ (1 M, 100 mL) while stirring vigorously. The resulting suspension was diluted with deionized water to a final volume of 2 L and held in a closed flask at 70°C for 60 hours, followed by washing to remove electrolytes.

Nontronite was purchased from the Clay Minerals Society (NAu-2) and has been extensively characterized by Keeling et al. (2000) (37.42% Fe_2O_3, 24.3% Fe)

Incubation initiation

Immediately upon recovery, cores were sealed and refrigerated at 4° C until incubations were initiated. Cores were visually inspected and the top ~5-7 cm sliced and sieved using coarse wire mesh to remove any rocks, carbonates, and other debris. Multiple cores from the same sampling site were homogenized in plastic bags and 2.5 mL of sediment aliquoted into 25 mL Balch tubes. Nutrients (4.7 mM NH_4^+, 0.4 mM PO_4^{3-}, PRO99 metal mix, F/2 media vitamin mix) were added to autoclaved and N_2-purged sulfate-free artificial sea water (ASW) and 7.5 mL of the ASW mixture were added to each tube (Lyman & Fleming, 1940). Each treatment was then amended as follows: control (unamended), killed control (chloramphenicol), sulfate (10 mM), Mn(III)-DFOB and Fe(III)-DFOB (1 mM, DFOB=desferrioxamine B). No Mn(III)-DFOB or Fe(III)-DFOB treatments were performed at sites 1 and 2. Minerals (manganite, birnessite, δ-MnO_2, nontronite, ferrihydrite, goethite) were suspended in deionized water and added such that the final concentration of added Mn or Fe was 10 mM. All treatments were prepared in triplicate, such that three tubes could be sacrificed at each timepoint. Incubation tubes were then sealed with black butyl stoppers (Geo-microbial Technologies) and aluminum crimps. Oxygen/air was removed from the headspace by inserting a needle attached to a mechanical vacuum pump (Gast) and evacuating for 10 seconds. ^{13}C-labeled methane (99%, ISOTEC) was added by injecting 1.5 mL by syringe. Unlabeled methane was then used to uniformly pressurize tubes to 29 PSI. As an initial timepoint, concentrations of iron, manganese, and sulfate as well as ^{13}C content of DIC were measured on the starting slurry, as described below.

Sampling

Incubations were stored upright in the dark at 4°C and sampled on days 35, 135, 189, and 259. Three replicate tubes per site and per treatment were sacrificed at each timepoint by venting, decrimping, and decanting overlying water for chemical and isotopic analyses as described below.

4.2.3 Chemical analyses

^{13}C-DIC measurements

Methane oxidation rates were measured as the rate of ^{13}C accumulation in the DIC pool. Samples for ^{13}C–DIC were prepared by addition of 24 µL of 0.2 µm freshly filtered overlying water from incubations to 20 mL headspace vials, crimp-sealed with gray butyl septa. Each sample was prepared and analyzed in duplicate. Concentrated phosphoric acid (10 µL) was then added to each vial to convert all DIC into CO_2 for analysis. Standards were prepared by addition of sodium bicarbonate powder (3.4 mg, 40 µmol) to pre-evacuated Tedlar bags followed by dilution with N_2-purged deionized water (400 mL) to produce 100 µM stock solutions. Two such stocks were produced, one using unlabeled bicarbonate and one using ^{13}C-labeled bicarbonate (99%, Cambridge Isotope Laboratories). Stock solutions were mixed gravimetrically through injection by Hamilton syringe into pre-weighed and crimp sealed 20 mL headspace vials (Restek) to produce standards varying from 0 to 9% ^{13}C. Phosphoric acid was added as described above. All standards were prepared in triplicate and showed excellent agreement between measured and predicted values ($r^2 \geq 0.99$). To allow for removal of any air blank from empty vials, vials containing no added bicarbonate were run alongside standards. The resulting CO_2 was then purified and trapped on a modified TraceGas (IsoPrime, Inc.) purge and trap system coupled with a Gilson autosampler before isotopic analysis on an isotope ratio mass spectrometer (IRMS) (IsoPrime 100, Elementar Inc.). Comparison of replicate samples showed typical reproducibility of ±10‰ for less enriched samples (ie. 100-200‰) and ±50‰ for highly enriched samples (ie. 500-600‰). Corrections were applied to account for any air present in the headspace of the vial. Incubation replicates were averaged, and moles of methane oxidized were calculated using Equation 1. This calculation assumes no net removal of DIC occurs and that methane is the only additional source of DIC (i.e., there is no degradation of organic matter or dissolution of carbonates). Methane oxidized vs. time was plotted and a best fit line was calculated using linear regression, where the slope is the rate of

AOM. Error was estimated by calculating the same regression with data points adjusted plus and minus one standard deviation from the mean for each data point.

Sulfate concentrations

Sulfate concentrations were measured using the barium chloride method (Vacu-vials kit, CHEMitrics). Overlying water was 0.2 µm filtered and diluted as necessary, before the addition of acid and barium chloride to the sample. The resulting turbidity due to the formation of suspended barium sulfate crystals was measured by absorbance at 420 nm. Expected accuracy was ±15% error at 75.0 ppm, ±20% error at 25.0 ppm, and ±30% at 10.0 ppm.

Iron concentrations

All iron concentration measurements were made using the ferrozine method (Viollier et al. 2000). Immediately after collection of overlying water, samples for dissolved iron were 0.2 µm filtered and 9 µL of 10% v/v HCl was added to 700 µL of filtered sample to stabilize the solution. To measure dissolved iron (II) (dFe(II)), acidified samples were then aliquoted (230 µL) into three wells of a 96 well plate and 12 µL of 6 M ammonium acetate and 12 µL of 0.01 M ferrozine were added to each well. After 1 hour, absorbance at 562 nm was measured on a microplate reader. For total dissolved iron (dFe(T)) measurements, 6 µL of 1.4 M hydroxylamine was added to each well following dFe(II) measurement and allowed to react for 2 hours. Dissolved Fe(III) was calculated by difference.

For total iron (dissolved + particulate) measurements, 9 µL of 10% v/v HCl was added to 700 µL of unfiltered overlying water and allowed to digest overnight. Sample was aliquoted (230 µL) into three replicate wells and 12 µL 6 M ammonium acetate, 12 µL 0.01 M ferrozine, and 6 µL 1.4 M hydroxylamine were added to each well. Color was allowed to develop 1 hour before measuring absorbance. Measurement of pyritic iron samples was conducted by overnight treatment with 66 µL of 10% v/v HNO_3 per 700 µL of unfiltered sample. Reagent additions and measurements were conducted as described above.

During the initial and final timepoint (t4), digests of the sediment were also performed by diluting sediment slurry 1:10 with deionized water and adding 10% v/v HCl as described for total iron

measurements above. Samples were then filtered and measured as described for dFe(II) and dFe(T). Sediment pyritic iron was also measured as described above.

Standard curves were prepared daily from stock solutions of ferrous sulfate ($FeSO_4$). Precision between replicates was generally better than 0.5 μM. Both Mn(III)-DFOB and Fe(III)-DFOB additions visibly altered the color of the samples, causing interference with absorption measurements. As such, absorbance of samples from these treatments was measured prior to addition of ferrozine, to allow for a background subtraction from final absorption measurements at 562 nm.

Gibbs free energy calculations

Gibbs free energy of formation values at 1 bar and 25° C were taken from literature (Bellotti et al 2021; Stumm and Morgan 1996; Viellard 2000). Reaction with nontronite was assumed to reduce Fe(III) to Fe(II) without significant disturbance of the mineral structure, as has been demonstrated in microbial studies (Zhao et al. 2015). The following conditions were used for *in-situ* ΔG calculations: $[CH_4]$ = 1.5 mM, $[HCO_3^-]$ = 11 mM, $[SO_4^{2-}]$ = 10 mM, $[HS^-]$ = 2 mM, [Fe(III)-DFOB] = [Mn(III)-DFOB] = 1 mM, $[Fe^{2+}] = [Mn^{2+}]$ = 1 μM, $[H^+] = 10^{-8}$ M, temperature = 4° C. Concentrations are taken either from the known amount added to incubations (CH_4, HCO_3^-, SO_4^{2-}, Fe(III)-DFOB, Mn(III)-DFOB), average of measurement performed on starting slurry (Fe^{2+}), or literature values from the site (HS^-, Mn^{2+}, H^+) (Luff and Wallman 2003).

4.3 Results

4.3.1 Methane oxidation rates

Site 1 was located close to an active bubble plume and carbonate mound at Hydrate Ridge (temperature: 4.2° C, depth: 797 m, salinity: 34.3). Methane oxidation rate in the control sediments was 3.7 ± 0.7 μmol CH_4 cm^{-3} yr^{-1} (Figure 2a, Figure 3a, Table 1). No treatments significantly increased rates of AOM. However, both manganite and δ-MnO_2 additions significantly lowered rates of AOM compared to the control as did the killed control treatment ($p < 0.05$).

Site 2 was also at Hydrate Ridge and close to Site 1 but was positioned 20 m away from any visible features of seep activity at a sediment-water interface free from carbonate structures, mats, or macrofauna (temperature: 4.3° C, depth: 787 m, salinity: 34.3). Overall compared to Site 1, Site 2

had slightly lower rates of AOM (Figure 2b, Figure 3b, Table 1). The control treatment had an AOM rate of 2.7 ± 0.2 μmol CH_4 cm^{-3} yr^{-1}. Addition of sulfate was the only treatment to show significant increases above the control (3.6 ± 0.5 μmol CH_4 cm^{-3} yr^{-1}) ($p < 0.05$). As at Site 1, rates in manganite and δ-MnO_2 treatments were both significantly lower than the control. Nontronite and killed control treatments also had noticeable declines in measured AOM rate relative to the control.

Site 3 was located near a dark microbial mat and active bubble flares at McArthur Canyon (temperature: 4.0° C, depth: 832 m, salinity: 34.4). Of all the sites examined in this study, Site 3 had the highest overall rates of AOM (Figure 2c, Figure 3c, Table 1). In many treatments, δ^{13}C-DIC values did not increase between t3 and t4 and thus rates for these treatments were calculated using data only up to t3. The unamended control had a rate of 17.8 ± 1.0 μmol CH_4 cm^{-3} yr^{-1} , nearly 5 times higher than Site 1 at Hydrate Ridge, which was also located near an area of active bubbling. Similar to Site 2, the addition of sulfate showed a significant increase in AOM rate. All four Mn treatments (manganite, birnessite, δ-MnO_2, and Mn(III)-DFOB) had markedly lower rates compared to the control. Two iron treatments (ferrihydrite and goethite) and the killed control also had significantly lower rates of AOM.

Site 4 at McArthur Canyon was close to Site 3, but positioned 20 m away from cold seep features (temperature: 4.0° C, depth: 833 m, salinity: 34.3). Rates at this site were close in magnitude to those observed at Site 1 and Site 2, and much lower than Site 3 (Figure 2d, Figure 3d, Table 1). The control treatment exhibited an AOM rate of 3.4 ± 0.5 μmol CH_4 cm^{-3} yr^{-1}. No treatments had higher rates than the control. Three out of four Mn treatments, and all of the solid Mn oxide mineral additions, (manganite, birnessite, and δ-MnO_2) had significantly lower rates of AOM compared to the unamended control. Goethite and the killed control also showed depressed AOM rates.

Among the four study sites, there were several notable trends in measured AOM rates. In both sets of geographically paired sites (Sites 1+2, Sites 3+4), the site closer to the active cold seep had higher rates of AOM overall. Addition of sulfate caused significant increases in AOM at Sites 2 and 3. Across all study sites, no oxidized metal addition significantly increased rates of AOM above those of the unamended control treatment. However, both manganite and δ-MnO_2

consistently yielded significant reductions in methane oxidation rates. There was variability across the sites as to which other Mn or Fe treatments were found to depress rates of AOM.

4.3.2 Sulfate concentrations

Sulfate concentrations were measured in the starting slurries, at t2 (control and sulfate treatments only), and t4 (all treatments) (Table 2, Figure 4). Sites 1-3 had sulfate concentrations 1-2 mM in the starting slurry, while Site 4 started at 4 mM. Site 2 and Site 4 had higher concentrations of sulfate than their corresponding near-seep sites (Site 1 and Site 3, respectively). By t2, control treatments saw large decreases in sulfate concentrations with sites 1-3 $\leq$ 0.5 mM and Site 4 measuring 2.3 mM. In the sulfate treatment at Site 3, sulfate concentration was nearly zero at t2. At the conclusion of the experiment, all sites and treatments were $\leq$ 0.4 mM. Site 3 had the lowest concentrations of sulfate overall, followed by Site 1. Excluding treatments with solid manganese mineral additions, the site closer to active seeps within geographically paired sites had lower sulfate concentrations ($p < 0.05$).

4.3.3 Iron concentrations

Dissolved iron concentrations in the incubation water (dissolved Fe(II), dissolved Fe(III), total Fe, pyritic Fe) were measured in the starting slurries and at t1, t2, and t4 (Table 3-9, Figure 5-8). Overall, iron concentrations were consistently much lower at Site 3 (maximum $\leq$ 30 μM) compared to the other sites (maximum $\geq$ 100 μM).

At Site 1, 2, and 4, control, sulfate, and birnessite treatments generally displayed increases in [dFe(II)] between t1 and t2, then decreases between t2 and t4. Concentrations of dFe(II) at the t2 maximum were comparable in control and sulfate treatments (averages: 122 μM, 132 μM respectively), but lower in birnessite treatments (average: 72 μM). At Site 2, these treatments also had increases in particulate Fe (total Fe - dFe) concentrations between t2 and t4. Pyritic iron concentrations also increased in the control and sulfate treatments. At Site 3, relatively few changes were observed among these treatments and most iron concentrations were close to zero, though a small increase in dFe(II) was observed in the sulfate treatment at t2 (8 μM).

Generally stable, near zero iron concentrations were observed in the water among the killed, manganite, and δ-MnO_2 treatments. At Site 1, a steady increase in [dFe(II)] was noted in the killed treatment. In the manganite treatment at Site 2 and Site 4, an increase in [dFe(II)] and small increase in [dFe(III)] occurred between t2 and t4. At Site 3, dFe(II) and particulate Fe concentrations rose between t2 and t4 in the δ-MnO_2 treatment.

Ferrihydrite and goethite treatments generally behaved similarly at Site 2, with an increase in pyritic iron concentration between t1 and t2 followed by a decrease between t2 and t4. Additionally, particulate iron and dFe(III) concentrations rose between t2 and t4. Similar dynamics in pyritic iron concentration were observed at Site 1 and Site 4; however, increases in particulate iron and dFe(III) concentrations were only observed in the ferrihydrite treatment. At Sites 1, 2, and 4, nontronite treatments had similar pyritic iron dynamics as ferrihydrite and goethite treatments with generally lower maxima at t2 (averages: 52 μM, 116 μM, 82 μM respectively). Particulate iron concentrations also increased between t1 and t2 and either decreased or remained constant between t2 and t4. At Site 3, iron concentrations for the goethite treatment remained close to zero and only small changes were observed in the nontronite treatment.

At Site 3, both the Mn(III)-DFOB and Fe(III)-DFOB treatments remained close to zero for all iron measurements. At Site 4, concentrations of dFe(II), dFe(III), and particulate Fe rose between t1 and t2 and then fell between t2 and t4 in the Mn(III)-DFOB treatment. Similarly to other oxidized iron treatments, the Fe(III)-DFOB treatment had a peak in pyritic iron concentration at t2 while dFe(III) and particulate iron concentration rose between t2 and t4 at Site 4.

To complement the iron measurements from the incubation waters, sediment digests (total Fe(II) and total Fe(III)) were also performed at the conclusion of the experiments (t4). Across all sites and treatments, no Fe(III) was detectable. Total Fe(II) concentration between sites and treatments varied between ~600 and 1000 μM. All iron treatments had statistically significantly higher total Fe(II) concentrations compared to control treatments at all sites ($p < 0.05$). No significant differences were found between total Fe(II) concentrations in kill or any manganese treatments compared to the control treatment.

4.4 Discussion

Rates of AOM were overall comparable to those of previous studies; however, in contrast to prior work, addition of oxidized iron or manganese did not increase measured rates of AOM above those from unamended controls. Two manganese treatments, in fact, caused rates to decrease at all four sites, which we hypothesis may be due to competition from heterotrophs. This divergence in results may also be due to other studies "pre-aging" sediments to entirely remove sulfate which may have allowed the slow growing ANME organisms to shift to metal-AOM based metabolisms prior the initiation of those experiments (Beal et al. 2009). We hypothesize the microbial community may have oxidized less methane overall in some metal treatments as metal-AOM results in higher theoretical energy yields per mole of methane. Finally, we infer the presence of metal-AOM at a site with low sulfate which suggests metal-AOM may occur under certain environmental conditions.

4.4.1 Comparison to previously reported rates of AOM

The marine sediments of the Cascadia Margin hosted substantial rates of AOM in our incubations. In environments of this type, AOM is thought to occur primarily in the sulfate-methane transition zone (SMTZ), a region found in anoxic sediments where the diffusion of sulfate downward and methane upward in the sediment overlap (Barnes and Goldberg 1976; Martens and Berner 1974; Reeburgh 2007). The depth of the SMTZ below the sediment-water interface varies widely (mm to >200 m) depending on several geochemical parameters including the input of organic matter and the rate of diffusion compared to factors controlling the microbially regulated rates of consumption of sulfate and methane (Knittel and Boetius 2009). Rates of sulfate-AOM in the environment have been found to vary across several orders of magnitude from several μmol cm^{-3} day^{-1} in cold seeps with surface methane hydrates to <1 nmol cm^{-3} day^{-1} in anoxic marine water columns. Substrate availability and oxygen concentration are believed to be the primary factors controlling the wide range of rates, with other environmental parameters such as pH, salinity, pressure, and temperature playing smaller roles (Knittel and Boetius 2009).

In contrast to expectations, the addition of oxidized forms of Fe and Mn did not universally increase rates of AOM. Generally, rates of metal-AOM in the environment have been reported from 1-60 μmol CH_4 cm^{-3} yr^{-1}, although isolating metal-AOM rates from concurrently occurring

sulfate-AOM has not always been possible (Table 12; Norði et al. 2013). Laboratory experiments have provided additional insights into estimating rates of metal-AOM and have varied from a few nmol to tens of μmol CH_4 cm^{-3} yr^{-1} (Table 13; Beal et al. 2009; Ettwig et al. 2016; Li et al. 2021; Segarra et al. 2013; Scheller et al. 2016). Several studies have also compared rates when treated with different forms of iron oxides. Scheller et al. (2016) incubated seep sediments from Santa Monica Basin with either Fe(III)-citrate, Fe(III)-EDTA, or Fe(III)-NTA. Fe(III)-citrate showed the highest rates of Fe-AOM, followed by Fe(III)-EDTA, and finally Fe(III)-NTA, suggesting the strength of the ligand may play a role in the observed reactivity and rate of metal-coupled AOM (Scheller et al. 2016). Solubility and surface area were also suggested to play an important role in determining metal-AOM rates in culture experiments conducted by Ettwig et al. (2016). Compared to nano-particulate ferrihydrite, soluble Fe(III)-citrate had approximately 13 times faster rates of Fe-AOM per g of protein day^{-1} (Ettwig et al. 2016). Li et al. (2021) compared different solid iron oxides (magnetite, goethite, and ferrihydrite) with goethite displaying the highest rates, followed by ferrihydrite, and magnetite; however, all rates were roughly comparable and the researchers cautioned that recycling of dissolved Fe(II) back to Fe(III) by putative iron oxidizer *Chlorobium* bacterium present at high relative abundance could confound their results.

Compared to literature rates, our results from oxidized metal treatments (Table 1, 0.8 - 18 μmol CH_4 cm^{-3} yr^{-1}) are similar in magnitude to other metal-addition incubations using natural aquatic sediments (Table 13, 0 - 14 μmol CH_4 cm^{-3} yr^{-1}) (Beal et al. 2009; Egger et al. 2015; Segarra et al. 2013; Sivan et al. 2011). Indeed, the rates measured in our incubations were most comparable to those of Beal et al. 2009, which also used sediments collected from marine methane seeps. However, in several of these studies, the addition of oxidized metals caused rates of AOM to increase above those of unamended control treatments, while our study did not observe any metal treatment consistently increasing rates of AOM. Instead, no individual oxidized metal treatment elevated rates of AOM above that of the live control. In all four incubations, manganite and δ-MnO_2 amendments resulted in significantly depressed rates of AOM compared to control treatments ($p < 0.05$). Similarly lowered rates of AOM were observed in rice paddy soil and lake sediments upon addition of δ-MnO_2 and in North Sea sediments upon addition of birnessite (Aromokeye et al. 2020; Kumaraswamy et al. 2001; Vigderovich et al. 2022). We speculate that our lowered rates of AOM may have been due to preferential organoclastic Mn reduction compared

to Mn-AOM. This could lower rates of AOM below that of the control if the heterotroph community stimulated by addition of manganite and δ-MnO_2 were able to outcompete ANME for a limiting nutrient required by both groups. Alternatively, the release of unlabeled CO_2 from natural organic material could depress the $\delta^{13}C$-CO_2 signal. We further discuss additional potential explanations for these results below. As in other studies, the addition of sulfate increased rates of AOM significantly, but only at Site 2 and 3 ($p < 0.05$, Beal et al. 2009; Segarra et al. 2013). Site 1 and Site 4 also had higher concentrations of sulfate at t2 compared to Site 2 and Site 3, potentially suggesting overall slower rates of sulfate-AOM (Figure 4).

4.4.2 Community energy yields

In order to compare the relative reactivities of the oxidized metals used in our incubation experiments, we calculated both ΔG^0 (at standard state conditions) and ΔG (at *in-situ* conditions) (Table 10). Notably, the *in-situ* ΔG of AOM coupled to goethite reduction was positive, indicating it would be thermodynamically unfavorable under the reaction conditions of this experiment.

Examination of Gibbs free energy yields for AOM coupled to different electron acceptors also reveals that microbes could potentially generate the same energy yield while oxidizing fewer moles of methane coupled to oxidized metal compared to sulfate (Segarra et al. 2013). For instance, using calculated *in-situ* ΔG values, oxidation of the same amount of methane yields 7 times more energy when coupled to reduction of birnessite compared to reduction of sulfate. At Site 3, we observe a rate of 33 μmol CH_4 cm^{-3} yr^{-1} for the sulfate treatment and 9.4 μmol CH_4 cm^{-3} yr^{-1} for birnessite. If we consider the energy yields, sulfate-AOM at this rate yields only 1.64 J cm^{-3} yr^{-1} compared to 3.53 J cm^{-3} yr^{-1} for birnessite-AOM (Figure 9, Table 11). In fact, we find equivalent or larger theoretical energy yields in all oxidized metal treatments across all sites compared to calculated theoretical energy yields for sulfate. This approach assumes microbes are only utilizing the added electron acceptor (i.e., no sulfate-AOM occurs in the birnessite treatment) and that solid minerals do not need to be broken down to be used; however, it illustrates the large potential gain in energy yield using oxidized metals compared to sulfate. If we instead assume the community need only produce the same energy yield as observed in the sulfate treatment, it is possible to calculate the minimum fraction of the AOM rate measured in the study that must be metal-AOM (Equation 2,3, Figure 10). Following from this, it is evident in most treatments that even a relatively modest

fraction of metal-AOM (on average ~15%) could provide the community with equivalent energy yield to that of our added sulfate treatment. These two approaches suggest potential minima and maxima for the predicted energy yields from our treatments.

Microbes performing AOM (ANME) are known to double extremely slowly (1.5 - 8 months) and thus the community may not have been able to expand rapidly when offered increased access to substrates over the course of the experiment (8.5 months) (Nauhaus et al. 2007; Zhang et al. 2011). Reports on similar incubation approaches have "aged" sediments for 12 months to eliminate residual sulfate and thereby allowed the microbial community to slowly adapt to sulfate-free conditions, thus possibly priming them for metal-AOM (Beal et al. 2009). Additionally, many questions remain as to the exact mechanisms of electron transfer between methane and solid metal oxides (Liang et al. 2019; Dang et al. 2021; Zhang et al. 2021). If ANME are in fact participating in direct interspecies electron transfer (DIET) as some researchers suggest, this could also be impeded by our incubation set-up. Li et al. (2021) found that additions of iron oxides (magnetite, goethite, and ferrihydrite) to a bioreactor containing an enrichment *Ca. "M. ferrireducens"* appreciably lowered Fe-AOM rates for >100 days and suggested that this may be due to disruption of archaeal-Fe oxide particle aggregates necessary for DIET (Li et al. 2021).

4.4.3 Inferring metal-AOM from other elements

Using the sulfate concentration data collected, we calculated overall sulfate removal rates and compared them to the AOM rates. Assuming a 1:1 stoichiometry of SO_4^{2-} to CH_4, even if all sulfate present went towards sulfate-AOM there was insufficient sulfate present to support measured methane consumption rates in nearly all treatments at site 3, including the control, all Mn treatments excluding δ-MnO_2, and all four Fe treatments. This indicates that metal-AOM must have been occurring in these treatments, even though their overall rates were not higher than the control or sulfate treatments. Inferred metal-AOM rates from Mn and Fe addition treatments varied from 5 - 13 μmol CH_4 cm^{-3} yr^{-1}. As no additional Mn or Fe was added to the control, oxidized metals already present in the sediment at Site 3 could have been responsible for this posited metal-AOM which accounted for ~40% of its overall AOM rate (13 μmol CH_4 cm^{-3} yr^{-1}). Site 3 had the lowest starting [SO_4^{2-}] of the four sites and thus its native microbial community may have been

better able to adapt to using metals in the place of sulfate or have already been performing metal-AOM *in-situ* prior to the initiation of the experiment.

It is difficult to fully close mass balance for iron as only the overlying water was measured at the majority of the timepoints. There was an intermediate accumulation of dFe(II) at t2 in several treatments including control, sulfate, and birnessite treatments from all four sites up to 163 μM (1.2 μmol total). Assuming this release of Fe^{2+} was related to Fe-AOM, this would only account for 0.2 μmol of CH_4 oxidized. This example illustrates that while rates of metal-AOM may not be as high as those of sulfate-AOM, these reactions could still significantly impact other biogeochemical cycles. The relative stoichiometry (8:1 for Fe/CH_4, 4:1 for Mn/CH_4) of metal-AOM reactions causes them to potentially be more impactful to metal cycling than carbon. Further, iron(II) can be removed from solution by reaction with sulfide to form authigenic iron sulfide minerals such as mackinawite. However, due to the constraints imposed by the method of Fe measurement used we were unable to directly measure their formation within the sediments and thus estimates of Fe-AOM solely from Fe measurements were unfeasible. Speciation of Mn in solution was not performed.

4.5 Conclusion

As the climate changes, it grows ever more urgent to understand the processes controlling the emissions of greenhouse gases such as methane. Other studies have suggested metal-AOM may be responsible for a portion of the removal of seafloor methane, thereby preventing its release to the atmosphere; however, the rates and mechanisms by which this process occurs are still poorly understood. In this study, we measured the rates of AOM from cold-seep sediments collected from four sites along the Cascadia Margin incubated with a diverse array of potentially environmentally relevant oxidized iron and manganese species. While we did not observe any consistently elevated rates of AOM due to these additions, many oxidized metal treatments in fact decreased rates of AOM below that of an unamended control, including manganite and δ-MnO_2 which lowered rates in all four incubations. We hypothesize this finding could have been related to increased energy yields to the microbial community related to coupling AOM to metal. Additionally, ANME are known to grow particularly slowly so they may not have been able to take full advantage of an increase in substrate on the timescale of the experiment. Finally, manganite and δ-MnO_2 may have

stimulated heterotrophs which competed for nutrients with ANME. Nevertheless, in the site with the lowest recorded sulfate, rates of up to 13 μmol CH_4 cm^{-3} yr^{-1} of inferred metal-AOM were observed, suggesting its role in marine sediments is non-negligible. Further study will be necessary to continue to expand our understanding of how and why different forms of oxidized iron and manganese impact rates of AOM in the environment.

$$^{12}\mathrm{CH_4} + ^{13}\mathrm{CH_4} = (1 + \frac{(1+F_{13}^*)}{F_{13}^*}) \frac{F_{13}\,^{12}\mathrm{DIC} + F_{13}\,^{13}\mathrm{DIC} + ^{13}\mathrm{DIC}}{1 - F_{13}(1 + \frac{(1-F_{13}^*)}{F_{13}^*})}$$

$$F_{13}^* = \frac{^{13}\mathrm{CH_4^*}}{^{12}\mathrm{CH_4^*} + ^{13}\mathrm{CH_4^*}}$$

$$F_{13} = \frac{^{13}\mathrm{DIC} + ^{13}\mathrm{CH_4}}{^{12}\mathrm{DIC} + ^{13}\mathrm{DIC} + ^{12}\mathrm{CH_4} + ^{13}\mathrm{CH_4}}$$

$^{12}\mathrm{CH_4}$ = moles of ^{12}C-methane oxidized

$^{13}\mathrm{CH_4}$ = moles of ^{13}C-methane oxidized

$^{12}\mathrm{CH_4^*}$ = moles of ^{12}C-methane at t_0

$^{13}\mathrm{CH_4^*}$ = moles of ^{13}C-methane at t_0

$^{12}\mathrm{DIC}$ = moles of ^{12}C-DIC at t_0

$^{13}\mathrm{DIC}$ = moles of ^{13}C-DIC at t_0

Equation 1: Formula to calculate overall moles of methane oxidized using F_{13} = the isotopic composition of total DIC measured on IRMS at a given time. For this experiment, F_{13}^* = 0.06044, ^{12}DIC = 2354 μmol, ^{13}DIC = 26.2 μmol

$$\text{AOM rate} = \text{Sulfate-AOM rate} + \text{Metal-AOM rate}$$

$$\begin{aligned}\text{Energy yield} &= \text{Sulfate-AOM energy yield} + \text{Metal-AOM energy yield} \\ &= \Delta G_{SO4}(\text{Sulfate-AOM rate}) + \Delta G_{Metal}(\text{Metal-AOM rate})\end{aligned}$$

Equations 2, 3: Calculations used to produce Figure 5. AOM rate = measured by δ^{13}C, Energy yield = energy yield from the sulfate treatment at a given site.

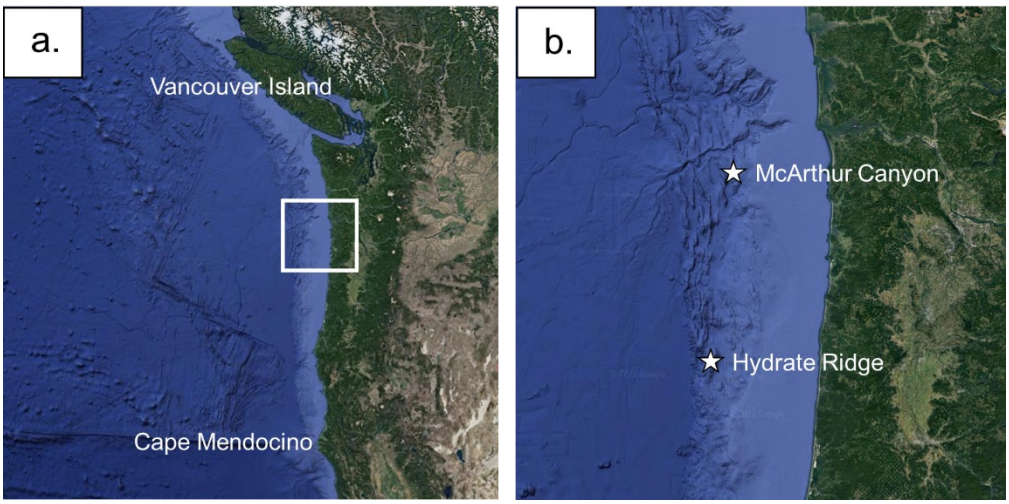

Figure 1: a. Satellite image of the west coast of the United States and Canada showing the full range of the Cascadia Margin, white box is magnified in b. Satellite image of the coast of Oregon with two major study areas marked.

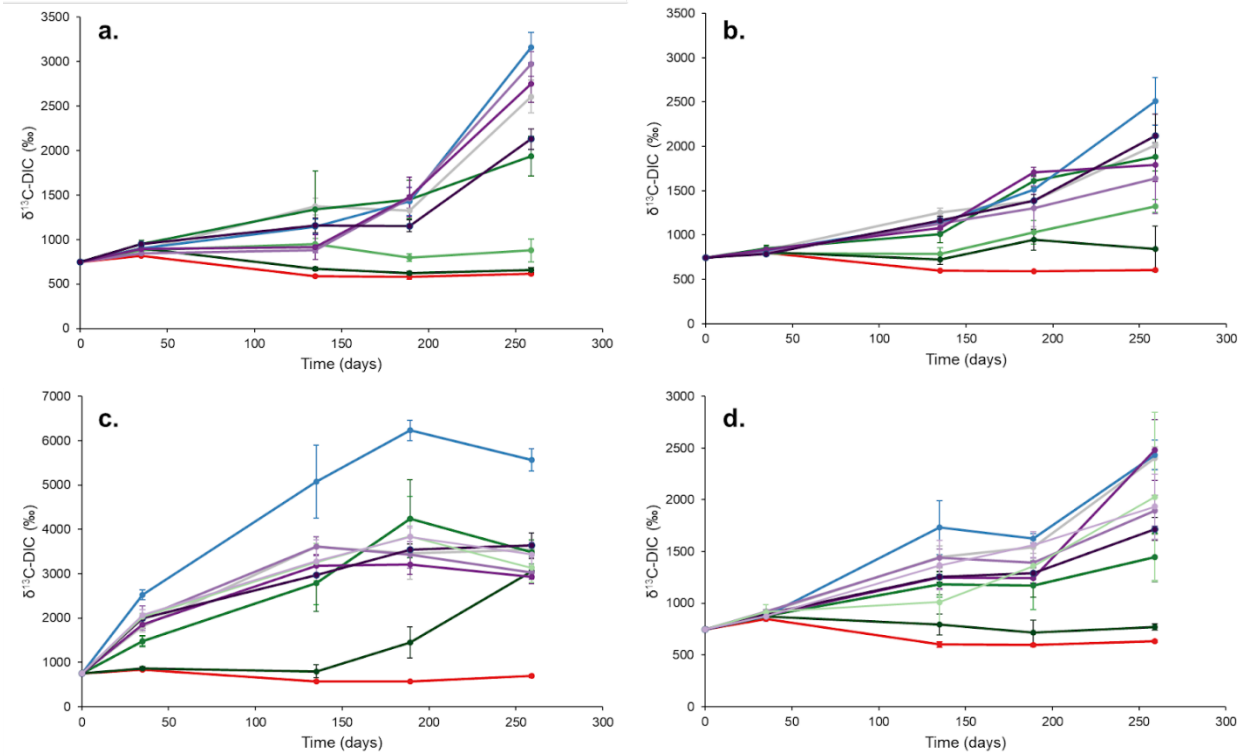

Figure 2: δ^{13}C-DIC (‰) vs. time (days) from all four incubations a. Site 1: Hydrate Ridge, near bubbles, b. Site 2: Hydrate Ridge, 20m from bubbles, c. Site 3: McArthur Canyon, microbial mat, d. Site 4: McArthur Canyon, 20m from bubbles. Oxidized Mn additions are colored in green and oxidized Fe additions are colored in purple (full color key below). No Mn(III)-DFOB or Fe(III)-DFOB treatments were conducted at Site 1 or Site 2. Error bars represent the standard deviation between three replicate tubes, measured in duplicate.

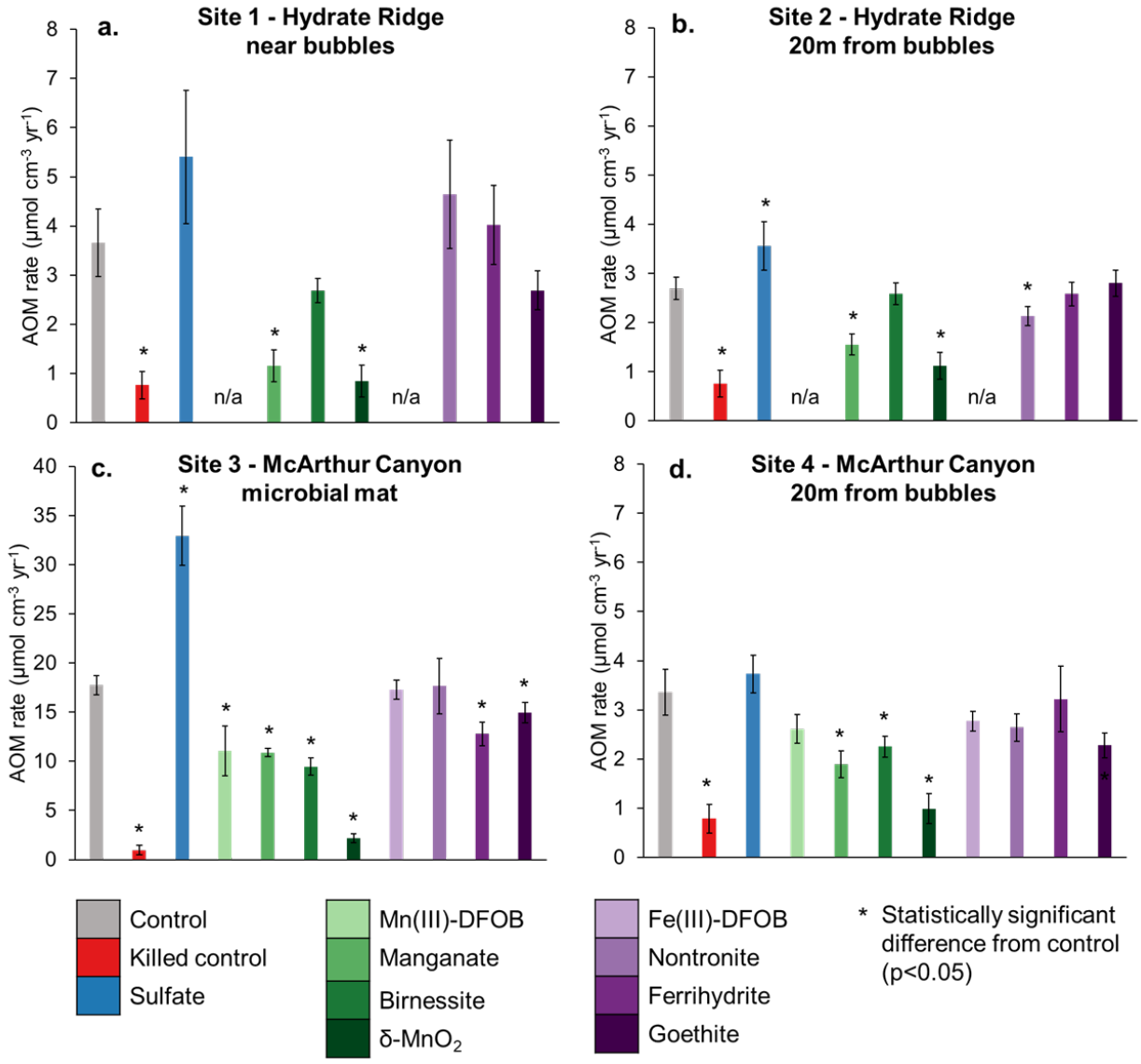

Figure 3: Rates of AOM (µmol CH_4 cm^{-3} yr^{-1}) from all four incubations. Oxidized Mn additions are colored green and oxidized Fe additions are colored purple. No Mn(III)-DFOB or Fe(III)-DFOB treatments were conducted at Site 1 or Site 2. Bars marked with a * have a statistically significant difference from the control treatment ($p < 0.05$). Error bars represent the standard deviation between three replicate tubes.

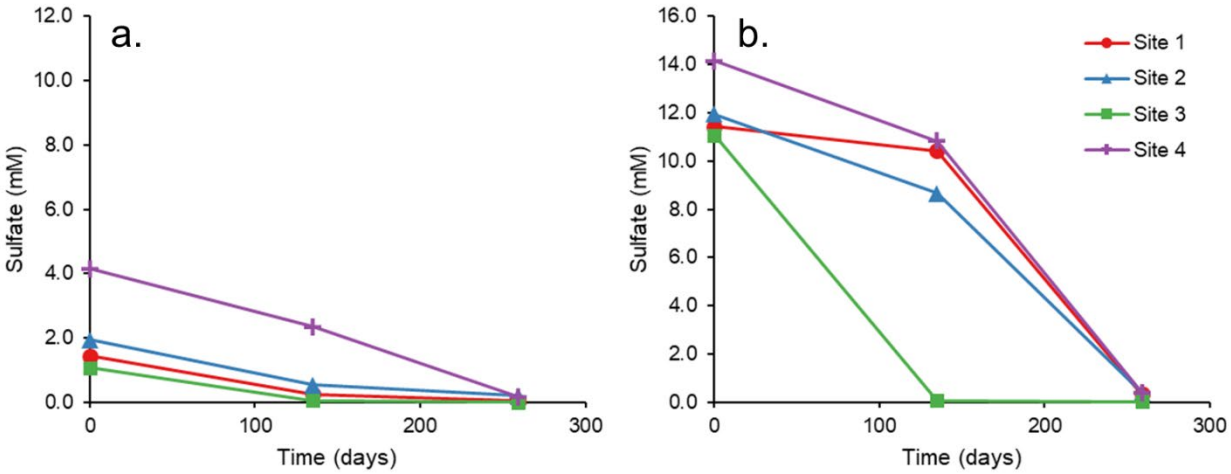

Figure 4: Sulfate concentrations (mM) vs. time (days) for the starting slurry (t0) and a. Control treatments (t2 and t4), b. Sulfate treatments (t2 and t4). t0 for sulfate treatments is calculated by adding the control values to the amount added (10mM).

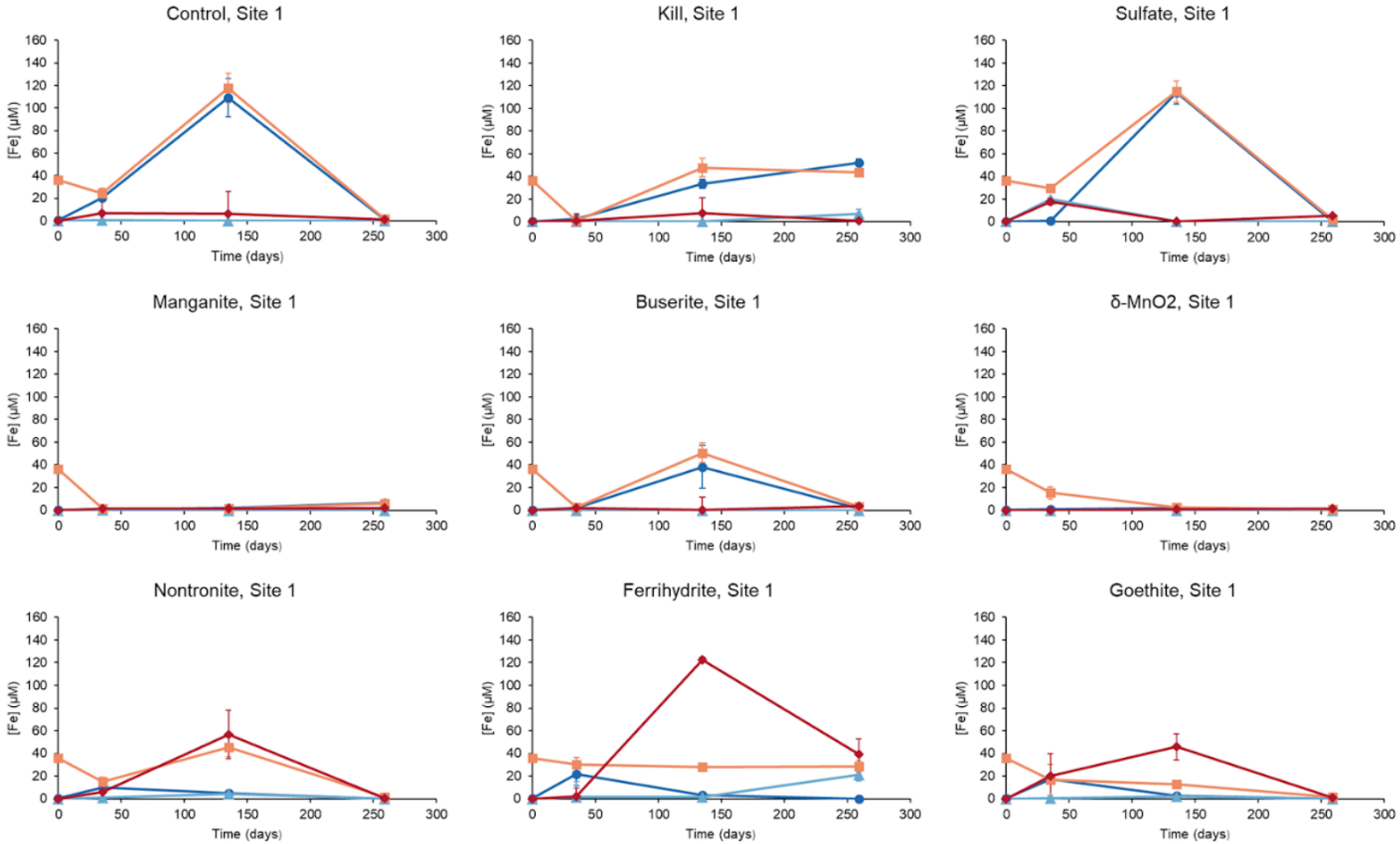

Figure 5: Site 1 iron concentrations from incubation liquid only. Dark blue: dFe(II), light blue: dFe(III), orange: total Fe (unfiltered), red: pyritic iron

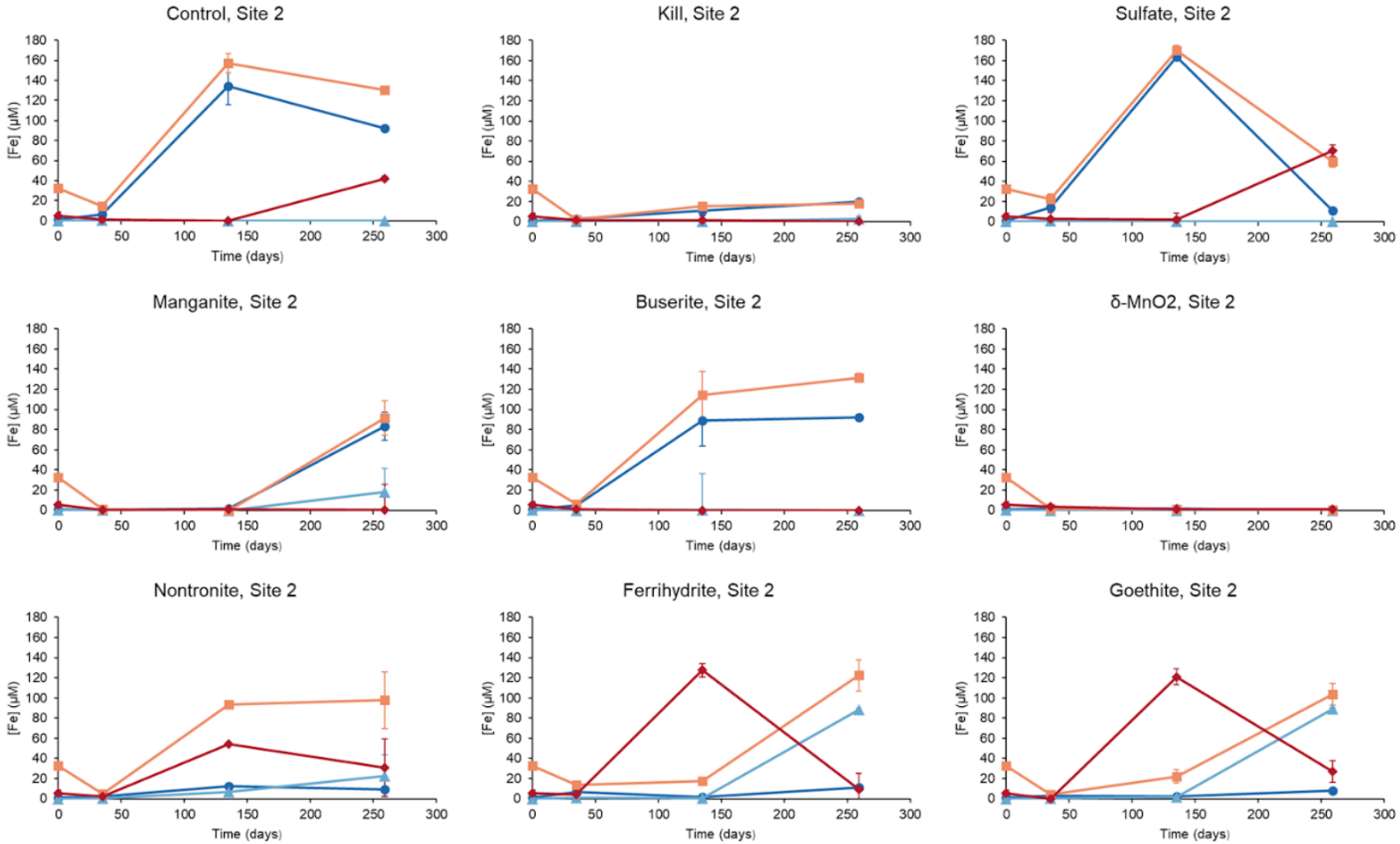

Figure 6: Site 2 iron concentrations from incubation liquid only. Dark blue: dFe(II), light blue: dFe(III), orange: total Fe (unfiltered), red: pyritic iron

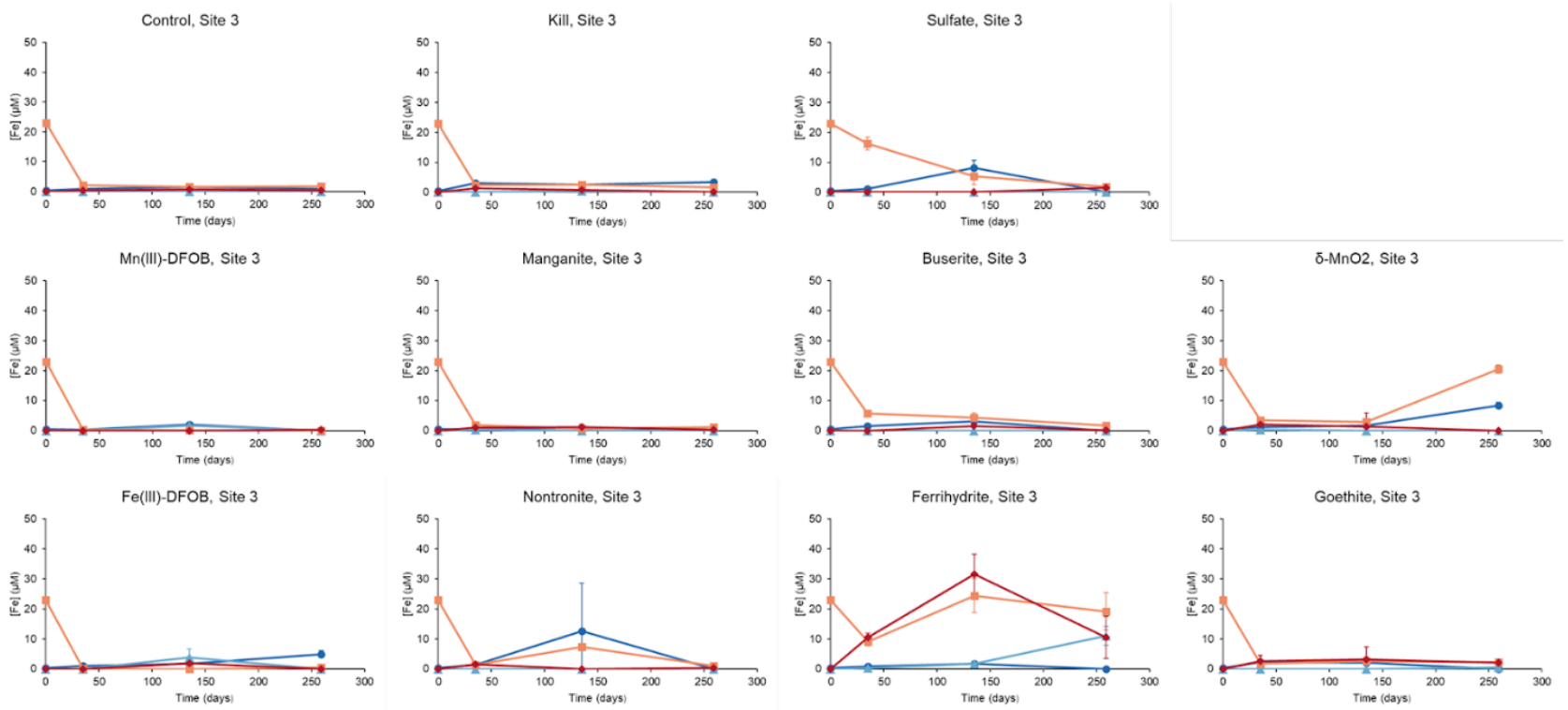

Figure 7: Site 3 iron concentrations from incubation liquid only. Dark blue: dFe(II), light blue: dFe(III), orange: total Fe (unfiltered), red: pyritic iron

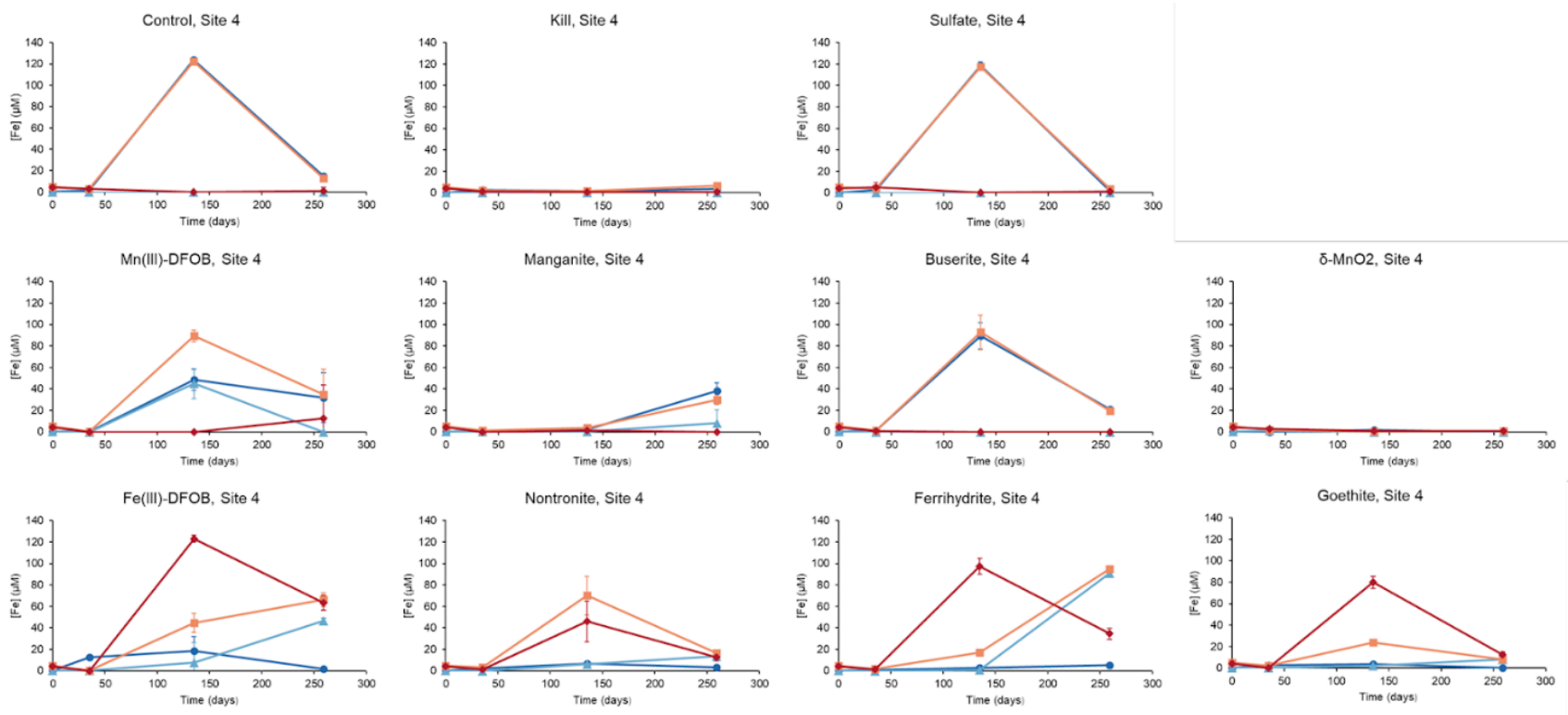

Figure 8: Site 4 iron concentrations from incubation liquid only. Dark blue: dFe(II), light blue: dFe(III), orange: total Fe (unfiltered), red: pyritic iro

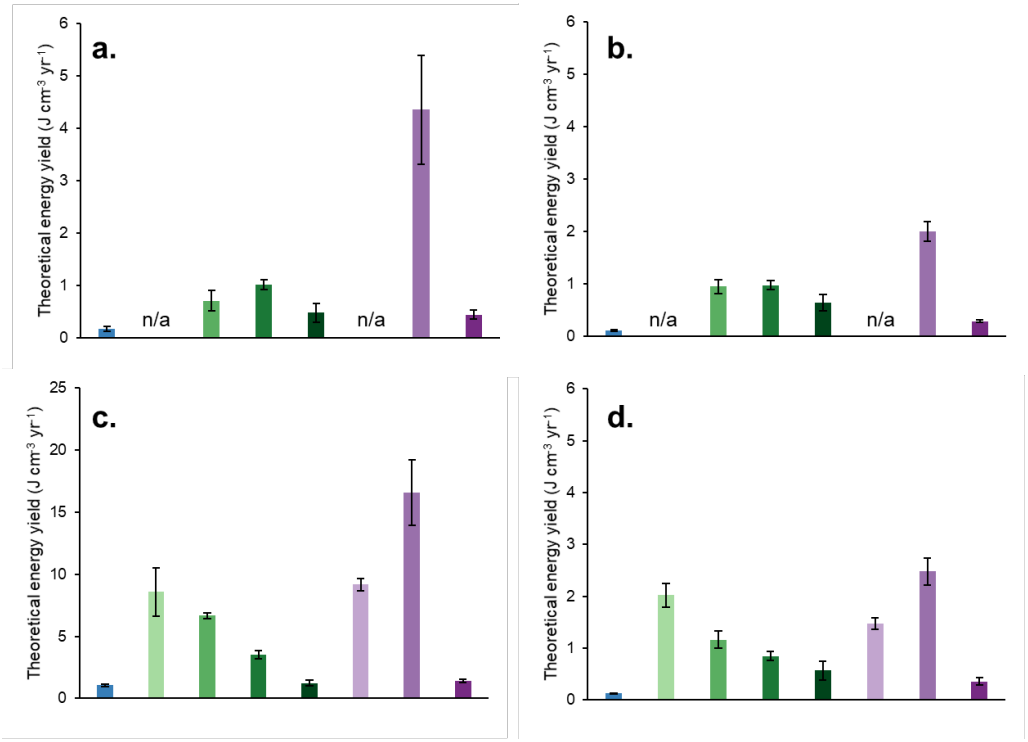

Figure 9: Theoretical energy yields assuming all measured AOM was due to the added electron acceptor.

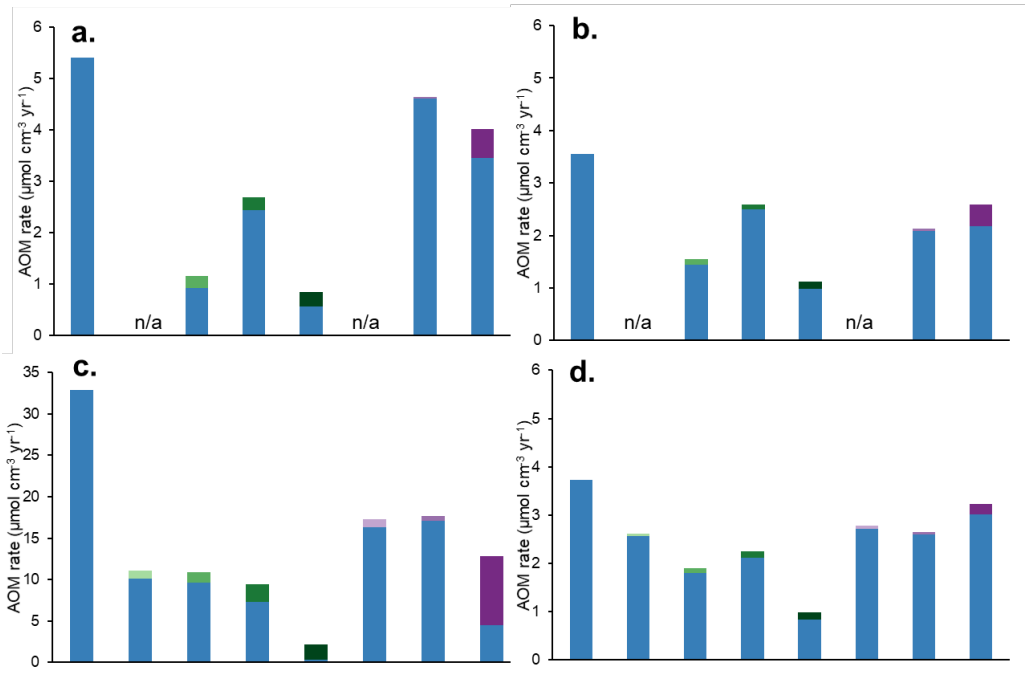

Figure 10: Total heights of bars represent the measured AOM rate at each site. Fractions are calculated such that total energy yield from the sum of sulfate-AOM and metal-AOM are equal in each bar.

Treatment	Site 1	Site 2	Site 3	Site 4
Control	3.7 ± 0.7	2.7 ± 0.2	17.8 ± 1.0	3.4 ± 0.5
Kill	0.8 ± 0.3	0.8 ± 0.3	1.0 ± 0.5	0.8 ± 0.3
Mn(III)-DFOB	n/a	n/a	11.1 ± 2.5	2.6 ± 0.3
Manganite	1.2 ± 0.3	1.6 ± 0.2	10.9 ± 0.4	1.9 ± 0.3
Birnessite	2.7 ± 0.3	2.6 ± 0.2	9.4 ± 0.9	2.3 ± 0.2
δ-MnO_2	0.8 ± 0.3	1.1 ± 0.3	2.2 ± 0.4	1.0 ± 0.3
Sulfate	5.4 ± 1.4	3.6 ± 0.5	32.9 ± 2.3	3.7 ± 0.4
Fe(III)-DFOB	n/a	n/a	17.3 ± 0.9	2.8 ± 0.2
Nontronite	4.6 ± 1.1	2.1 ± 0.2	17.6 ± 2.8	2.6 ± 0.3
Ferrihydrite	4.0 ± 0.8	2.6 ± 0.2	12.8 ± 1.2	3.2 ± 0.7
Goethite	2.7 ± 0.4	2.8 ± 0.3	15.0 ± 1.0	2.3 ± 0.3

Table 1: Rates of AOM (μmol CH_4 cm^{-3} yr^{-1}) from four incubation experiments treated with a variety of oxidized iron and manganese species, as well as sulfate and live/killed controls. Errors represent one standard deviation between three replicate tubes.

Timepoint	Treatment	Site 1	Site 2	Site 3	Site 4
t0	Starting slurry	1.44	1.95	1.06	4.15
t2	Control	0.26	0.54	0.05	2.34
	Sulfate	10.43	8.67	0.06	10.82
t4	Control	0.04	0.20	n.d.	0.16
	Kill	0.09	0.19	0.07	0.10
	Mn(III)-DFOB			0.01	0.18
	Manganite	0.24	0.23	0.01	0.26
	Buserite	0.16	0.17	0.02	0.10
	δ-MnO_2	0.25	0.22	0.03	0.18
	Sulfate	0.34	0.40	0.03	0.41
	Fe(III)-DFOB			0.03	0.25
	Nontronite	0.11	0.24	0.01	0.22
	Ferrihydrite	0.09	0.19	0.02	0.19
	Goethite	0.11	0.20	0.01	0.19

Table 2: Sulfate concentrations (mM) from starting slurry and incubation timepoints. n.d. = below detection limit. Accuracy expectations are ±15% error at 0.78 mM, ±20% error at 0.26 mM, and ±30% at 0.10 mM.

	Timepoint	Control	Kill	Manganite	Buserite	δ-MnO_2	Sulfate	Nontronite	Ferrihydrite	Goethite
dFe(II)	t0	0.28 ± 0.10	0.28 ± 0.10	0.28 ± 0.10	0.28 ± 0.10	0.28 ± 0.10	0.28 ± 0.10	0.28 ± 0.10	0.28 ± 0.10	0.28 ± 0.10
	t1	20.58 ± 0.15	2.57 ± 0.15	0.63 ± 0.28	1.74 ± 0.47	1.13 ± 0.15	1.02 ± 0.09	9.80 ± 3.51	21.56 ± 9.70	17.40 ± 0.40
	t2	109.04 ± 17.08	33.46 ± 4.19	1.77 ± 0.69	38.22 ± 18.71	2.21 ± 0.59	113.96 ± 10.17	4.77 ± 0.68	3.08 ± 0.37	2.75 ± 0.56
	t4	0.94 ± 0.60	52.05 ± 3.10	6.65 ± 0.97	1.24 ± 0.16	n.d.	n.d.	n.d.	n.d.	n.d.
dFe(T)	t0	0.28 ± 0.07	0.28 ± 0.07	0.28 ± 0.07	0.28 ± 0.07	0.28 ± 0.07	0.28 ± 0.07	0.28 ± 0.07	0.28 ± 0.07	0.28 ± 0.07
	t1	21.02 ± 0.32	2.52 ± 0.21	0.96 ± 0.25	1.48 ± 0.58	1.10 ± 0.17	20.94 ± 1.05	10.58 ± 3.21	23.04 ± 9.47	17.52 ± 1.09
	t2	108.68 ± 17.21	33.30 ± 4.10	1.66 ± 0.73	38.21 ± 18.64	1.88 ± 0.59	113.32 ± 10.31	8.92 ± 1.39	4.32 ± 0.19	4.74 ± 1.07
	t4	0.75 ± 0.60	59.26 ± 2.17	5.89 ± 1.30	0.86 ± 0.41	n.d.	n.d.	n.d.	21.01 ± 5.66	n.d.
dFe(III)	t0	n.d.	n.d.	n.d.	n.d.	n.d.	n.d.	n.d.	n.d.	n.d.
	t1	0.43 ± 0.36	n.d.	0.33 ± 0.37	n.d.	n.d.	19.91 ± 1.06	0.78 ± 4.76	1.47 ± 13.55	0.12 ± 1.16
	t2	n.d.	n.d.	n.d.	n.d.	n.d.	n.d.	4.14 ± 1.55	1.24 ± 0.42	2.00 ± 1.21
	t4	n.d.	7.21 ± 3.78	n.d.	n.d.	n.d.	n.d.	n.d.	21.01 ± 5.68	n.d.
Fe(III)%	t0	0.00	0.00	0.00	0.00	0.00	0.00	0.00	0.00	0.00
	t1	2.05	0.00	34.61	0.00	0.00	95.11	7.34	6.40	0.67
	t2	0.00	0.00	0.00	0.00	0.00	0.00	46.45	28.74	42.10
	t4	0.00	12.17	0.00	0.00	n/a	n/a	n/a	100.00	n/a
Total Fe	t0	36.06 ± 0.19	36.06 ± 0.19	36.06 ± 0.19	36.06 ± 0.19	36.06 ± 0.19	36.06 ± 0.19	36.06 ± 0.19	36.06 ± 0.19	36.06 ± 0.19
	t1	24.50 ± 4.01	1.02 ± 0.02	1.44 ± 0.58	2.72 ± 0.16	15.22 ± 5.48	29.38 ± 1.32	15.14 ± 3.57	30.14 ± 6.18	16.86 ± 13.43
	t2	117.64 ± 13.13	47.62 ± 8.19	1.41 ± 1.10	50.61 ± 8.53	2.54 ± 1.51	114.88 ± 9.25	45.50 ± 8.71	28.06 ± 2.34	12.67 ± 0.72
	t4	1.46 ± 0.36	43.46 ± 2.93	5.65 ± 1.29	2.88 ± 0.29	0.87 ± 0.04	1.71 ± 0.13	1.75 ± 0.78	28.48 ± 4.83	1.54 ± 0.14
FeS	t0	n.d.	n.d.	n.d.	n.d.	n.d.	n.d.	n.d.	n.d.	n.d.
	t1	6.70 ± 13.06	1.04 ± 5.89	1.66 ± 1.04	1.91 ± 1.29	n.d.	17.80 ± 2.71	6.11 ± 4.48	1.95 ± 7.27	19.82 ± 19.85
	t2	6.27 ± 19.67	7.43 ± 13.46	1.23 ± 1.39	0.10 ± 11.26	1.12 ± 1.99	n.d.	56.62 ± 21.62	122.52 ± 2.39	45.76 ± 11.47
	t4	1.08 ± 0.96	1.04 ± 5.89	2.24 ± 3.10	3.70 ± 0.88	1.56 ± 0.25	5.35 ± 0.58	0.58 ± 0.91	39.07 ± 13.60	0.86 ± 0.29
Digest Fe(II)	t4	648.15 ± 110.89	702.79 ± 19.07	812.03 ± 29.12	853.60 ± 22.06	780.79 ± 26.16	919.06 ± 9.64	928.62 ± 33.21	953.63 ± 23.95	957.58 ± 9.82
Digest Fe(T)	t4	628.73 ± 108.07	698.40 ± 20.45	806.70 ± 31.03	844.83 ± 21.29	731.72 ± 22.88	910.90 ± 10.28	920.65 ± 32.22	943.38 ± 21.83	943.81 ± 8.91
Digest Fe(III)	t4	n.d.	n.d.	n.d.	n.d.	n.d.	n.d.	n.d.	n.d.	n.d.

Table 3: Site 1 iron concentrations (μM). Errors represent the standard deviations between three replicate incubation tubes measured in triplicate. n.d. = below detection limit.

	Timepoint	Control	Kill	Manganite	Buserite	δ-MnO_2	Sulfate	Nontronite	Ferrihydrite	Goethite
dFe(II)	t0	0.97 ± 0.05	0.97 ± 0.05	0.97 ± 0.05	0.97 ± 0.05	0.97 ± 0.05	0.97 ± 0.05	0.97 ± 0.05	0.97 ± 0.05	0.97 ± 0.05
	t1	6.07 ± 1.02	2.52 ± 0.02	0.51 ± 0.10	4.68 ± 0.71	1.29 ± 0.38	14.49 ± 0.64	2.09 ± 0.65	6.94 ± 2.75	2.83 ± 0.66
	t2	134.53 ± 19.03	11.14 ± 0.98	1.91 ± 0.70	89.07 ± 25.60	1.63 ± 0.11	163.75 ± 3.28	12.59 ± 0.85	1.82 ± 0.37	2.32 ± 0.19
	t4	92.49 ± 0.54	20.15 ± 2.49	83.58 ± 13.94	92.30 ± 1.05	n.d.	11.14 ± 1.04	9.33 ± 0.21	10.90 ± 1.16	7.81 ± 0.73
dFe(T)	t0	1.05 ± 0.04	1.05 ± 0.04	1.05 ± 0.04	1.05 ± 0.04	1.05 ± 0.04	1.05 ± 0.04	1.05 ± 0.04	1.05 ± 0.04	1.05 ± 0.04
	t1	6.60 ± 1.63	2.41 ± 0.04	0.90 ± 0.15	4.51 ± 0.75	1.28 ± 0.41	15.18 ± 0.97	2.43 ± 1.10	8.19 ± 2.84	3.08 ± 0.79
	t2	134.07 ± 18.95	10.95 ± 1.09	1.78 ± 0.70	89.36 ± 25.56	1.52 ± 0.06	162.90 ± 2.72	19.15 ± 0.27	2.53 ± 0.38	4.06 ± 0.59
	t4	91.64 ± 0.57	22.74 ± 1.24	101.82 ± 18.76	90.77 ± 1.52	n.d.	10.79 ± 1.36	31.74 ± 21.03	99.05 ± 1.34	97.15 ± 1.00
dFe(III)	t0	0.08 ± 0.06	0.08 ± 0.06	0.08 ± 0.06	0.08 ± 0.06	0.08 ± 0.06	0.08 ± 0.06	0.08 ± 0.06	0.08 ± 0.06	0.08 ± 0.06
	t1	0.53 ± 1.93	n.d.	0.39 ± 0.18	n.d.	n.d.	0.68 ± 1.16	0.34 ± 1.28	1.25 ± 3.95	0.25 ± 1.03
	t2	n.d.	n.d.	n.d.	0.29 ± 36.17	n.d.	n.d.	6.56 ± 0.89	0.71 ± 0.53	1.74 ± 0.62
	t4	n.d.	2.58 ± 2.78	18.24 ± 23.37	n.d.	n.d.	n.d.	22.40 ± 21.03	88.15 ± 1.77	89.35 ± 1.23
Fe(III)%	t0	7.92	7.92	7.92	7.92	7.92	7.92	7.92	7.92	7.92
	t1	8.04	0.00	43.65	0.00	0.00	4.49	14.02	15.29	8.19
	t2	0.00	0.00	0.00	0.33	0.00	0.00	34.27	27.93	42.84
	t4	0.00	11.36	17.92	0.00	n/a	0.00	70.60	89.00	91.96
Total Fe	t0	32.60 ± 2.35	32.60 ± 2.35	32.60 ± 2.35	32.60 ± 2.35	32.60 ± 2.35	32.60 ± 2.35	32.60 ± 2.35	32.60 ± 2.35	32.60 ± 2.35
	t1	14.63 ± 0.15	2.18 ± 0.06	1.20 ± 0.25	6.32 ± 0.76	1.37 ± 0.43	22.27 ± 5.08	4.55 ± 3.17	13.72 ± 2.46	4.04 ± 0.38
	t2	157.07 ± 9.52	15.72 ± 2.58	n.d.	114.17 ± 23.76	0.88 ± 1.03	170.29 ± 4.87	93.78 ± 1.79	17.45 ± 3.34	22.09 ± 6.68
	t4	130.25 ± 1.23	18.06 ± 1.83	91.54 ± 16.82	131.66 ± 3.91	0.64 ± 0.05	59.51 ± 5.65	97.63 ± 28.43	122.47 ± 15.69	103.54 ± 10.89
FeS	t0	5.24 ± 3.36	5.24 ± 3.36	5.24 ± 3.36	5.24 ± 3.36	5.24 ± 3.36	5.24 ± 3.36	5.24 ± 3.36	5.24 ± 3.36	5.24 ± 3.36
	t1	0.90 ± 1.76	1.74 ± 1.90	0.54 ± 0.76	0.96 ± 1.15	3.61 ± 0.57	2.74 ± 6.31	2.27 ± 3.77	4.45 ± 4.93	n.d.
	t2	n.d.	1.52 ± 4.72	0.71 ± 0.18	n.d.	0.81 ± 1.09	2.39 ± 5.78	54.13 ± 1.82	127.57 ± 6.68	121.02 ± 8.01
	t4	42.12 ± 2.21	n.d.	0.38 ± 25.04	n.d.	1.26 ± 0.79	70.73 ± 5.69	31.00 ± 28.43	9.31 ± 15.72	26.95 ± 10.90
Digest Fe(II)	t4	813.57 ± 26.50	762.58 ± 23.19	868.48 ± 23.17	890.19 ± 17.61	835.31 ± 22.23	928.75 ± 44.75	947.52 ± 26.42	988.56 ± 19.03	1012.40 ± 29.95
Digest Fe(T)	t4	779.56 ± 30.48	759.37 ± 23.05	861.63 ± 24.26	882.57 ± 17.55	793.81 ± 20.85	920.46 ± 45.38	939.72 ± 24.54	980.15 ± 18.73	999.80 ± 30.88
Digest Fe(III)	t4	n.d.	n.d.	n.d.	n.d.	n.d.	n.d.	n.d.	n.d.	n.d.

Table 4: Site 2 iron concentrations (μM). Errors represent the standard deviations between three replicate incubation tubes measured in triplicate. n.d. = below detection limit.

	Timepoint	Control	Kill	Mn(III)-DFOB	Manganite	Buserite	δ-MnO_2	Sulfate	Fe(III)-DFOB	Nontronite	Ferrihydrite	Goethite
dFe(II)	t0	0.37 ± 0.22	0.37 ± 0.22	0.37 ± 0.22	0.37 ± 0.22	0.37 ± 0.22	0.37 ± 0.22	0.37 ± 0.22	0.37 ± 0.22	0.37 ± 0.22	0.37 ± 0.22	0.37 ± 0.22
	t1	0.89 ± 0.05	3.01 ± 0.07	0.20 ± 0.18	0.42 ± 0.07	1.45 ± 0.07	1.13 ± 0.07	1.10 ± 0.14	0.91 ± 0.04	1.31 ± 0.35	0.78 ± 0.12	2.25 ± 0.06
	t2	1.51 ± 0.36	2.45 ± 0.01	2.10 ± 0.21	1.03 ± 0.07	3.03 ± 0.12	1.72 ± 0.27	9.45 ± 1.61	1.63 ± 2.33	12.60 ± 16.01	1.73 ± 0.24	2.04 ± 0.97
	t4	0.89 ± 0.76	3.40 ± 0.60	n.d.	0.20 ± 0.15	n.d.	8.33 ± 1.09	n.d.	4.94 ± 1.21	n.d.	n.d.	n.d.
dFe(T)	t0	0.18 ± 0.03	0.18 ± 0.03	0.18 ± 0.03	0.18 ± 0.03	0.18 ± 0.03	0.18 ± 0.03	0.18 ± 0.03	0.18 ± 0.03	0.18 ± 0.03	0.18 ± 0.03	0.18 ± 0.03
	t1	0.79 ± 0.07	2.90 ± 0.06	n.d.	0.77 ± 0.05	0.99 ± 0.22	1.37 ± 0.30	1.06 ± 0.15	0.45 ± 0.05	1.15 ± 0.43	1.00 ± 0.24	2.27 ± 0.09
	t2	1.36 ± 0.27	2.91 ± 1.12	3.77 ± 0.20	1.00 ± 0.04	3.00 ± 0.09	1.51 ± 0.31	8.08 ± 2.63	5.38 ± 1.84	11.92 ± 15.42	3.47 ± 0.90	1.54 ± 0.85
	t4	0.80 ± 0.80	2.17 ± 0.84	n.d.	n.d.	n.d.	6.84 ± 0.44	n.d.	3.55 ± 0.78	n.d.	10.98 ± 3.16	0.44 ± 0.30
dFe(III)	t0	n.d.	n.d.	n.d.	n.d.	n.d.	n.d.	n.d.	n.d.	n.d.	n.d.	n.d.
	t1	n.d.	n.d.	n.d.	0.35 ± 0.09	n.d.	0.25 ± 0.31	n.d.	n.d.	n.d.	0.22 ± 0.27	0.02 ± 0.11
	t2	n.d.	0.46 ± 1.12	1.67 ± 0.29	n.d.	n.d.	n.d.	n.d.	3.74 ± 2.97	n.d.	1.73 ± 0.93	n.d.
	t4	n.d.	n.d.	n.d.	n.d.	n.d.	n.d.	n.d.	n.d.	n.d.	10.98 ± 3.16	0.44 ± 0.43
Fe(III)%	t0	0.00	0.00	0.00	0.00	0.00	0.00	0.00	0.00	0.00	0.00	0.00
	t1	0.00	0.00	0.00	45.68	0.00	17.92	0.00	0.00	0.00	22.30	0.83
	t2	0.00	15.82	44.36	0.00	0.00	0.00	0.00	69.63	0.00	50.01	0.00
	t4	0.00	0.00	n/a	0.00	n/a	0.00	n/a	n/a	0.00	100.00	100.00
Total Fe	t0	22.92 ± 0.62	22.92 ± 0.62	22.92 ± 0.62	22.92 ± 0.62	22.92 ± 0.62	22.92 ± 0.62	22.92 ± 0.62	22.92 ± 0.62	22.92 ± 0.62	22.92 ± 0.62	22.92 ± 0.62
	t1	2.18 ± 0.61	2.33 ± 0.06	0.26 ± 0.26	1.86 ± 0.13	5.68 ± 0.43	3.49 ± 0.82	16.21 ± 2.09	0.08 ± 0.02	1.39 ± 0.19	9.05 ± 1.43	1.66 ± 0.43
	t2	1.61 ± 0.16	2.60 ± 0.28	0.04 ± 0.01	0.57 ± 0.63	4.37 ± 1.58	2.84 ± 3.01	5.27 ± 2.67	n.d.	7.30 ± 0.64	24.47 ± 5.64	2.55 ± 1.41
	t4	1.68 ± 0.40	1.72 ± 0.18	n.d.	1.19 ± 0.25	1.61 ± 0.23	20.47 ± 1.41	1.90 ± 0.11	0.52 ± 0.02	1.06 ± 0.20	19.17 ± 6.30	2.31 ± 0.17
FeS	t0	n.d.	n.d.	n.d.	n.d.	n.d.	n.d.	n.d.	n.d.	n.d.	n.d.	n.d.
	t1	0.26 ± 0.83	1.29 ± 0.36	n.d.	1.05 ± 0.66	n.d.	2.03 ± 0.82	n.d.	n.d.	1.46 ± 0.56	10.46 ± 1.49	2.63 ± 1.82
	t2	0.66 ± 0.43	0.71 ± 0.31	n.d.	1.15 ± 0.89	1.45 ± 2.92	1.29 ± 4.64	n.d.	1.82 ± 0.95	n.d.	31.66 ± 6.64	3.19 ± 4.21
	t4	0.40 ± 0.47	n.d.	0.25 ± 0.18	0.28 ± 0.40	0.17 ± 0.67	n.d.	1.53 ± 0.49	n.d.	0.36 ± 0.28	10.51 ± 7.08	2.07 ± 0.44
Digest Fe(II)	t4	647.11 ± 19.25	619.30 ± 28.85	712.30 ± 25.72	760.74 ± 81.71	704.27 ± 34.35	731.95 ± 17.34	788.20 ± 9.29	845.94 ± 10.80	805.12 ± 44.19	889.71 ± 20.41	876.78 ± 37.48
Digest Fe(T)	t4	638.78 ± 25.14	614.95 ± 27.50	707.50 ± 24.88	752.92 ± 80.32	696.36 ± 33.44	709.16 ± 19.28	781.58 ± 9.42	834.61 ± 10.44	794.77 ± 45.44	877.78 ± 20.38	869.40 ± 35.66
Digest Fe(III)	t4	n.d.	n.d.	n.d.	n.d.	n.d.	n.d.	n.d.	n.d.	n.d.	n.d.	n.d.

Table 5: Site 3 iron concentrations (μM). Errors represent the standard deviations between three replicate incubation tubes measured in triplicate. n.d. = below detection limit.

	Timepoint	Control	Kill	Mn(III)-DFOB	Manganite	Buserite	δ-MnO_2	Sulfate	Fe(III)-DFOB	Nontronite	Ferrihydrite	Goethite
dFe(II)	t0	0.25 ± 0.05	0.25 ± 0.05	0.25 ± 0.05	0.25 ± 0.05	0.25 ± 0.05	0.25 ± 0.05	0.25 ± 0.05	0.25 ± 0.05	0.25 ± 0.05	0.25 ± 0.05	0.25 ± 0.05
	t1	1.26 ± 0.49	2.46 ± 0.06	0.21 ± 0.07	0.56 ± 0.34	1.06 ± 0.08	n.d.	2.62 ± 0.71	12.76 ± 1.22	2.49 ± 0.32	0.95 ± 0.10	2.66 ± 0.18
	t2	123.82 ± 1.91	1.56 ± 0.03	48.42 ± 9.87	2.19 ± 0.40	89.48 ± 12.44	1.59 ± 0.22	118.42 ± 3.70	18.41 ± 13.37	6.80 ± 0.37	2.64 ± 0.27	3.46 ± 0.82
	t4	14.86 ± 2.57	3.47 ± 0.67	31.92 ± 23.21	38.31 ± 7.26	20.79 ± 0.30	n.d.	1.86 ± 0.16	1.95 ± 1.01	3.37 ± 0.54	5.04 ± 0.63	n.d.
dFe(T)	t0	0.36 ± 0.21	0.36 ± 0.21	0.36 ± 0.21	0.36 ± 0.21	0.36 ± 0.21	0.36 ± 0.21	0.36 ± 0.21	0.36 ± 0.21	0.36 ± 0.21	0.36 ± 0.21	0.36 ± 0.21
	t1	1.24 ± 0.55	2.38 ± 0.04	n.d.	0.90 ± 1.31	0.65 ± 0.06	1.31 ± 0.26	2.61 ± 0.84	12.85 ± 1.24	2.55 ± 0.47	0.97 ± 0.20	2.75 ± 0.22
	t2	123.47 ± 1.84	1.41 ± 0.13	93.34 ± 9.80	2.22 ± 0.46	89.36 ± 12.68	1.40 ± 0.8	115.45 ± 2.51	25.92 ± 13.65	13.07 ± 0.59	3.48 ± 0.64	5.79 ± 1.26
	t4	14.61 ± 2.52	2.84 ± 1.75	31.39 ± 23.81	46.56 ± 10.07	20.66 ± 0.19	n.d.	1.54 ± 0.29	48.78 ± 2.22	16.93 ± 2.83	96.23 ± 0.24	8.00 ± 1.02
dFe(III)	t0	0.11 ± 0.22	0.11 ± 0.22	0.11 ± 0.22	0.11 ± 0.22	0.11 ± 0.22	0.11 ± 0.22	0.11 ± 0.22	0.11 ± 0.22	0.11 ± 0.22	0.11 ± 0.22	0.11 ± 0.22
	t1	n.d.	n.d.	n.d.	0.35 ± 0.46	n.d.	1.31 ± 0.27	n.d.	0.09 ± 1.75	0.06 ± 0.57	0.02 ± 0.23	0.10 ± 0.28
	t2	n.d.	n.d.	44.92 ± 13.91	0.03 ± 0.61	n.d.	n.d.	n.d.	7.51 ± 19.11	6.27 ± 0.70	0.84 ± 0.69	2.32 ± 1.51
	t4	n.d.	n.d.	n.d.	8.25 ± 12.42	n.d.	n.d.	n.d.	46.83 ± 2.44	13.56 ± 2.88	91.19 ± 0.68	8.00 ± 1.02
Fe(III)%	t0	30.29	30.29	30.29	30.29	30.29	30.29	30.29	30.29	30.29	30.29	30.29
	t1	0.00	0.00	0.00	38.21	0.00	100.00	0.00	0.67	2.43	1.58	3.48
	t2	0.00	0.00	48.12	1.22	0.00	0.00	0.00	28.96	47.95	24.20	40.17
	t4	0.00	0.00	0.00	17.72	0.00	n/a	0.00	96.01	80.10	94.77	100.00
Total Fe	t0	4.98 ± 0.65	4.98 ± 0.65	4.98 ± 0.65	4.98 ± 0.65	4.98 ± 0.65	4.98 ± 0.65	4.98 ± 0.65	4.98 ± 0.65	4.98 ± 0.65	4.98 ± 0.65	4.98 ± 0.65
	t1	2.69 ± 1.59	1.94 ± 0.57	0.12 ± 0.08	1.28 ± 0.42	1.18 ± 0.11	1.85 ± 0.57	4.27 ± 1.29	0.34 ± 0.06	3.36 ± 0.74	1.69 ± 0.18	2.20 ± 0.89
	t2	122.21 ± 1.89	1.59 ± 0.54	89.50 ± 5.29	3.83 ± 2.05	92.68 ± 15.83	0.44 ± 0.69	117.21 ± 2.38	44.67 ± 8.69	70.05 ± 18.01	17.25 ± 0.75	23.58 ± 1.91
	t4	12.81 ± 2.09	6.38 ± 0.04	34.61 ± 23.93	30.03 ± 4.44	19.39 ± 1.00	0.61 ± 0.04	3.61 ± 1.01	66.35 ± 6.50	16.76 ± 2.33	94.78 ± 1.49	8.10 ± 0.45
FeS	t0	4.17 ± 0.72	4.17 ± 0.72	4.17 ± 0.72	4.17 ± 0.72	4.17 ± 0.72	4.17 ± 0.72	4.17 ± 0.72	4.17 ± 0.72	4.17 ± 0.72	4.17 ± 0.72	4.17 ± 0.72
	t1	2.72 ± 2.04	0.95 ± 1.30	n.d.	n.d.	0.65 ± 0.72	2.57 ± 1.50	4.93 ± 4.57	n.d.	1.27 ± 0.92	1.10 ± 0.89	0.40 ± 0.95
	t2	n.d.	0.45 ± 0.63	n.d.	1.13 ± 2.20	n.d.	0.70 ± 0.79	n.d.	123.15 ± 3.22	45.92 ± 18.91	97.39 ± 7.36	79.80 ± 5.63
	t4	1.13 ± 3.16	0.87 ± 1.43	12.54 ± 31.30	n.d.	n.d.	0.72 ± 0.29	1.42 ± 1.05	63.41 ± 6.71	12.77 ± 3.69	34.60 ± 5.36	12.55 ± 2.49
Digest Fe(II)	t4	624.96 ± 41.14	592.50 ± 16.45	723.31 ± 36.96	681.46 ± 18.51	709.19 ± 29.05	655.89 ± 17.76	826.06 ± 6.90	838.13 ± 23.58	811.93 ± 8.02	853.39 ± 37.24	916.63 ± 14.13
Digest Fe(T)	t4	623.71 ± 38.60	601.89 ± 16.89	721.12 ± 34.66	678.80 ± 17.65	706.02 ± 28.82	642.42 ± 26.54	819.62 ± 7.26	831.36 ± 23.42	808.76 ± 8.50	848.19 ± 34.90	902.86 ± 15.98
Digest Fe(III)	t4	n.d.	n.d.	n.d.	n.d.	n.d.	n.d.	n.d.	n.d.	n.d.	n.d.	n.d.

Table 6: Site 4 iron concentrations (μM). Errors represent the standard deviations between three replicate incubation tubes measured in triplicate. n.d. = below detection limit.

		dFe(II)				dFe(III)				Fe(III) %			
Timepoint	**Treatment**	**Site 1**	**Site 2**	**Site 3**	**Site 4**	**Site 1**	**Site 2**	**Site 3**	**Site 4**	**Site 1**	**Site 2**	**Site 3**	**Site 4**
t0	Starting slurry	0.28 ± 0.10	0.97 ± 0.05	0.37 ± 0.22	0.25 ± 0.05	n.d.	0.08 ± 0.06	n.d.	0.11 ± 0.22	0.00	7.92	0.00	30.29
t1	Control	20.58 ± 0.15	6.07 ± 1.02	0.89 ± 0.05	1.26 ± 0.49	0.43 ± 0.36	0.53 ± 1.93	n.d.	n.d.	2.05	8.04	0.00	0.00
	Kill	2.57 ± 0.15	2.52 ± 0.02	3.01 ± 0.07	2.46 ± 0.06	n.d.	n.d.	n.d.	n.d.	0.00	0.00	0.00	0.00
	Mn(III)-DFOB			0.20 ± 0.18	0.21 ± 0.07			n.d.	n.d.			0.00	0.00
	Manganite	0.63 ± 0.28	0.51 ± 0.10	0.42 ± 0.07	0.56 ± 0.34	0.33 ± 0.37	0.39 ± 0.18	0.35 ± 0.09	0.35 ± 0.46	34.61	43.65	45.68	38.21
	Buserite	1.74 ± 0.47	4.68 ± 0.71	1.45 ± 0.07	1.06 ± 0.08	n.d.	n.d.	n.d.	n.d.	0.00	0.00	0.00	0.00
	δ-MnO_2	1.13 ± 0.15	1.29 ± 0.38	1.13 ± 0.07	n.d.	n.d.	n.d.	0.25 ± 0.31	1.31 ± 0.27	0.00	0.00	17.92	100.00
	Sulfate	1.02 ± 0.09	14.49 ± 0.64	1.10 ± 0.14	2.62 ± 0.71	19.91 ± 1.06	0.68 ± 1.16	n.d.	n.d.	95.11	4.49	0.00	0.00
	Fe(III)-DFOB			0.91 ± 0.04	12.76 ± 1.22			n.d.	0.09 ± 1.75			0.00	0.67
	Nontronite	9.80 ± 3.51	2.09 ± 0.65	1.31 ± 0.35	2.49 ± 0.32	0.78 ± 4.76	0.34 ± 1.28	n.d.	0.06 ± 0.57	7.34	14.02	0.00	2.43
	Ferrihydrite	21.56 ± 9.70	6.94 ± 2.75	0.78 ± 0.12	0.95 ± 0.10	1.47 ± 13.55	1.25 ± 3.95	0.22 ± 0.27	0.02 ± 0.23	6.40	15.29	22.30	1.58
	Goethite	17.40 ± 0.40	2.83 ± 0.66	2.25 ± 0.06	2.66 ± 0.18	0.12 ± 1.16	0.25 ± 1.03	0.02 ± 0.11	0.10 ± 0.28	0.67	8.19	0.83	3.48
t2	Control	109.04 ± 17.08	134.53 ± 19.03	1.51 ± 0.36	123.82 ± 1.91	n.d.	n.d.	n.d.	n.d.	0.00	0.00	0.00	0.00
	Kill	33.46 ± 4.19	11.14 ± 0.98	2.45 ± 0.01	1.56 ± 0.03	n.d.	n.d.	0.46 ± 1.12	n.d.	0.00	0.00	15.82	0.00
	Mn(III)-DFOB			2.10 ± 0.21	48.42 ± 9.87			1.67 ± 0.29	44.92 ± 13.91			44.36	48.12
	Manganite	1.77 ± 0.69	1.91 ± 0.70	1.03 ± 0.07	2.19 ± 0.40	n.d.	n.d.	n.d.	0.03 ± 0.61	0.00	0.00	0.00	1.22
	Buserite	38.22 ± 18.71	89.07 ± 25.60	3.03 ± 0.12	89.48 ± 12.44	n.d.	0.29 ± 36.17	n.d.	n.d.	0.00	0.33	0.00	0.00
	δ-MnO_2	2.21 ± 0.59	1.63 ± 0.11	1.72 ± 0.27	1.59 ± 0.22	n.d.	n.d.	n.d.	n.d.	0.00	0.00	0.00	0.00
	Sulfate	113.96 ± 10.17	163.75 ± 3.28	8.08 ± 2.63	118.42 ± 3.70	n.d.	n.d.	n.d.	n.d.	0.00	0.00	0.00	0.00
	Fe(III)-DFOB			1.63 ± 2.33	18.41 ± 13.37			3.74 ± 2.97	7.51 ± 19.11			69.63	28.96
	Nontronite	4.77 ± 0.68	12.59 ± 0.85	12.60 ± 16.01	6.80 ± 0.37	4.14 ± 1.55	6.56 ± 0.89	n.d.	6.27 ± 0.70	46.45	34.27	0.00	47.95
	Ferrihydrite	3.08 ± 0.37	1.82 ± 0.37	1.73 ± 0.24	2.64 ± 0.27	1.24 ± 0.42	0.71 ± 0.53	1.73 ± 0.93	0.84 ± 0.69	28.74	27.93	50.01	24.20
	Goethite	2.75 ± 0.56	2.32 ± 0.19	2.04 ± 0.97	3.46 ± 0.82	2.00 ± 1.21	1.74 ± 0.62	n.d.	2.32 ± 1.51	42.10	42.84	0.00	40.17
t4	Control	0.94 ± 0.60	92.49 ± 0.54	0.89 ± 0.76	14.86 ± 2.57	n.d.	n.d.	n.d.	n.d.	0.00	0.00	0.00	0.00
	Kill	52.05 ± 3.10	20.15 ± 2.49	3.40 ± 0.60	3.47 ± 0.67	7.21 ± 3.78	2.58 ± 2.78	n.d.	n.d.	12.17	11.36	0.00	0.00
	Mn(III)-DFOB			n.d.	31.92 ± 23.21			n.d.	n.d.			n/a	0.00
	Manganite	6.65 ± 0.97	83.58 ± 13.94	0.20 ± 0.15	38.31 ± 7.26	n.d.	18.24 ± 23.37	n.d.	8.25 ± 12.42	0.00	17.92	0.00	17.72
	Buserite	1.24 ± 0.16	92.30 ± 1.05	n.d.	20.79 ± 0.30	n.d.	n.d.	n.d.	n.d.	0.00	0.00	n/a	0.00
	δ-MnO_2	n.d.	n.d.	8.33 ± 1.09	n.d.	n.d.	n.d.	n.d.	n.d.	n/a	n/a	0.00	n/a
	Sulfate	n.d.	11.14 ± 1.04	n.d.	1.86 ± 0.16	n.d.	n.d.	n.d.	n.d.	n/a	0.00	n/a	0.00
	Fe(III)-DFOB			4.94 ± 1.21	1.95 ± 1.01			n.d.	46.83 ± 2.44			0.00	96.01
	Nontronite	n.d.	9.33 ± 0.21	n.d.	3.37 ± 0.54	n.d.	22.40 ± 21.03	n.d.	13.56 ± 2.88	n/a	70.60	n/a	80.10
	Ferrihydrite	n.d.	10.90 ± 1.16	n.d.	5.04 ± 0.63	21.01 ± 5.68	88.15 ± 1.77	10.98 ± 3.16	91.19 ± 0.68	100.00	89.00	100.00	94.77
	Goethite	n.d.	7.81 ± 0.73	n.d.	n.d.	n.d.	89.35 ± 1.23	0.44 ± 0.43	8.00 ± 1.02	n/a	91.96	100.00	100.00

Table 7: Dissolved iron concentrations (μM) from all four sites. Errors represent the standard deviations between three replicate incubation tubes measured in triplicate. n.d. = below detection limit.

		Total Fe				FeS			
Timepoint	**Treatment**	**Site 1**	**Site 2**	**Site 3**	**Site 4**	**Site 1**	**Site 2**	**Site 3**	**Site 4**
t0	Starting slurry	36.06 ± 0.19	32.60 ± 2.35	22.92 ± 0.62	4.98 ± 0.65	n.d.	5.24 ± 3.36	n.d.	4.17 ± 0.72
t1	Control	24.50 ± 4.01	14.63 ± 0.15	2.18 ± 0.61	2.69 ± 1.59	6.70 ± 13.06	0.90 ± 1.76	0.26 ± 0.83	2.72 ± 2.04
	Kill	1.02 ± 0.02	2.18 ± 0.06	2.33 ± 0.06	1.94 ± 0.57	1.04 ± 5.89	1.74 ± 1.90	1.29 ± 0.36	0.95 ± 1.30
	Mn(III)-DFOB			0.26 ± 0.26	0.12 ± 0.08			n.d.	n.d.
	Manganite	1.44 ± 0.58	1.20 ± 0.25	1.86 ± 0.13	1.28 ± 0.42	1.66 ± 1.04	0.54 ± 0.76	1.05 ± 0.66	n.d.
	Buserite	2.72 ± 0.16	6.32 ± 0.76	5.68 ± 0.43	1.18 ± 0.11	1.91 ± 1.29	0.96 ± 1.15	n.d.	0.65 ± 0.72
	δ-MnO_2	15.22 ± 5.48	1.37 ± 0.43	3.49 ± 0.82	1.85 ± 0.57	n.d.	3.61 ± 0.57	2.03 ± 0.82	2.57 ± 1.50
	Sulfate	29.38 ± 1.32	22.27 ± 5.08	16.21 ± 2.09	4.27 ± 1.29	17.80 ± 2.71	2.74 ± 6.31	n.d.	4.93 ± 4.57
	Fe(III)-DFOB			0.08 ± 0.02	0.34 ± 0.06			n.d.	n.d.
	Nontronite	15.14 ± 3.57	4.55 ± 3.17	1.39 ± 0.19	3.36 ± 0.74	6.11 ± 4.48	2.27 ± 3.77	1.46 ± 0.56	1.27 ± 0.92
	Ferrihydrite	30.14 ± 6.18	13.72 ± 2.46	9.05 ± 1.43	1.69 ± 0.18	1.95 ± 7.27	4.45 ± 4.93	10.46 ± 1.49	1.10 ± 0.89
	Goethite	16.86 ± 13.43	4.04 ± 0.38	1.66 ± 0.43	2.20 ± 0.89	19.82 ± 19.85	n.d.	2.63 ± 1.82	0.40 ± 0.95
t2	Control	117.64 ± 13.13	157.07 ± 9.52	1.61 ± 0.16	122.21 ± 1.89	6.27 ± 19.67	n.d.	0.66 ± 0.43	n.d.
	Kill	47.62 ± 8.19	15.72 ± 2.58	2.60 ± 0.28	1.59 ± 0.54	7.43 ± 13.46	1.52 ± 4.72	0.71 ± 0.31	0.45 ± 0.63
	Mn(III)-DFOB			0.04 ± 0.01	89.50 ± 5.29			n.d.	n.d.
	Manganite	1.41 ± 1.10	n.d.	0.57 ± 0.63	3.83 ± 2.05	1.23 ± 1.39	0.71 ± 0.18	1.15 ± 0.89	1.13 ± 2.20
	Buserite	50.61 ± 8.53	114.17 ± 23.76	4.37 ± 1.58	92.68 ± 15.83	0.10 ± 11.26	n.d.	1.45 ± 2.92	n.d.
	δ-MnO_2	2.54 ± 1.51	0.88 ± 1.03	2.84 ± 3.01	0.44 ± 0.69	1.12 ± 1.99	0.81 ± 1.09	1.29 ± 4.64	0.70 ± 0.79
	Sulfate	114.88 ± 9.25	170.29 ± 4.87	5.27 ± 2.67	117.21 ± 2.38	n.d.	2.39 ± 5.78	n.d.	n.d.
	Fe(III)-DFOB			n.d.	44.67 ± 8.69			1.82 ± 0.95	123.15 ± 3.22
	Nontronite	45.50 ± 8.71	93.78 ± 1.79	7.30 ± 0.64	70.05 ± 18.01	56.62 ± 21.62	54.13 ± 1.82	n.d.	45.92 ± 18.91
	Ferrihydrite	28.06 ± 2.34	17.45 ± 3.34	24.47 ± 5.64	17.25 ± 0.75	122.52 ± 2.39	127.57 ± 6.68	31.66 ± 6.64	97.39 ± 7.36
	Goethite	12.67 ± 0.72	22.09 ± 6.68	2.55 ± 1.41	23.58 ± 1.91	45.76 ± 11.47	121.02 ± 8.01	3.19 ± 4.21	79.80 ± 5.63
t4	Control	1.46 ± 0.36	130.25 ± 1.23	1.68 ± 0.40	12.81 ± 2.09	1.08 ± 0.96	42.12 ± 2.21	0.40 ± 0.47	1.13 ± 3.16
	Kill	43.46 ± 2.93	18.06 ± 1.83	1.72 ± 0.18	6.38 ± 0.04	1.04 ± 5.89	n.d.	n.d.	0.87 ± 1.43
	Mn(III)-DFOB			n.d.	34.61 ± 23.93			0.25 ± 0.18	12.54 ± 31.30
	Manganite	5.65 ± 1.29	91.54 ± 16.82	1.19 ± 0.25	30.03 ± 4.44	2.24 ± 3.10	0.38 ± 25.04	0.28 ± 0.40	n.d.
	Buserite	2.88 ± 0.29	131.66 ± 3.91	1.61 ± 0.23	19.39 ± 1.00	3.70 ± 0.88	n.d.	0.17 ± 0.67	n.d.
	δ-MnO_2	0.87 ± 0.04	0.64 ± 0.05	20.47 ± 1.41	0.61 ± 0.04	1.56 ± 0.25	1.26 ± 0.79	n.d.	0.72 ± 0.29
	Sulfate	1.71 ± 0.13	59.51 ± 5.65	1.90 ± 0.11	3.61 ± 1.01	5.35 ± 0.58	70.73 ± 5.69	1.53 ± 0.49	1.42 ± 1.05
	Fe(III)-DFOB			0.52 ± 0.02	66.35 ± 6.50			n.d.	63.41 ± 6.71
	Nontronite	1.75 ± 0.78	97.63 ± 28.43	1.06 ± 0.20	16.76 ± 2.33	0.58 ± 0.91	31.00 ± 28.43	0.36 ± 0.28	12.77 ± 3.69
	Ferrihydrite	28.48 ± 4.83	122.47 ± 15.69	19.17 ± 6.30	94.78 ± 1.49	39.07 ± 13.60	9.31 ± 15.72	10.51 ± 7.08	34.60 ± 5.36
	Goethite	1.54 ± 0.14	103.54 ± 10.89	2.31 ± 0.17	8.10 ± 0.45	0.86 ± 0.29	26.95 ± 10.90	2.07 ± 0.44	12.55 ± 2.49

Table 8: Particulate iron concentrations (μM) from all four sites. Errors represent the standard deviations between three replicate incubation tubes measured in triplicate. n.d. = below detection limit.

	Digest Fe(II)				Digest Fe(III)			
Treatment	**Site 1**	**Site 2**	**Site 3**	**Site 4**	**Site 1**	**Site 2**	**Site 3**	**Site 4**
Control	648.15 ± 110.89	813.57 ± 26.50	647.11 ± 19.25	624.96 ± 41.14	n.d.	n.d.	n.d.	n.d.
Kill	702.79 ± 19.07	762.58 ± 23.19	619.30 ± 28.85	592.50 ± 16.45	n.d.	n.d.	n.d.	n.d.
Mn(III)-DFOB			712.30 ± 25.72	723.31 ± 36.96			n.d.	n.d.
Manganite	812.03 ± 29.12	868.48 ± 23.17	760.74 ± 81.71	681.46 ± 18.51	n.d.	n.d.	n.d.	n.d.
Buserite	853.60 ± 22.06	890.19 ± 17.61	704.27 ± 34.35	709.19 ± 29.05	n.d.	n.d.	n.d.	n.d.
δ-MnO_2	780.79 ± 26.16	835.31 ± 22.23	731.95 ± 17.34	655.89 ± 17.76	n.d.	n.d.	n.d.	n.d.
Sulfate	919.06 ± 9.64	928.75 ± 44.75	788.20 ± 9.29	826.06 ± 6.90	n.d.	n.d.	n.d.	n.d.
Fe(III)-DFOB			845.94 ± 10.80	838.13 ± 23.58			n.d.	n.d.
Nontronite	928.62 ± 33.21	947.52 ± 26.42	805.12 ± 44.19	811.93 ± 8.02	n.d.	n.d.	n.d.	n.d.
Ferrihydrite	953.63 ± 23.95	988.56 ± 19.03	889.71 ± 20.41	853.39 ± 37.24	n.d.	n.d.	n.d.	n.d.
Goethite	957.58 ± 9.82	1012.40 ± 29.95	876.78 ± 37.48	916.63 ± 14.13	n.d.	n.d.	n.d.	n.d.

Table 9: Iron digest concentrations (μM) from all four sites at the end of the experiment. Errors represent the standard deviations between three replicate incubation tubes measured in triplicate. n.d. = below detection limit.

Addition	Balanced reaction	Free energy (kJ mol CH_4^{-1})	
		ΔG^0	ΔG
Sulfate	$CH_4 + SO_4^{2-} \rightarrow HCO_3^- + HS^- + H_2O$	-32.94	-32.06
Mn(III)-DFOB	$CH_4 + 8Mn(III)\text{-}DFOB + 3H_2O \rightarrow HCO_3^- + 8Mn(II)\text{-}DFOB + 9H^+$	-650.96	-773.64
Manganite	$CH_4 + 8MnOOH + 15H^+ \rightarrow HCO_3^- + 8Mn^{2+} + 13H_2O$	-998.15	-611.76
Birnessite	$CH_4 + 4MnO_2 + 7H^+ \rightarrow HCO_3^- + 4Mn^{2+} + 5H_2O$	-550.31	-376.03
δ-MnO_2	$CH_4 + 4MnO_2 + 7H^+ \rightarrow HCO_3^- + 4Mn^{2+} + 5H_2O$	-790.31	-567.22
Fe(III)-DFOB	$CH_4 + 8Fe(III)\text{-}DFOB + 3H_2O \rightarrow HCO_3^- + 8Fe(II)\text{-}DFOB + 9H^+$	-26.07	-530.55
Nontronite	$CH_4 + 8Fe(III)\text{-clay} + 3H_2O \rightarrow HCO_3^- + 8Fe(II)\text{-clay} + 9H^+$	-560.87	-938.08
Ferrihydrite	$CH_4 + 8Fe(OH)_3 + 15H^+ \rightarrow HCO_3^- + 8Fe^{2+} + 21H_2O$	-496.15	-109.76
Goethite	$CH_4 + 8FeOOH + 15H^+ \rightarrow HCO_3^- + 8Fe^{2+} + 13H_2O$	-357.91	28.48

Table 10: Balanced reaction for AOM and Gibbs free energy calculations for the electron acceptors added in this study. Nontronite calculation assumes Fe^{3+} was reduced in place without significantly disturbing the mineral structure.

Addition	Theoretical energy yield (J cm^{-3} yr^{-1})			
	Site 1	Site 2	Site 3	Site 4
Sulfate	0.17 ± 0.04	0.11 ± 0.02	1.06 ± 0.07	0.12 ± 0.01
Mn(III)-DFOB			8.56 ± 1.96	2.02 ± 0.23
Manganite	0.71 ± 0.20	0.95 ± 0.13	6.65 ± 0.26	1.16 ± 0.17
Birnessite	1.01 ± 0.09	0.97 ± 0.08	3.35 ± 0.33	0.85 ± 0.08
δ-MnO_2	0.48 ± 0.18	0.64 ± 0.16	1.24 ± 0.25	0.56 ± 0.17
Fe(III)-DFOB			9.17 ± 0.50	1.47 ± 0.11
Nontronite	4.35 ± 1.03	2.00 ± 0.19	16.55 ± 2.62	2.48 ± 0.26
Ferrihydrite	0.44 ± 0.09	0.28 ± 0.03	1.40 ± 0.13	0.35 ± 0.07
Goethite				

Table 11: Theoretical energy yields, assuming only the added electron acceptor is utilized for AOM.

Environment	Rate		Description	Reference
Marine	6 - 14	µmol CO_2 cm^{-3} yr^{-1}	Marine methane-seep sediments, Eel River Basin	Beal et al. 2009
	1.32	µmol CO_2 cm^{-3} yr^{-1}	Brackish coastal sediments, Bothnian Sea	Egger et al. 2015
	59	µmol CH_4 cm^{-3} yr^{-1}	Metalliferous hydrothermal sediments, Chowder Hill	Wankel et al. 2012
	n/a		Marine sediments, Argentine Basin	Riedinger et al. 2014
	n/a		Brackish coastal sediments, Georgia	Segarra et al. 2013
	1 - 33	µmol CO_2 cm^{-3} yr^{-1}	Marine methane-seep sediments, Cascadia Margin	*This study*
Freshwater	13	µmol CH_4 cm^{-3} yr^{-1} *	Freshwater sediments from an iron-rich lake, Lake Ørn	Norði et al. 2013
	1.3	µmol CO_2 cm^{-3} yr^{-1}	Freshwater sediments from a deep lake, Lake Kinneret	Sivan et al. 2011
	n/a		Crude oil-contaminated groundwater near Bemidiji	Amos et al. 2012
	n/a		Sediments from a mud volcano, eastern Taiwan	Chang et al. 2012
	n/a		Fresh water from a deep ferruginous lake, Lake Matano	Crowe et al. 2011
	n/a		Freshwater sediments from an iron-rich lake, Lake Ørn	Mostovaya et al. 2021
	n/a		Freshwater sediments, Lake Baikal	Torres et al. 2014

Table 12: Rates of metal-AOM measured in various environments (modified from He et al. 2018). Wankel et al. 2012 and Norði et al. 2013 rates are the maximum rates reported in these publications. * includes sulfate-AOM

Metal oxide/complex	Sample	Rate		Reference
Ferrihydrite	Marine sediments, Eel River Basin	6	µmol CO_2 cm^{-3} yr^{-1}	Beal et al. 2009
	Enrichment from freshwater sediment, Australia	23	µmol CH_4 cm^{-3} yr^{-1}	Cai et al. 2018
	Coastal sediments, Bothnian Sea	1.3	µmol CH_4 cm^{-3} yr^{-1}	Egger et al. 2015
	Culture of nitrate-AOM	144	µmol CO_2 $g_{(protein)}^{-1}$ d^{-1}	Ettwig et al. 2016
	Co-culture of nitrate-AOM and *S. oneidensis* MR-1	29	µmol CH_4 $g_{(biomass)}^{-1}$ d^{-1}	Fu et al. 2016
	Culture of nitrate-AOM	0	µmol CH_4 $g_{(biomass)}^{-1}$ d^{-1}	Fu et al. 2016
	Culture from Cai et al. 2018	1.1	µmol CH_4 cm^{-3} yr^{-1}	Li et al. 2021
	Brackish salt marsh sediment, Georgia	1.4	µmol CH_4 cm^{-3} yr^{-1}	Segarra et al. 2013
	Freshwater tidal creek sediment, Georgia	4.6	µmol CH_4 cm^{-3} yr^{-1}	Segarra et al. 2013
	Marine methane-seep sediments, Cascadia Margin	3 - 13	µmol CO_2 cm^{-3} yr^{-1}	*This study*
Goethite/iron oxyhydroxide	Marine sediments, Eel River Basin	0	µmol CO_2 cm^{-3} yr^{-1}	Beal et al. 2009
	Culture from Cai et al. 2018	464	µmol CH_4 cm^{-3} yr^{-1}	Li et al. 2021
	Freshwater sediments, Lake Kinneret	1.3	µmol CH_4 cm^{-3} yr^{-1}	Sivan et al. 2011
	Marine methane-seep sediments, Cascadia Margin	2 - 15	µmol CO_2 cm^{-3} yr^{-1}	*This study*
Magnetite	Culture from Cai et al. 2018	330	µmol CH_4 cm^{-3} yr^{-1}	Li et al. 2021
Fe(III)-citrate	Culture of nitrate-AOM	1920	µmol CO_2 $g_{(protein)}^{-1}$ d^{-1}	Ettwig et al. 2016
	Culture of sulfate-AOM	290	µmol CO_2 cm^{-3} yr^{-1}	Scheller et al. 2016
	Enrichment from freshwater sediment, Zoibe wetland	1410	µmol CH_4 cm^{-3} yr^{-1}	Chen et al. 2022
Fe(III)-EDTA	Culture of sulfate-AOM	44	µmol CO_2 cm^{-3} yr^{-1}	Scheller et al. 2016
Fe(III)-NTA	Culture of sulfate-AOM	15	µmol CO_2 cm^{-3} yr^{-1}	Scheller et al. 2016
Birnessite	Marine sediments, Eel River Basin	14	µmol CO_2 cm^{-3} yr^{-1}	Beal et al. 2009
	Culture of nitrate-AOM	504	µmol CO_2 $g_{(protein)}^{-1}$ d^{-1}	Ettwig et al. 2016
	Culture from Cai et al. 2018	16	µmol CH_4 cm^{-3} yr^{-1}	Leu et al. 2020
	Brackish salt marsh sediment, Georgia	0.88	µmol CH_4 cm^{-3} yr^{-1}	Segarra et al. 2013
	Freshwater tidal creek sediment, Georgia	1.3	µmol CH_4 cm^{-3} yr^{-1}	Segarra et al. 2013
	Marine methane-seep sediments, Cascadia Margin	2 - 9	µmol CO_2 cm^{-3} yr^{-1}	*This study*

Table 13: Rates of metal-AOM from laboratory experiments using a variety of metal oxides or metal-ligand complexes (modified from He et al. 2018).

References

Amos, R. T., Bekins, B. A., Cozzarelli, I. M., Voytek, M. A., Kirshtein, J. D., Jones, E. J. P., & Blowes, D. W. (2012). Evidence for iron-mediated anaerobic methane oxidation in a crude oil-contaminated aquifer. *Geobiology*, *10*(6), 506–517.

Aromokeye, D. A., Kulkarni, A. C., Elvert, M., Wegener, G., Henkel, S., Coffinet, S., Eickhorst, T., Oni, O. E., Richter-Heitmann, T., Schnakenberg, A., Taubner, H., Wunder, L., Yin, X., Zhu, Q., Hinrichs, K. U., Kasten, S., & Friedrich, M. W. (2020). Rates and Microbial Players of Iron-Driven Anaerobic Oxidation of Methane in Methanic Marine Sediments. *Frontiers in Microbiology*, *10*, 3041.

Arshad, A., Speth, D. R., de Graaf, R. M., Op den Camp, H. J. M., Jetten, M. S. M., & Welte, C. U. (2015). A metagenomics-based metabolic model of nitrate-dependent anaerobic oxidation of methane by Methanoperedens-like archaea. *Frontiers in Microbiology*, *6*(DEC).

Barnes, F. O., & Goldberg, E. D. (1976). Methane production and consumption in anoxic marine sediments - NASA/ADS. *Geology*, *4*(5), 297.

Bar-Or, I., Elvert, M., Eckert, W., Kushmaro, A., Vigderovich, H., Zhu, Q., Ben-Dov, E., & Sivan, O. (2017). Iron-Coupled Anaerobic Oxidation of Methane Performed by a Mixed Bacterial-Archaeal Community Based on Poorly Reactive Minerals. *Environmental Science and Technology*, *51*(21), 12293–12301.

Beal, E. J., House, C. H., & Orphan, V. J. (2009). Manganese- and iron-dependent marine methane oxidation. *Science*, *325*(5937), 184–187.

Bellotti, D., & Remelli, M. (2021). Deferoxamine B: A Natural, Excellent and Versatile Metal Chelator. *Molecules*, *26*(11).

Boetius, A., Ravenschlag, K., Schubert, C. J., Rickert, D., Widdel, F., Gleseke, A., Amann, R., Jørgensen, B. B., Witte, U., & Pfannkuche, O. (2000). A marine microbial consortium apparently mediating anaerobic oxidation of methane. *Nature*, *407*(6804), 623–626.

Cai, C., Leu, A. O., Xie, G. J., Guo, J., Feng, Y., Zhao, J. X., Tyson, G. W., Yuan, Z., & Hu, S. (2018). A methanotrophic archaeon couples anaerobic oxidation of methane to Fe(III) reduction. *ISME Journal*, *12*(8), 1929–1939.

Cai, C., Li, K., Liu, D., John, C. M., Wang, D., Fu, B., Fakhraee, M., He, H., Feng, L., & Jiang, L. (2021). Anaerobic oxidation of methane by Mn oxides in sulfate-poor environments. *Geology*, *49*(7), 761–766.

Callahan, B. J., McMurdie, P. J., Rosen, M. J., Han, A. W., Johnson, A. J. A., & Holmes, S. P. (2016). DADA2: High-resolution sample inference from Illumina amplicon data. *Nature Methods*, *13*(7), 581–583.

Callahan, B. J., Sankaran, K., Fukuyama, J. A., Mcmurdie, P. J., Holmes, S. P., Lahti, L., & Garud, N. R. (2016). Bioconductor Workflow for Microbiome Data Analysis: from raw reads to community analyses. *F1000Research*, *5*, 1492.

Chang, Y. H., Cheng, T. W., Lai, W. J., Tsai, W. Y., Sun, C. H., Lin, L. H., & Wang, P. L. (2012). Microbial methane cycling in a terrestrial mud volcano in eastern Taiwan. *Environmental Microbiology*, *14*(4), 895–908.

Chen, H., Gan, Q., & Fan, C. (2020). Methyl-Coenzyme M Reductase and Its Post-translational Modifications. *Frontiers in Microbiology*, *11*.

Chen, L., Li, L., Zhang, S., Zhang, W., Xue, K., Wang, Y., & Dong, X. (2022). Anaerobic methane oxidation linked to Fe(III) reduction in a Candidatus Methanoperedens-enriched

consortium from the cold Zoige wetland at Tibetan Plateau. *Environmental Microbiology*, *24*(2), 614–625.

Crowe, S. A., Katsev, S., Leslie, K., Sturm, A., Magen, C., Nomosatryo, S., Pack, M. A., Kessler, J. D., Reeburgh, W. S., Roberts, J. A., González, L., Douglas Haffner, G., Mucci, A., Sundby, B., & Fowle, D. A. (2011). The methane cycle in ferruginous Lake Matano. *Geobiology*, *9*(1), 61–78.

Cui, M., Ma, A., Qi, H., Zhuang, X., & Zhuang, G. (2015). Anaerobic oxidation of methane: an "active" microbial process. *MicrobiologyOpen*, *4*(1), 1.

Dang, C. C., Xie, G. J., Liu, B. F., Xing, D. F., Ding, J., & Ren, N. Q. (2021). Heavy metal reduction coupled to methane oxidation：Mechanisms, recent advances and future perspectives. *Journal of Hazardous Materials*, *405*, 124076.

Dong, Q. Y., Wang, Z., Shi, L. D., Lai, C. Y., & Zhao, H. P. (2019). Anaerobic methane oxidation coupled to chromate reduction in a methane-based membrane biofilm batch reactor. *Environmental Science and Pollution Research International*, *26*(25), 26286–26292.

Duckworth, O. W., & Sposito, G. (2005). Siderophore-manganese (III) interactions. I. Air-oxidation of manganese(II) promoted by desferrioxamine B. *Environmental Science and Technology*, *39*(16), 6037–6044.

Egger, M., Rasigraf, O., Sapart, C. J., Jilbert, T., Jetten, M. S. M., Röckmann, T., van der Veen, C., Bânda, N., Kartal, B., Ettwig, K. F., & Slomp, C. P. (2015). Iron-mediated anaerobic oxidation of methane in brackish coastal sediments. *Environmental Science and Technology*, *49*(1), 277–283.

Etminan, M., Myhre, G., Highwood, E. J., & Shine, K. P. (2016). Radiative forcing of carbon dioxide, methane, and nitrous oxide: A significant revision of the methane radiative forcing. *Geophysical Research Letters*, *43*(24), 12,614-12,623.

Ettwig, K. F., Butler, M. K., le Paslier, D., Pelletier, E., Mangenot, S., Kuypers, M. M. M., Schreiber, F., Dutilh, B. E., Zedelius, J., de Beer, D., Gloerich, J., Wessels, H. J. C. T., van Alen, T., Luesken, F., Wu, M. L., van de Pas-Schoonen, K. T., Op Den Camp, H. J. M., Janssen-Megens, E. M., Francoijs, K. J., … Strous, M. (2010). Nitrite-driven anaerobic methane oxidation by oxygenic bacteria. *Nature*, *464*(7288), 543–548.

Ettwig, K. F., Shima, S., van de Pas-Schoonen, K. T., Kahnt, J., Medema, M. H., Op Den Camp, H. J. M., Jetten, M. S. M., & Strous, M. (2008). Denitrifying bacteria anaerobically oxidize methane in the absence of Archaea. *Environmental Microbiology*, *10*(11), 3164–3173.

Ettwig, K. F., Zhu, B., Speth, D., Keltjens, J. T., Jetten, M. S. M., & Kartal, B. (2016). Archaea catalyze iron-dependent anaerobic oxidation of methane. *Proceedings of the National Academy of Sciences of the United States of America*, *113*(45), 12792–12796.

Fu, L., Li, S. W., Ding, Z. W., Ding, J., Lu, Y. Z., & Zeng, R. J. (2016). Iron reduction in the DAMO/Shewanella oneidensis MR-1 coculture system and the fate of Fe(II). *Water Research*, *88*, 808–815.

Hansel, C. M., Lentini, C. J., Tang, Y., Johnston, D. T., Wankel, S. D., & Jardine, P. M. (2015). Dominance of sulfur-fueled iron oxide reduction in low-sulfate freshwater sediments. *ISME Journal*, *9*(11), 2400–2412.

Hansel, C. M., & Lentini, C. L. (2011). *Mineralogical Controls on Microbial Reduction of Fe(III) (Hydr)oxides* (J. Stolz & R. Oremland, Eds.).

Haroon, M. F., Hu, S., Shi, Y., Imelfort, M., Keller, J., Hugenholtz, P., Yuan, Z., & Tyson, G. W. (2013). Anaerobic oxidation of methane coupled to nitrate reduction in a novel archaeal lineage. *Nature*, *500*(7464), 567–570.

He, Z., Zhang, Q., Feng, Y., Luo, H., Pan, X., & Gadd, G. M. (2018). Microbiological and environmental significance of metal-dependent anaerobic oxidation of methane. *Science of the Total Environment*, *610–611*, 759–768.

Holmkvist, L., Ferdelman, T. G., & Jørgensen, B. B. (2011). A cryptic sulfur cycle driven by iron in the methane zone of marine sediment (Aarhus Bay, Denmark). *Geochimica et Cosmochimica Acta*, *75*(12), 3581–3599.

Johnson, H. P., Miller, U. K., Salmi, M. S., & Solomon, E. A. (2015). Analysis of bubble plume distributions to evaluate methane hydrate decomposition on the continental slope. *Geochemistry, Geophysics, Geosystems*, *16*(11), 3825–3839.

Keeling, J. L., Raven, M. D., & Gates, W. P. (2000). Geology and characterization of two hydrothermal nontronites from weathered metamorphic rocks at the Uley Graphite Mine, South Australia. *Clays and Clay Minerals*, *48*(5), 537–548.

Knittel, K., & Boetius, A. (2009). Anaerobic oxidation of methane: Progress with an unknown process. *Annual Review of Microbiology*, *63*, 311–334.

Kulm, L. D., Suess, E., Moore, J. C., Carson, B., Lewis, B. T., Ritger, S. D., Kadko, D. C., Thornburg, T. M., Embley, R. W., Rugh, W. D., Massoth, G. J., Langseth, M. G., Cochrane, G. R., & Scamman, R. L. (1986). Oregon subduction zone: Venting, fauna, and carbonates. *Science*, *231*(4738), 561–566.

Kumaraswamy, S., Ramakrishnan, B., & Sethunathan, N. (2001). Methane Production and Oxidation in an Anoxic Rice Soil as Influenced by Inorganic Redox Species. *Journal of Environmental Quality*, *30*(6), 2195–2201.

Lai, C. Y., Dong, Q. Y., Rittmann, B. E., & Zhao, H. P. (2018). Bioreduction of Antimonate by Anaerobic Methane Oxidation in a Membrane Biofilm Batch Reactor. *Environmental Science and Technology*, *52*(15), 8693–8700.

Larsen, I., Little, B., Nealson, K. H., Ray, R., Stone, A., & Tlan, J. (1998). Manganite reduction by Shewanella putrefaciens MR-4. *American Mineralogist*, *83*(11-12_Part_2), 1564–1572.

Leu, A. O., Cai, C., McIlroy, S. J., Southam, G., Orphan, V. J., Yuan, Z., Hu, S., & Tyson, G. W. (2020). Anaerobic methane oxidation coupled to manganese reduction by members of the Methanoperedenaceae. *ISME Journal*, *14*(4), 1030–1041.

Li, W., Cai, C., Song, Y., Ni, G., Zhang, X., & Lu, P. (2021). The Role of Crystalline Iron Oxides in Methane Mitigation through Anaerobic Oxidation of Methane. *ACS ES&T Water*, *1*(5), 1153–1160.

Liang, L., Wang, Y., Sivan, O., & Wang, F. (2019). Metal-dependent anaerobic methane oxidation in marine sediment: Insights from marine settings and other systems. *Science China Life Sciences*, *62*(10), 1287–1295.

Liu, J., Zhang, Y., Gu, Q., Sheng, A., & Zhang, B. (2020). Tunable Mn Oxidation State and Redox Potential of Birnessite Coexisting with Aqueous Mn(II) in Mildly Acidic Environments. *Minerals*, *10*(8), 690.

Lovley, D. R., Holmes, D. E., & Nevin, K. P. (2004). Dissimilatory Fe(III) and Mn(IV) reduction. *Advances in Microbial Physiology*, *49*, 219–286.

Luff, R., & Wallmann, K. (2003). Fluid flow, methane fluxes, carbonate precipitation and biogeochemical turnover in gas hydrate-bearing sediments at Hydrate Ridge, Cascadia

Margin: numerical modeling and mass balances. *Geochimica et Cosmochimica Acta*, *67*(18), 3403–3421.
Lyman, J., & Fleming, R. (1940). Composition of seawater. *Journal of Marine Research*, *3*, 134–146.
Mandernack, K. W., Post, J., & Tebo, B. M. (1995). Manganese mineral formation by bacterial spores of the marine Bacillus, strain SG-1: Evidence for the direct oxidation of Mn(II) to Mn(IV). *Geochimica et Cosmochimica Acta*, *59*(21), 4393–4408.
Martens, C. S., & Berner, R. A. (1974). Methane production in the interstitial waters of sulfate-depleted marine sediments. *Science*, *185*(4157), 1167–1169.
Martinez-Cruz, K., Leewis, M. C., Herriott, I. C., Sepulveda-Jauregui, A., Anthony, K. W., Thalasso, F., & Leigh, M. B. (2017). Anaerobic oxidation of methane by aerobic methanotrophs in sub-Arctic lake sediments. *Science of The Total Environment*, *607–608*, 23–31.
McMurdie, P. J., & Holmes, S. (2013). phyloseq: An R Package for Reproducible Interactive Analysis and Graphics of Microbiome Census Data. *PLOS ONE*, *8*(4), e61217.
Merle, S. G., Embley, R. W., Johnson, H. P., Lau, T. K., Phrampus, B. J., Raineault, N. A., & Gee, L. J. (2021). Distribution of Methane Plumes on Cascadia Margin and Implications for the Landward Limit of Methane Hydrate Stability. *Frontiers in Earth Science*, *9*, 104.
Moran, J. J., House, C. H., Freeman, K. H., & Ferry, J. G. (2005). Trace methane oxidation studied in several Euryarchaeota under diverse conditions. *Archaea*, *1*(5), 303–309.
Mostovaya, A., Wind-Hansen, M., Rousteau, P., Bristow, L. A., & Thamdrup, B. (2022). Sulfate- and iron-dependent anaerobic methane oxidation occurring side-by-side in freshwater lake sediment. *Limnology and Oceanography*, *67*(1), 231–246.
Myhre, G., Shindell, D., Bréon, F.-M., Collins, W., Fuglestvdt, J., Huang, J., & Koch, D. (2013). Anthropogenic and natural radiative forcing. *Climate Change 2013 the Physical Science Basis: Working Group I Contribution to the Fifth Assessment Report of the Intergovernmental Panel on Climate Change*, *9781107057999*, 659–740.
Nauhaus, K., Albrecht, M., Elvert, M., Boetius, A., & Widdel, F. (2007). In vitro cell growth of marine archaeal-bacterial consortia during anaerobic oxidation of methane with sulfate. *Environmental Microbiology*, *9*(1), 187–196.
Nauhaus, K., Boetius, A., Krüger, M., & Widdel, F. (2002). In vitro demonstration of anaerobic oxidation of methane coupled to sulphate reduction in sediment from a marine gas hydrate area. *Environmental Microbiology*, *4*(5), 296–305.
Nealson, K. H., Belz, A., & McKee, B. (2002). Breathing metals as a way of life: geobiology in action. *Antonie van Leeuwenhoek*, *81*(1–4), 215–222.
Nealson, K. H., & Saffarini, D. (1994). Iron and manganese in anaerobic respiration: environmental significance, physiology, and regulation. *Annual Review of Microbiology*, *48*, 311–343.
Nordi, K. Á., Thamdrup, B., & Schubert, C. J. (2013). Anaerobic oxidation of methane in an iron-rich Danish freshwater lake sediment. *Limnology and Oceanography*, *58*(2), 546–554.
Oni, O., Miyatake, T., Kasten, S., Richter-Heitmann, T., Fischer, D., Wagenknecht, L., Kulkarni, A., Blumers, M., Shylin, S. I., Ksenofontov, V., Costa, B. F. O., Klingelhöfer, G., & Friedrich, M. W. (2015). Distinct microbial populations are tightly linked to the profile of

dissolved iron in the methanic sediments of the Helgoland mud area, North Sea. *Frontiers in Microbiology*,

Orphan, V. J., Hinrichs, K. U., Ussler, W., Paull, C. K., Taylor, L. T., Sylva, S. P., Hayes, J. M., & Delong, E. F. (2001). Comparative Analysis of Methane-Oxidizing Archaea and Sulfate-Reducing Bacteria in Anoxic Marine Sediments. *Applied and Environmental Microbiology*, *67*(4), 1922.

Raghoebarsing, A. A., Pol, A., van de Pas-Schoonen, K. T., Smolders, A. J. P., Ettwig, K. F., Rijpstra, W. I. C., Schouten, S., Sinninghe Damsté, J. S., Op Den Camp, H. J. M., Jetten, M. S. M., & Strous, M. (2006). A microbial consortium couples anaerobic methane oxidation to denitrification. *Nature*, *440*(7086), 918–921.

Reeburgh, W. S. (2007). Oceanic Methane Biogeochemistry. *Chemical Reviews*, *107*(2), 486–513.

Riedinger, N., Formolo, M. J., Lyons, T. W., Henkel, S., Beck, A., & Kasten, S. (2014). An inorganic geochemical argument for coupled anaerobic oxidation of methane and iron reduction in marine sediments. *Geobiology*, *12*(2), 172–181.

Roden, E. E., & Zachara, J. M. (1996). Microbial Reduction of Crystalline Iron(III) Oxides: Influence of Oxide Surface Area and Potential for Cell Growth. *Environmental Science and Technology*, *30*(5), 1618–1628.

Rooze, J., Egger, M., Tsandev, I., & Slomp, C. P. (2016). Iron-dependent anaerobic oxidation of methane in coastal surface sediments: Potential controls and impact. *Limnology and Oceanography*, *61*, S267–S282.

Ruff, S. E., Biddle, J. F., Tesked, A. P., Knittel, K., Boetius, A., & Ramette, A. (2015). Global dispersion and local diversification of the methane seep microbiome. *Proceedings of the National Academy of Sciences of the United States of America*, *112*(13), 4015–4020.

Scheller, S., Yu, H., Chadwick, G. L., McGlynn, S. E., & Orphan, V. J. (2016). Artificial electron acceptors decouple archaeal methane oxidation from sulfate reduction. *Science*, *351*(6274), 703–707.

Schnakenberg, A., Aromokeye, D. A., Kulkarni, A., Maier, L., Wunder, L. C., Richter-Heitmann, T., Pape, T., Ristova, P. P., Bühring, S. I., Dohrmann, I., Bohrmann, G., Kasten, S., & Friedrich, M. W. (2021). Electron Acceptor Availability Shapes Anaerobically Methane Oxidizing Archaea (ANME) Communities in South Georgia Sediments. *Frontiers in Microbiology*, *12*.

Schwertmann U, & Cornell R. (2000). *Iron Oxides in the Laboratory: Preparation and Characterization, 2nd, Completely Revised and Enlarged Edition*.

Segarra, K. E. A., Comerford, C., Slaughter, J., & Joye, S. B. (2013). Impact of electron acceptor availability on the anaerobic oxidation of methane in coastal freshwater and brackish wetland sediments. *Geochimica et Cosmochimica Acta*, *115*, 15–30.

Sivan, O., Adler, M., Pearson, A., Gelman, F., Bar-Or, I., John, S. G., & Eckert, W. (2011). Geochemical evidence for iron-mediated anaerobic oxidation of methane. *Limnology and Oceanography*, *56*(4), 1536–1544.

Sivan, O., Antler, G., Turchyn, A. v., Marlow, J. J., & Orphan, V. J. (2014). Iron oxides stimulate sulfate-driven anaerobic methane oxidation in seeps. *Proceedings of the National Academy of Sciences of the United States of America*, *111*(40), E4139–E4147.

Spasojević, I., Armstrong, S. K., Brickman, T. J., & Crumbliss, A. L. (1999). Electrochemical behavior of the Fe(III) complexes of the cyclic hydroxamate siderophores alcaligin and desferrioxamine E. *Inorganic Chemistry*, *38*(3), 449–454.

Stumm, W., & Morgan, J. J. (1996). *Aquatic chemistry: chemical equilibria and rates in natural waters*. 1022.

Su, G., Zopfi, J., Yao, H., Steinle, L., Niemann, H., & Lehmann, M. F. (2020). Manganese/iron-supported sulfate-dependent anaerobic oxidation of methane by archaea in lake sediments. *Limnology and Oceanography*, *65*(4), 863–875.

Thamdrup, B. (2000). Bacterial Manganese and Iron Reduction in Aquatic Sediments. *Advances in Microbial Ecology*, *16*(1), 41–84.

Timmers, P. H. A., Welte, C. U., Koehorst, J. J., Plugge, C. M., Jetten, M. S. M., & Stams, A. J. M. (2017). Reverse Methanogenesis and Respiration in Methanotrophic Archaea. *Archaea*, *2017*.

Torres, N. T., Och, L. M., Hauser, P. C., Furrer, G., Brandl, H., Vologina, E., Sturm, M., Bürgmann, H., & Müller, B. (2014). Early diagenetic processes generate iron and manganese oxide layers in the sediments of Lake Baikal, Siberia. *Environmental Sciences: Processes and Impacts*, *16*(4), 879–889.

Vieillard, P. (2000). A new method for the prediction of Gibbs free energies of formation of hydrated clay minerals based on the electronegativity scale. *Clays and Clay Minerals*, *48*(4), 459–473.

Vigderovich, H., Eckert, W., Elul, M., Rubin-Blum, M., Elvert, M., & Sivan, O. (2022). Long-term incubations provide insight into the mechanisms of anaerobic oxidation of methane in methanogenic lake sediments. *Biogeosciences*, *19*(8), 2313–2331.

Villalobos, M., Toner, B., Bargar, J., & Sposito, G. (2003). Characterization of the manganese oxide produced by pseudomonas putida strain MnB1. *Geochimica et Cosmochimica Acta*, *67*(14), 2649–2662.

Viollier, E., Inglett, P. W., Hunter, K., Roychoudhury, A. N., & van Cappellen, P. (2000). The ferrozine method revisited: Fe(II)/Fe(III) determination in natural waters. *Applied Geochemistry*, *15*(6), 785–790.

Wang, F. P., Zhang, Y., Chen, Y., He, Y., Qi, J., Hinrichs, K. U., Zhang, X. X., Xiao, X., & Boon, N. (2014). Methanotrophic archaea possessing diverging methane-oxidizing and electron-Transporting pathways. *ISME Journal*, *8*(5), 1069–1078.

Wang, Z., Shi, L. D., Lai, C. Y., & Zhao, H. P. (2019). Methane oxidation coupled to vanadate reduction in a membrane biofilm batch reactor under hypoxic condition. *Biodegradation*, *30*(5–6), 457–466.

Wankel, S. D., Adams, M. M., Johnston, D. T., Hansel, C. M., Joye, S. B., & Girguis, P. R. (2012). Anaerobic methane oxidation in metalliferous hydrothermal sediments: Influence on carbon flux and decoupling from sulfate reduction. *Environmental Microbiology*, *14*(10), 2726–2740.

Wasmund, K., Pelikan, C., Schintlmeister, A., Wagner, M., Watzka, M., Richter, A., Bhatnagar, S., Noel, A., Hubert, C. R. J., Rattei, T., Hofmann, T., Hausmann, B., Herbold, C. W., & Loy, A. (2021). Genomic insights into diverse bacterial taxa that degrade extracellular DNA in marine sediments. *Nature Microbiology*, *6*(7), 885–898.

Weber, H. S., Habicht, K. S., & Thamdrup, B. (2017). Anaerobic methanotrophic archaea of the ANME-2d cluster are active in a low-sulfate, iron-rich freshwater sediment. *Frontiers in Microbiology*, *8*(APR), 619.

Weber, T., Wiseman, N. A., & Kock, A. (2019). Global ocean methane emissions dominated by shallow coastal waters. *Nature Communications 2019 10:1*, *10*(1), 1–10.

Wu, M. L., Ettwig, K. F., Jetten, M. S. M., Strous, M., Keltjens, J. T., & van Niftrik, L. (2011). A new intra-aerobic metabolism in the nitrite-dependent anaerobic methane-oxidizing bacterium Candidatus "Methylomirabilis oxyfera." *Biochemical Society Transactions*, *39*(1), 243–248.

Yan, Z., Joshi, P., Gorski, C. A., & Ferry, J. G. (2018). A biochemical framework for anaerobic oxidation of methane driven by Fe(III)-dependent respiration. *Nature Communications*, *9*(1).

Yang, H., Yu, S., & Lu, H. (2021). Iron-Coupled Anaerobic Oxidation of Methane in Marine Sediments: A Review. *Journal of Marine Science and Engineering 2021, Vol. 9, Page 875*, *9*(8), 875.

Zehnder, A. J. B., & Brock, T. D. (1979). Methane formation and methane oxidation by methanogenic bacteria. *Journal of Bacteriology*, *137*(1), 420.

Zhang, X., Yuan, Z., & Hu, S. (2021). Anaerobic oxidation of methane mediated by microbial extracellular respiration. *Environmental Microbiology Reports*, *13*(6), 790–804.

Zhang, Y., Maignien, L., Zhao, X., Wang, F., & Boon, N. (2011). Enrichment of a microbial community performing anaerobic oxidation of methane in a continuous high-pressure bioreactor. *BMC Microbiology*, *11*.

Zhao, L., Dong, H., Kukkadapu, R. K., Zeng, Q., Edelmann, R. E., Pentrák, M., & Agrawal, A. (2015). Biological redox cycling of iron in nontronite and its potential application in nitrate removal. *Environmental Science & Technology*, *49*(9), 5493–5501.

5. Conclusion

In nature, abiotic and biotic reactions are often intertwined and rarely involve only a single element. The restrictions of scientific study require us to simplify and disentangle these processes in order to perform experiments with clear parameters. However, there are risks to systematically oversimplifying experiments and models to include only biotic processes and/or only a single element. The work of this thesis demonstrates that coupled cycling reactions are worthy of greater attention and that their study may illuminate important processes occurring in nature. Here, I summarize the results of the three data chapters and provide suggestions for future steps.

In Chapter 2, I presented results of an isotopic study of the abiotic oxidation of nitrite to nitrate by manganese(III)-pyrophosphate (Mn(III)-PP). An inverse isotope effect of -19.9 ± 0.7‰ was measured between the $\delta^{15}N$ of nitrite consumed and nitrate produced over a range of environmentally relevant pH values (5-8). Through the addition of mildly ^{15}N enriched nitrate at the beginning of the reaction, I demonstrate that this inverse isotope effect is kinetic in nature and that no back-reaction occurs. These results are widely congruent with that of its biological analog during nitrification, which also has an inverse kinetic isotope effect of similar magnitude. Experiments in ^{18}O-labeled water further showed that water is the source of the additional oxygen atom in nitrate associated with an isotope effect of +20.3 ± 1.5‰, again comparable to that of nitrite-oxidizing organisms. Additionally, I showed that the reaction is second-order with respect to Mn(III)-PP and first order with respect to nitrous acid; thus the reaction rate falls with increasing pH. Finally, the reaction was found to be "agnostic" to oxygen; that is, the rate of reaction is unaffected by the presence or absence of oxygen, suggesting ligand bound Mn(III) could oxidize nitrite in the environment even under functionally anoxic conditions. While this study was undertaken in a laboratory environment, these results suggest that results of anoxic nitrification in the environment could in fact be due to abiotic reactions which do not necessarily require oxygen as biological nitrification does. The similarity in isotope effect magnitude and direction to the corresponding biotic reactions also suggests reactions between Mn(III)-L and nitrite would go unnoticed by conventional stable isotope approaches.

There remain several open questions from Chapter 2. Firstly, Mn(III)-L complexes have not been well characterized and are thought to contain complex mixtures of humic substances (Oldham et

al. 2015). While Mn(III)-PP is seen as a model ligand, it is unclear what proportion of natural Mn(III)-L complexes also react with nitrite, and if so, what their rates of reactions would be (Qian et al. 2019). Nitrite is also a reactive species involved in several biological nitrogen cycling processes, including nitrification, denitrification, and anammox (Gruber 2008). It is unclear if the rate of reaction of abiotic oxidation by Mn(III)-L could compete with these biotic reactions. While the results of Chapter 2 suggest reactions between Mn(III)-L and nitrite could occur in the environment, further studies would be necessary to determine if this reaction is occurring in nature and, if so, to what extent. Estuarine environments, which can experience high concentrations of both nitrite and Mn(III)-L would be a probable location to begin environmental investigations of the process (Madison et al. 2013; Oldham et al. 2017). Lakes containing ferromanganese nodules might also be likely locations to investigate the potential for this reaction. For instance, Second Connecticut Lake contains abundant ferromanganese nodules and has an average pH of 6.6, which are conditions which would theoretically favor this reaction (Asikainen and Werle 2007). Incubations could be conducted in these waters using ^{15}N-labeled nitrite to measure rates of nitrite oxidation in filter-sterilized vs unfiltered water to separate abiotic and biotic nitrite oxidation. This approach yields "potential" rates since the addition of nitrite perturbs the system. Further experimentation in a variety of ecosystems would be necessary to determine the potential environmental relevance of this reaction. Overall, the results of this chapter open avenues for further exploration of "anoxic nitrification" in the environment and suggest that Mn(III)-L may play an important role in impacting the nitrogen cycle in natural waters of pH < 7.

In Chapter 3, I reported abiotic conversion of hydroxylamine to nitrous oxide by manganese(III)-PP (Mn(III)-PP) in artificial seawater. The site preference of the nitrous oxide was found to be +35.5 ± 0.6‰, identical to that produced by ammonia-oxidizing organisms. In addition to nitrous oxide, nitrite and another product (presumed to be dinitrogen gas) were also formed. The proportion of products was found to vary with the starting ratio of reactants with a peak in nitrous oxide production at 3:1 Mn(III)-PP to hydroxylamine. The potential for "hybrid" production of N_2O (i.e., two N atoms having different precursor sources) was investigated through addition of isotopically distinct nitrite added at the beginning of the reaction; however, this signal was not found in the nitrous oxide, indicating no further reaction of nitrite to nitrous oxide. Additionally, further consumption of nitrous oxide was ruled out due to the consistent site preference throughout

reaction progress and starting reactant ratios. The results of this chapter suggest abiotic formation of nitrous oxide by manganese(III) could occur in nature but also be thus far unnoticed due to the congruence of the isotope effect with biotic reactions. This study supports others that have suggested nitrous oxide production from nitrifiers may be a largely mixed biotic-abiotic process.

In the future, in order to fully close nitrogen mass-balance in this reaction, nitrogen gas and/or ammonium production would need to be quantified. As dinitrogen was present in the headspace of the experiments presented, it was not possible to determine if it was a reaction product. Changing the inert gas used to purge from nitrogen to helium, for example, would allow for quantification of N_2. Ammonium concentration can be quantified through persulfate oxidation, although this method often results in a high blank (Knapp et al. 2005). Measurement of Mn(III)-PP concentration using the leucoberbelin blue before and after reaction with hydroxylamine would also allow for more discrete redox accounting, which could further help to identify the "missing N." I also plan to perform future experiments in the presence of oxygen to determine if the reaction is able to proceed under oxic conditions. If the reaction produces N_2 in the presence of oxygen, that would contrast with conventional understanding the N_2 is generally produced by anammox and denitrification under anoxic conditions (Devol 2015). As in Chapter 2, a wider variety of Mn(III)-L complexes could also be tested to ensure natural Mn(III)-L is being emulated as closely as possible. Mn(IV) oxides have also been shown to react with NH_2OH, though to the best of my knowledge the isotopic composition of the resulting N_2O has not been characterized which could provide another interesting avenue of exploration (Cavazos et al. 2018). Further lab experiments could also investigate the potential of coupled biotic/abiotic reaction, by adding Mn(III)-L to cultures of AOA, AOB, and/or comammox bacteria and measure the resulting products (particularly N_2O) compared to controls with no added Mn(III)-L. This study also highlights the importance of abiotic controls when performing culture experiments. It is essential to perform abiotic media controls not only with the reactant (in this case NH_3), but also with any reactive intermediates that are formed by microbes (in this case NH_2OH). Similar incubation studies in natural waters with high natural rates of nitrification, such as above the oxic/anoxic interface in oxygen deficient zones would help to establish the relevance of the reaction in the environment.

The results of both Chapter 2 and 3 shed light on abiotic coupled cycling reactions between Mn and N. However, they are by no means exhaustive studies and there remains much important work to be done in this area. Firstly, pyrophosphate is only one among many potential ligands that can complex Mn(III) which may have different degrees of reactivity. Relatively little is known at this time about the identities of the organics able to complex Mn(III) which means most studies are performed with model ligands such as pyrophosphate or DFOB. These studies both focused on Mn(III)-L complexes; however, Mn(III,IV)oxyhydroxides are also commonly found in the environment could potentially react with many nitrogen species. Natural manganese oxides exist in many different mineral forms with varying reactivities. These chapters have also highlighted some of the challenges associated with studying coupled cycling reactions; for instance, that the potential for redox reactions between Mn and N also can result in interferences in the methods used to measure their concentrations. This remains a primary area of concern when performing studies of this nature and requires extensive testing and the use of multiple types of controls.

In Chapter 4, I described experiments designed to measure rates of anaerobic oxidation of methane (AOM) in presence of a variety of electron acceptors including sulfate and a variety of oxidized forms of manganese and iron ranging from solid mineral phases to dissolved ligand-bound species. Cold-seep sediments were collected from the Cascadia Margin and incubated for 8.5 months using ^{13}C to track the formation of carbon dioxide from methane. Generally, rates were comparable to those measured in other studies of cold-seep environments, however, in contrast to previous work AOM rates were not consistently elevated in the presence of additional oxidized iron and manganese. In fact, some metal treatments were found to depress rates of AOM below that of the unamended control treatment. It was hypothesized that these findings may be attributed to increased energy yields per mole of methane consumed compared to traditional sulfate-AOM and an inability of the slow-growing microbial community to adapt to the increase in new electron acceptors. While the result that metal additions depressed rates of AOM contrasted with previous work, I also did not age sediments before initiating the experiment as other studies did, thus slowly removing sulfate and allowing the community to adapt alongside. Generally, the results of my study suggest that microbes performing metal-AOM may not be able to take full advantage of a high input of oxidized metals without a period of adjustment.

Results of 16S rRNA extractions performed by collaborators will need to be incorporated into this study and may shed further light on any shifts in community composition. If community composition was not significantly altered between the initiation and end of the study, this would support the hypothesis that the microbial community was unable to quickly adapt to take advantage of provided oxidized metal sources. Furthermore, examination of the differences between treatments could lead to greater understanding of if community composition was altered depending on the particular mineral or complexed species added. Future studies could incorporate pre-aging of sediments or selection of locations already low in sulfate in order to maximize the ability to measure rates of metal-AOM. Additionally, new experiments would benefit from utilization of an IRMS prep system designed to process DIC samples which would minimize error in measurements.

Taken as a whole, this thesis illuminates both the complexity and necessity of studying coupled cycling reactions. While these experiments are often more difficult to perform than those that focus solely on one element, the insights gleaned from examining the interactions between multiple elements can be immensely rewarding.

References

Asikainen, C. A., & Werle, S. F. (2007). Accretion of ferromanganese nodules that form pavement in Second Connecticut Lake, New Hampshire. *Proceedings of the National Academy of Sciences of the United States of America*, *104*(45), 17579–17581.

Cavazos, A. R., Taillefert, M., Tang, Y., & Glass, J. B. (2018). Kinetics of nitrous oxide production from hydroxylamine oxidation by birnessite in seawater. *Marine Chemistry*, *202*, 49–57.

Devol, A. H. (2015). Denitrification, anammox, and N2 production in marine sediments. *Annual Review of Marine Science*, *7*(Volume 7, 2015), 403–423

Gruber, N. (2008). The Marine Nitrogen Cycle: Overview and Challenges. *Nitrogen in the Marine Environment*, 1–50.

Jones, M. R., Luther, G. W., Mucci, A., & Tebo, B. M. (2019). Concentrations of reactive Mn(III)-L and MnO2 in estuarine and marine waters determined using spectrophotometry and the leuco base, leucoberbelin blue. *Talanta*, *200*, 91–99.

Knapp, A. N., Sigman, D. M., & Lipschultz, F. (2005). N isotopic composition of dissolved organic nitrogen and nitrate at the Bermuda Atlantic Time-series study site. *Global Biogeochemical Cycles*, *19*(1), 1–15.

Madison, A. S., Tebo, B. M., Mucci, A., Sundby, B., & Luther, G. W. (2013). Abundant porewater Mn(III) is a major component of the sedimentary redox system. *Science*, *341*(6148), 875–878.

Oldham, V. E., Jones, M. R., Tebo, B. M., & Luther, G. W. (2017). Oxidative and reductive processes contributing to manganese cycling at oxic-anoxic interfaces. *Marine Chemistry*, *195*, 122–128.

Qian, A., Zhang, W., Shi, C., Pan, C., Giammar, D. E., Yuan, S., Zhang, H., & Wang, Z. (2019). Geochemical Stability of Dissolved Mn(III) in the Presence of Pyrophosphate as a Model Ligand: Complexation and Disproportionation. *Environmental Science and Technology*, *53*(10), 5768–5777.